4-28-2017

Cardiac Effects of Purinergic P2X Channel Activation

Ronghua Yang
University of Connecticut School of Medicine and Dentistry, ryang@uchc.edu

Cardiac Effects of Purinergic P2X Channel Activation

Ronghua Yang, PhD

University of Connecticut, 2017

ABSTRACT

Purinergic receptors respond to extracellular nucleotides and their metabolites. They act as important signaling transduction molecules in a variety of biological processes and are important in a number of pathophysiologic conditions that impact human health. A subset of these receptors acts as non-selective cation channels, designated as P2X receptors, which can induce electrical activities in the cellular membrane and thus impact cellular function. A number of longitudinal studies following surgically or genetically induced heart failure animals have demonstrated potential improvement of cardiac function with $P2X_4$ receptor overexpression. We explore here how P2X signaling affects cardiomyocyte excitability and leads to changes in contraction in both computational and experimental models. We confirm computational predictions of P2X induced membrane depolarization and subsequent changes in a number of cardiomyocyte currents using whole cell patch clamp techniques. Direct sodium cxxxentry via P2X channels leading to intracellular ion concentration changes were detected with an increase in Na^+-K^+ ATPase peak current and enhancement of the calcium entry mode of the Na^+-Ca^{2+} exchanger. The latter we show may play a role in the enhancement of contractile response by extracellular ATP. With the aid of computational prediction and interpretation, our findings highlight the value of dynamic considerations of channel currents and offer explanations for prior inconsistencies in the purinergic field. Moreover, we establish an interaction between the $P2X_4$ receptor and nitric oxide production that may underlie its cardioprotective effects after myocardial injury. This improved understanding of P2X action on the heart helps to improve our evaluation of its targeting in clinical applications.

Cardiac Effects of Purinergic P2X Channel Activation

Ronghua Yang

B.S., Johns Hopkins University, 2007

A Dissertation

Submitted in Partial Fulfillment of the

Requirements for the Degree of

DOCTOR OF PHILOSOPHY

at the

UNIVERSITY OF CONNECTICUT

2017

APPROVAL PAGE

Doctor of Philosophy Dissertation

Cardiac Effects of Purinergic P2X Channel Activation

Presented by

Ronghua Yang, B.S.

Major Advisor _____
Dr. Bruce Liang

Major Advisor _____
Dr. Leslie Loew

Associate Advisor_____
Dr. Kimberly Dodge-Kafka

Associate Advisor_____
Dr. Ion Moraru

Associate Advisor_____
Dr. Yi Wu

Associate Advisor_____
Dr. Lixia Yue

University of Connecticut
2017

ACKNOWLEDGMENTS

First and foremost I would like to thank my advisors, Dr. Bruce Liang and Dr. Leslie Loew for their mentorship during my Ph.D studies. It was an honor to have both highly achieved scientists take interest in my growth as a scientist and I am grateful for their steady support in resources and encouragements. I am also thankful for the scientific freedom I was given to grow and learn from my trials and errors. To be able to learn from the different scientific perspectives of both laboratories and both centers that they lead (the Pat and Jim Calhoun Cardiology Center and the Center for Cell Analysis and Modeling) was also particularly gratifying. The mix of biology and technology helped me appreciate the bigger picture and be confident in my training to take on new scientific endeavors.

From the Liang lab, many thanks to Dr. Jian-bing Shen for showing me patch clamp techniques in action and for much of the data that led to the studies included in this thesis. Dr. Chunxia Cronin and Carol McGuiness were instrumental in carrying out the animal studies, from taking care of the animals to establishing surgical cardiac injury models, and to performing echocardiograms. Drs. Hongquan Gan and Suying Fan taught me the delicate technique of the isolated working heart, and Dr. Ruibo Wang and Courtney Gold were helpful not only in their assistance in molecular techniques but also for being entertaining desk neighbors for these years.

Many of the members from the Loew lab and the Center for Cell Analysis and Modeling were invaluable in teaching me to use Virtual Cell and to appreciate the values of different modeling techniques beyond what I have done. Besides bothering Jim Schaff and the Virtual Cell team on numerous occasions, Paul Michalski and Cibele Falkenberg were also helpful for modeling tips and discussions. Additionally, Corey Acker offered helpful tips on instrumentation

and electrophysiology, and I have also learned from the projects of my fellow students, many of whom have been of assistance and support at different times.

I would also like to acknowledge the members of my thesis committee: Dr. Kimberly Dodge-Kafka, Dr. Ion Moraru, Dr. Yi Wu, and Dr. Lixia Yue. Not only were they helpful in discussions, they also opened up their respective laboratories for in depth technical assistance, some of which led to critical information that contributed to part of this thesis work. While not part of the committee, Dr. Achilles Pappano also offered valuable advice and encouragement.

Additionally, I would like to thank my previous mentors and teachers, who have shown me both knowledge and passion to prepare me well for the challenges of medical and graduate school. Special thanks go to Dr. Lili Barouch for encouraging an interest in cardiovascular medicine, by first opening up her clinic to me and subsequently giving me my first real job performing research in her laboratory at Hopkins.

More thanks go to the UCHC MD/PhD program. I am thankful to many of the members past and present, for scientific discussions and personal camaraderie. To my friends, some of whom I started medical school with but have since then moved onto residencies, thanks for your stories and examples that keep me looking forward to the days beyond the Ph.D.

Special and profound thanks to : 1) my husband who offered invaluable support and humor over the years, 2) my mother who constantly reminded and demonstrated to me that all I had to do was say the word and she would be here, if for nothing else than to just make dinner (more like food for the week), 3) my father, who designed my first ever experiment and taught me to keep asking questions, 4) my maternal grandparents, who have given up their comfort and relocated to provide the most loving care to my newborn while I continue to pursue my projects, and of course 5) my little boy who has provided me with new joy and inspiration.

Finally, I would like to dedicate this thesis to my paternal grandparents, Mrs. Muzhu and Mr. Liangyang Yang. Two years ago, he suffered a stroke that would forever change our interactions, but I will always remember him as the one who biked me to school every day and made sure that I was never late. They were my earliest teachers who instilled curiosity and a strong work ethic and they continue to teach me important lessons in life.

TABLE OF CONTENTS

LIST OF TABLES

Table

LIST OF FIGURES

Figure

LIST OF ABBREVIATIONS

2-meSATP	2-methylthioadenosine-5'-o-triphosphate
ADP	adenosine diphosphate
AMP	adenosine monophosphate
AP	action potential
APD90	action potential duration 90
ATP	adenosine triphosphate
AV	atrioventricular
bl	baseline
Ca^{2+}	calcium
cAMP	3'-5'-cyclic adenosine monophosphate
cGMP	3'-5'-cyclic guanosine monophosphate
CICR	calcium induced calcium release
CS	cell shortening
CSQ	calsequestrin
CTR	control
Cu_2(FL2E)	copper complex of 2-[4,5-bis[6-(2-ethoxy-2-oxoethoxy)-2-methylquinolin-8-ylamino]methyl]-6-hydroxy-3-oxo-3H-xanthen-9-yl}benzoic acid
DAF-FM DA	4-Amino-5-Methylamino-2',7'-Difluorofluorescein diacetate
dP/dt	rate of pressure change
E	equilibrium potential
EC50	effective concentration 50
eNOS	endothelial nitric oxide synthase
F	Faraday constant, 96,500 coulombs/mol
f_p	voltage-dependence parameter of Na^+-K^+ ATPase
FS	fractional shortening
HF	heart failure
HR	heart rate
I	current
I_{CaL}	L-type calcium current
I_f	funny current
I_{NCX}	sodium calcium exchanger current
I_p	sodium potassium ATPase current
$\overline{I_p}$	maximum Na^+-K^+ ATPase current
IP3	inositol triphosphate
Ive	ivermectin
JSR	junctional sarcoplasmic reticulum
K^+	potassium
KBR	KB-R7943, 2-[2-[4-(4-nitrobenzyloxyl)phenyl]ethyl]isothiourea
K_{m,K_o}	K^+ half-saturation constant for sodium potassium ATPase current
K_{m,Na_i}	Na^+ half-saturation constant for sodium potassium ATPase current
$K_{m,Na}$	Na^+ half-saturation constant for sodium calcium exchanger current
$K_{m,Ca}$	Ca^{2+} half-saturation constant for sodium calcium exchanger current
k_{NCX}	scaling factor of sodium calcium exchanger current
k_{sat}	saturation factor for sodium calcium exchanger current at very negative potentials
KO	knockout
LAD	left anterior descending (coronary artery)
L-NIO	L-N5-(1-iminoethyl)ornithine hydrochloride

LVEDD	left ventricular end diastolic dimension
LVESD	left ventricular end systolic dimension
LVIDs	left ventricular internal diameter at end systole
LVPW	left ventricular posterior wall
MI	myocardial infarction
Na^+	sodium
Na^+ pump	sodium potassium (Na^+-K^+) ATPase
NCX	sodium calcium exchanger
nNOS	neuronal nitric oxide synthase
NSR	nonjunctional sarcoplamic reticulum
OE	overexpression
P2X	ionotropic P2 channels
$P2X_4R$	P2X subtype 4 receptor
P2Y	metabotropic P2 G protein coupled receptors
PKG	protein kinase G, cGMP-dependent protein kinase
PLCβ	phospholipase C beta
PMCA	plasma membrane calcium ATPase
PPADS	pyridoxalphosphate-6-azophenyl-2′,4′-disulphonic acid
R	gas constant, 8.314 J/(°K×mol)
RyR	ryanodine receptor
SA	sinoatrial
SERCA	sarcoendoplasmic reticulum calcium ATPase
sGC	soluble guanylate cyclase
SNAP	S-nitroso-N-acetyl-D,L-penicillamine
SR	sarcoplasmic reticulum
T	absolute temperature in °K
TAC	transverse aortic constriction
Tg	transgenic
PH	pressure height (systolic pressure – diastolic pressure)
V	voltage
VT	ventricular tachycardiac
WO	washout
WT	wildtype
YM	YM 244769, N-(3-aminobenzyl)-6-{4-[(3-fluorobenzyl)oxyl]phenoxy} nicotinamide
σ	extracellular sodium concentration-dependence parameter of voltage-dependence parameter of Na^+-K^+ ATPase current
η	factor controlling voltage dependence of sodium calcium exchanger current

Chapter 1

Introduction[a]

The human heart is an amazingly efficient biological pump. It can adjust to a wide range of situations, providing blood flow to our bodies while we rest or exercise strenuously; and it works relentlessly, beating more than 2.5 billion times during an average lifetime. Diseases associated with this marvelous organ, however, remain the leading cause of death in the United States and are increasingly plaguing other developed and developing nations. The latest data suggest that 1 in every 4 deaths in the United States is attributable to heart disease and cardiovascular deaths represented 30% of all global deaths in 2008.[2, 3] More than half of these are due to coronary heart disease. Significant medical advances have been made in both interventional techniques and pharmacological treatments used to prevent major injuries to the heart and fatalities, but many questions remain regarding the progression of cardiac remodeling after injury. Heart failure, or the inability of the heart to pump enough blood and oxygen to support other organs in the body, affects 5.1 million people in the US and costs the nation an estimated $32 billion each year in the cost of health care services and lost productivity.[4] Treatment options, especially those that have been shown to prolong life rather than simply provide temporary symptom relief, remain limited.

In addition to treating the underlying pathology that led the heart to fail, heart failure is predominantly managed pharmacologically through the use of beta-blockers, angiotensin II receptors blockers, angiotensin converting enzyme inhibitors, diuretics, and in some cases, blood vessel dilators, aldosterone receptor antagonists, and digoxin. Inotropic therapy

[a] Part of this chapter, particular the information on summary of purinergic receptors have been published previously: Yang R, Liang BT. "Cardiac P2X4 Receptors: Targets in Ischemia and Heart Failure?" Circ Res. 111:397-401. 08/2012.

(dobutamine, milrinone) may be used in end-stage disease to make the heart pump harder, forcing the heart muscle to contract more forcefully, and often also speeding up the heart's rhythm. These therapeutics can relieve and control symptoms, but the risk of death rises if they are taken long term. Mechanical support in the form of a left ventricular assist device and ultimately heart transplant are last resort options.

Many of the aforementioned pharmacological compounds have been developed based on structural and functional insights from biologically active molecules that regulate heart function. Extracellular application of adenosine triphosphate (ATP) and its derivatives has been recognized to modify heart function for some time, with the first paper describing the effects of adenosine monophosphate (AMP) and adenosine published in 1929.[5] Since then, molecular cloning has been used to identify a number of cellular receptors that respond to these extracellular nucleotides, which are collectively referred to as purinergic receptors, and there has been a rapid expansion of the purinergic field. Within the purinergic receptor family, the ligand gated $P2X_4$ non-selective cation channel was previously identified as an important mediator of ATP's effects in the endogenous murine heart. More interestingly, when mice with cardiac specific overexpression of this receptor were subjected to different models of heart injury/failure, they had better survival and preserved heart function. With this result in mind, in this thesis, we undertake a number of studies to derive mechanistic insight into how activation of this purinergic receptor impacts cardiomyocyte electrophysiology and contraction and how its downstream signaling affects heart function. We begin with a review of the electrical activities of the heart and excitation contraction coupling that serve as the basis of cardiac function and for understanding how purinergic ion channels can impact heart function.

1.1 The cardiac action potential and its conduction

In order to maintain rhythmic contractions throughout one's life, the heart relies on an elegant electromechanically coupled system. Action potentials (APs), which coordinate contractions from muscles that pump blood to the rest of the body, are generated by defined ion fluxes through specific channels on the cardiomyocyte sarcolemma. The sinoatrial (SA) node residing in the right atrium of the heart is typically the dominant pacemaker, containing pacemaking cells capable of rhythmic spontaneous depolarizations. Their APs are distinct in that they contain an ionic flux known as the pacemaker current, or the "funny current" (I_f) (also described as Na^+ (f), Figure 1.1A). I_f passes through a channel distinct from the fast sodium channel responsible for rapid depolarization in ventricular muscle cells. Rather, the pacemaker channel is activated by hyperpolarization and is thus open during repolarization of the cell, as the membrane potential approaches its most negative values. The inward flow of Na^+ ions through the pacemaker channel then causes the membrane potential to become progressively less negative during repolarization and eventually, depolarizes the cell to its threshold voltage. The fast depolarization phase of the pacemaker cell AP is thought to rely mainly on Ca^{2+} influx, as the persistently less negative membrane voltage of pacemakers keep the fast sodium channels in these cells mainly inactivated. Repolarization relies on inactivation of the calcium channels and increased activation of potassium channels leading to K^+ efflux from cells (Figure 1.1A).

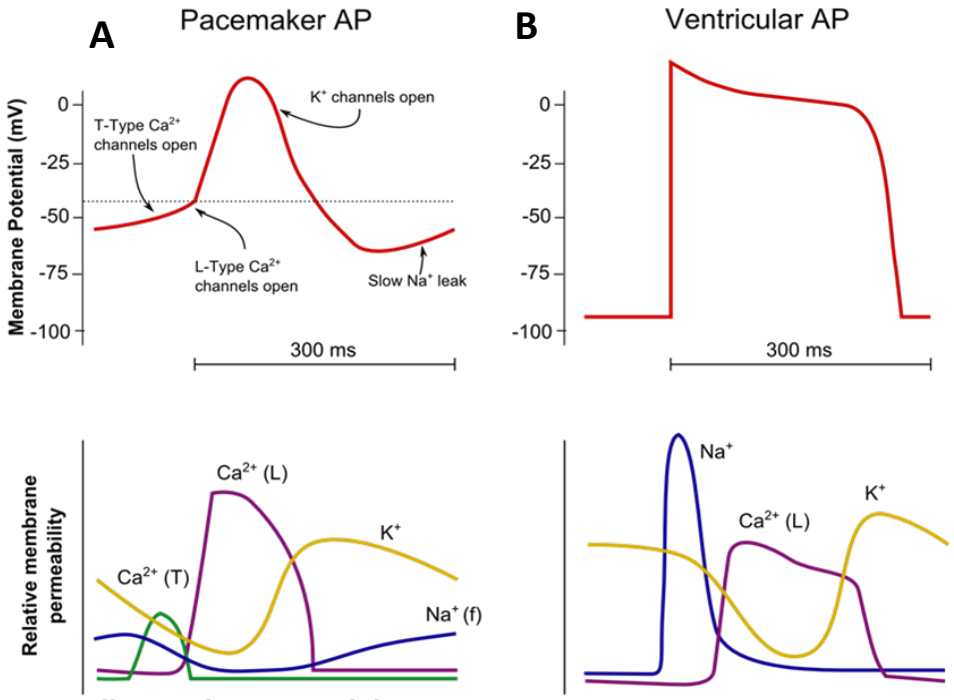

Figure 1.1 Cardiac Action Potentials
Action potentials from the SA node (A) and ventricular myocytes (B) with corresponding ion permeabilities. The funny current I_f, or Na^+ (f), gradually depolarizes SA pacemakers to reach threshold for opening of Ca^{2+} channels that are responsible for the AP upshoot. In ventricular myocytes, the membrane potential is stable until the depolarizing stimulus arrives, which leads to opening of fast Na^+ channels responsible for the rapid depolarization. Repolarization is a balance of Ca^{2+} and K^+ permeabilities. (Reproduced with permission from http://www.nataliescasebook.com/tag/cardiac-action-potentials)

During depolarization, the electrical impulse spreads rapidly between cardiac myocytes due to the presence of low-resistance connections known as gap junctions between neighboring cells. First, atrial muscle fibers propagate the impulse from the SA node to the atrioventricular (AV) node. Fibrous tissue surrounding the tricuspid and mitral valves ensures that there is no direct electrical connection between the atrial and ventricular chambers other than through the AV node. The speed of tissue depolarization and the conduction velocity along cells depend on a number of factors, including the number of sodium channels, the magnitude of the resting potential, and fiber arrangement. Specialized regions, such as Purkinje fibers, can contain more densely arranged fiber and/or tissues with a high concentration of Na^+ channels, which allow electrical impulse to spread quickly within and between cells for rapid conduction. After

traversing the AV node, the cardiac AP spreads into the rapidly conducting bundle of His and Purkinje fibers, which then distribute the electrical impulses to the bulk of the ventricular muscle cells. A visual summary is provided in Figure 1.2, which also demonstrates more detailed differences in AP among different regions of the heart.

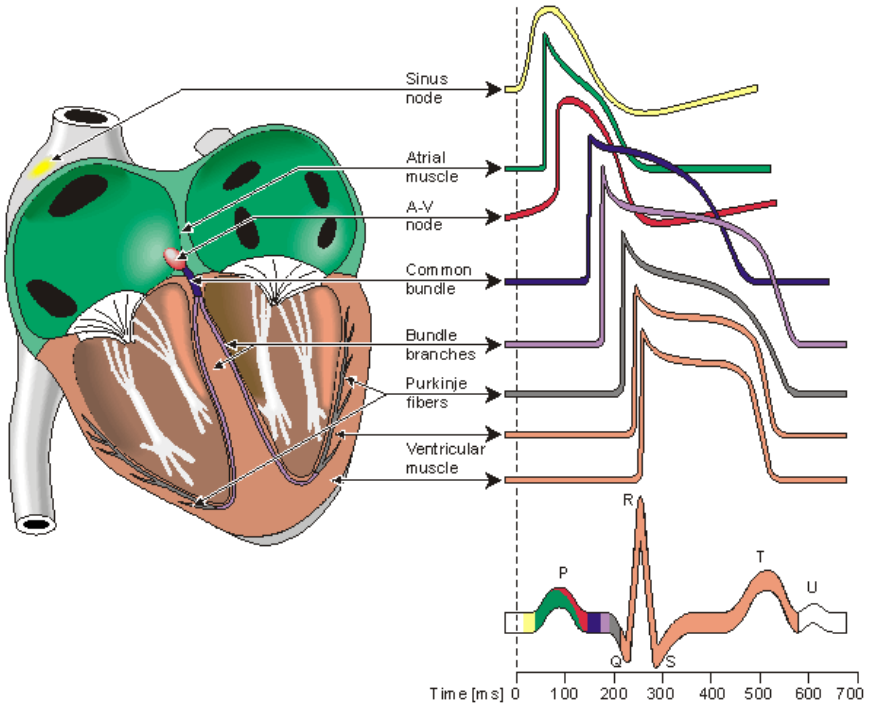

Figure 1.2 The Cardiac Conduction Pathway
The action potential is regularly initiated from the sinus node and propagated throughout the heart via specialized tracks and by cell to cell communication. The typical sequence of action potential travel and morphologies of different cell types found in each of the specialized regions of the heart are shown. The summation of these electrical signals gives rise to the electrocardiogram, which provides information about AP propagation. (Figure 6.7 from Malmivuo J and Plonsey R. “Bioelectromagnetism: Principles and Applications of Bioelectric and Biomagnetic Fields”. Reproduced with permission from Oxford University Press.)

The AP of the ventricular muscle cardiomyocytes is morphologically and ionically different than that of the pacemaker cells (Figure 1.1B). The resting potential is typically more negative than the pacemaker resting potential. When a depolarizing influence is encountered, some sodium channels can open and the entry of Na^+ ions into cells causes the transmembrane potential to become progressively less negative. When the threshold potential is reached,

enough of these fast Na^+ channels have opened to generate a self-sustaining inward Na^+ current, resulting in a prominent influx of Na^+ responsible for the rapid upstroke of the AP. The fast sodium channels then undergo rapid inactivation while transiently activated potassium channels are quickly activated by the large depolarization, which returns the membrane potential towards negative values. The plateau phase of the muscle AP is mediated by the balance of an outward K^+ current in competition with an inward Ca^{2+} current though the L-type calcium channels. These channels have a slower activation profile and remain open much longer compared with fast sodium channels. Calcium ions that enter the cell during this plateau phase are crucial in triggering additional internal calcium release from the sarcoplasmic reticulum for initiating myocyte contraction. Repolarization of the AP occurs with continued outward flow of K^+ while Ca^{2+} channels gradually inactivate.

1.2 Sarcolemmal ion channels and currents in the cardiomyocyte

As previously mentioned, Na^+ and Ca^{2+} influx are responsible for membrane depolarization and a number of K^+ channels are responsible for repolarization. The voltage gated Na^+ and K^+ channels all consist of a primary α- and multiple secondary β-subunits. The α-subunit is responsible for passing current while the β-subunits modify channel expression levels and regulate gating and channel kinetics. In contrast, the calcium channel is a combination of as many as 5 subunits, α1, α2, β, γ, and δ. A list of these currents, with their respective proteins for the primary α-subunits along with the encoding genes is included in Table 1.1. In addition to these voltage sensitive channel currents, a number of transporters act to return Na^+ and Ca^{2+} ions that enter the cell during depolarization to the extracellular environment and to bring K^+ back into the cell. Ca^{2+} ions are removed by the Na^+-Ca^{2+} exchanger (NCX) and to a lesser extent by the plasma membrane Ca^{2+} ATPase pump (PMCA), while the Na^+/K^+-ATPase pump makes the corrective exchange of Na^+ and K^+. All three of these transporters are electrogenic, capable of generating currents that influence the AP and resting potential.

Current	Description	Activation mechanism	Clone	Gene
α-subunit of inward current channels				
I_{Na}	Sodium current	Voltage, depolarization	$Na_v1.5$	SCN5A
$I_{Ca,L}$	Calcium current, L-type	Voltage, depolarization	$Ca_v1.2$	CACNA1C
$I_{Ca,T}$	Calcium current, T-type	Voltage, depolarization	$Ca_v3.1$/ $Ca_v3.2$	CACNA1G
α-subunit of outward (K^+) current channels				
$I_{to,f}$	Transient outward current, fast	Voltage, depolarization	KV4.2/4.3	KCNF2/3
$I_{to,s}$	Transient outward current, slow	Voltage, depolarization	KV1.4/1.7/3.4	KCNA4/7, KCNC4
I_{Kur}	Delayed rectifier, ultrarapid	Voltage, depolarization	KV1.5/3.1	KCNA5/KCNC1
I_{Kr}	Delayed rectifier, fast	Voltage, depolarization	HERG	KCNH2
I_{Ks}	Delayed rectifier, slow	Voltage, depolarization	KVLQT1	KCNQ1
I_{K1}	Inward rectifier	Voltage, depolarization	Kir 2.1/2.2	KCNJ2/12
Specialized Outward Current				
I_f	Pacemaker current	Voltage, hyperpolarization	HCN2/4	HCN2/4

Table 1.1 Membrane Currents that underlie the Action Potential
Modified with permission from Grant AO, "Cardiac Ion Channels". *Circulation: Arrhythmia and Electrophysiology* 2009.[6]

1.3 From Excitation to Contraction

In response to APs generated by sarcolemmal ionic currents, cardiomyocytes contract by cycling calcium between the sarcoplasmic reticulum (SR) and the cytoplasm. Activation of L-type Ca^{2+} channels results in a small influx of Ca^{2+} ions into the cell that is insufficient to cause contraction, but triggers a greater Ca^{2+} release from the SR, known as Ca^{2+} induced Ca^{2+} release (CICR). The T-tubule invaginations of the sarcolemmal membrane bring the L-type channels into close apposition with ryanodine receptors (RyRs) on the SR, which undergo a conformational change in response to the L-type channel Ca^{2+} influx to allow a much greater

release of Ca^{2+} from the SR. A single L-type calcium channel can trigger SR Ca^{2+} release only from a locally apposed cluster of RyRs, and statistical recruitment of release clusters brings about graded release,[7] in which the Ca^{2+} released from the SR is graded according to the amount of trigger Ca^{2+} entering the cell via L-type Ca^{2+} channels.[8]

The sensitivity of troponin C to Ca^{2+} is the crucial link from Ca^{2+} transients to mechanical activity. Troponin is composed of three subunits; in addition to troponin C that binds Ca^{2+}, troponin T links the troponin complex to actin and tropomyosin molecules, and troponin I inhibits the ATPase activity of the actin-myosin interaction that leads to crossbridge formation. Actin and myosin are the chief force generating molecules in contraction. Myosin molecules are arranged in thick filaments, which are tethered by titin to the z-lines of sarcomeres. Actin is arranged in thin filaments as an α-helix of two strands that interdigitate between the thick myosin filaments. Under resting conditions, tropomyosin lies in the grooves between the actin filaments and inhibits the interaction between myosin heads and actin, preventing contraction. Ca^{2+} binding to tryponin leads to conformational change in tropomyosin, exposing active sites between actin and myosin filaments, allowing crossbridge formation and for the filaments to slide across each other. As long as the cytosolic Ca^{2+} concentration remains sufficiently high to inhibit the troponin-tropomyosin blocking action of crossbridge formation between actin and myosin, progressive ATP-dependent reactions between the myosin head and actin causes the muscle fiber to shorten by increasing the overlap between the myofilaments within each sarcomere. Relaxation occurs when Ca^{2+} is removed from the cytosolic space, largely through sequestration back into the SR by the sarcoendoplasmic reticulum Ca^{2+} ATPase (SERCA) pump, while a smaller fraction is extruded into the extracellular space by the NCX and the PMCA.

1.4 Computational Models of Cardiac Electrophysiology and Contraction

The generation of the AP followed by excitation-contraction coupling is a highly dynamic process with a carefully timed sequence of events that occur on the millisecond scale. To understand these complex interactions, quantitative modeling has been utilized to analyze each process, and is exemplified by the original Hodgkin-Huxley description of the squid giant axon AP, which has been the standard for describing voltage-dependent membrane ion current dynamics for over 60 years.[9] This model introduced the concept of channel gating, and related currents through ensembles of channels to the state of these gates. The first computational model of a cardiac myocyte, the Purkinje cell, was developed based on the Hodgkin-Huxley formalism and was presented by Denis Noble in the early 1960s.[10] Early models explored mechanisms underlying the long AP duration observed in cardiac myocytes compared to neurons, which was explained as a balance between a maintained inward Na^+ current and a slowly activating outward K^+ current. Relative Na^+ and K^+ conductances could be adjusted to produce a stable resting potential or a stable oscillation that mimicked the oscillatory long duration APs of the cardiac Purkinje fiber. While we now know that the inward current during the plateau phase of the cardiac AP is primarily due to membrane Ca^{2+} permeability and that the conclusions of the earliest models were inaccurate, they were nonetheless fundamentally important in trying to achieve detailed mechanistic and quantitative understanding of the cardiomyocyte AP. Subsequent elaborations led to the development of the 1985 DiFrancesco-Noble model [11], which has become a template for pacemaking cell models. In addition to including hyperpolarization activated I_f conductance for pacemaking in the Purkinje fiber, it also incorporated time-varying concentration of ions in the cell, activities of the Na^+/K^+ ATPase and NCX, and voltage and calcium dependent inactivation of the calcium current. It also introduced components of subcellular Ca^{2+} movement, where Ca^{2+} is taken into the SR by SERCA and can diffuse from the nonjunctional SR (NSR) to the junctional SR (JSR) for CICR from the JSR. All subsequent models of the cardiomyocyte have been built based on this framework.

The first ventricular cell model based on voltage clamp recordings obtained from isolated myocytes was reported in 1991.[12] This first Luo and Rudy model based on data from guinea pig ventricular myocytes described six distinct membrane currents and substantially progressed the field, as current descriptions were carefully based on existing experimental data and model equations were fully published to enable implementation by other investigators. Their second model published in 1994 included sarcolemmal pumps and exchangers, intracellular Ca^{2+} buffers, CICR and Ca^{2+} cycling. The development of quantitative models greatly benefited from technical advances in the spatiotemporal control of single cell voltage clamping, which allowed for increasingly sophisticated experiments to generate more detailed data and even leading to single channel measurements. Concurrent with these new technical advances, subsequent models have become increasingly biophysically detailed. Markov chain models are now commonly used to describe gating behavior, and are comprised of a number of different states that loosely correspond to different conformations of channel proteins as they undergo activation and inactivation, with transition rates between certain states being voltage-dependent. The Markov property of “memorylessness” assures that the future evolution of the process state depends only on the current state and overcomes the limiting assumption of Hodgkin-Huxley that channel gates behave independently. More detailed descriptions of CICR mechanisms represent another area of advance in the modern model of the cardiac myocyte. Statistical recruitment of calcium release units underlying graded calcium release can be modeled by including a population of dyadic Ca^{2+} release units in which local interactions of individual sarcolemmal L-type calcium channels and nearby RyR are simulated stochastically[13]. As the computational resources involved in such modeling can be overwhelming, simplified local control models of CICR are often formulated by applying a carefully chosen set of approximations that allow for the ensemble behavior of Ca^{2+} release units to be represented by simple ordinary differential equations[14]. These important modeling features are included in the Bondarenko model[15] (Figure 1.3), which was parameterized to fit experimental observations

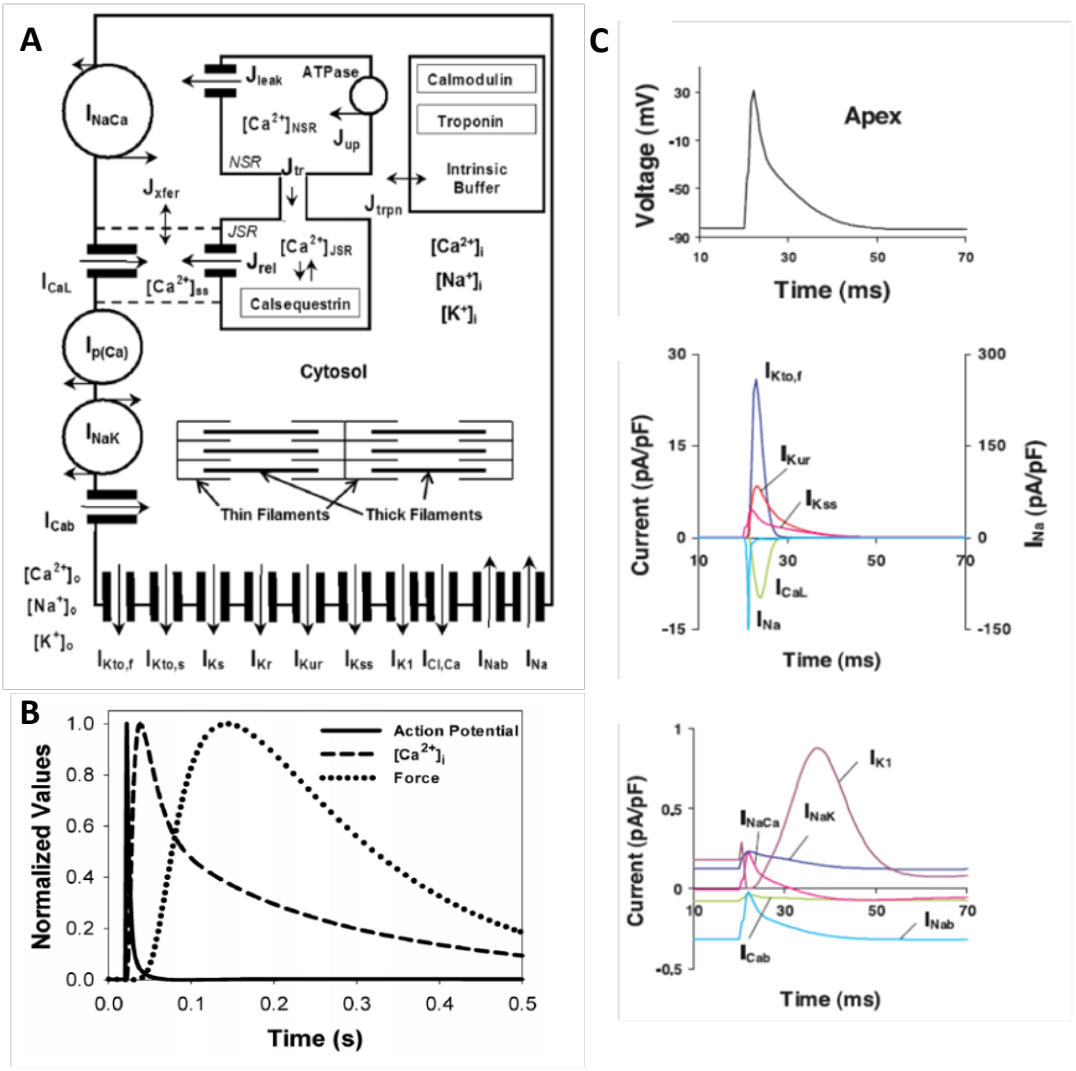

Figure 1.3 Excitation-Contraction Coupling as presented in an Integrated Cardiomyocyte Model

(A) Major membrane ionic currents that give rise to the AP are shown, with L-type calcium channel current I_{CaL} coupled to calcium release from the junctional SR. Rising cytosolic Ca2+ can bind to tryponin, leading to myofilament overlap that generates contraction. Depolarizing currents I_{Na} and I_{CaL}, repolarizing K^+ currents $I_{Kto,f}$, $I_{Kto,s}$, I_{Ks}, I_{Kr}, I_{Kur}, I_{Kss}, I_{K1}, transporter and pump currents I_{NaK}, $I_{NaCa,}$ $I_{p(Ca)}$, background currents I_{Nab}, I_{Cab}, and a calcium activated chloride current $I_{Cl,Ca}$ were included in this model of the murine ventricular myocyte. Markov descriptions of gating mechanisms were implemented for I_{Na}, $I_{Ca,L}$, and I_{Kur}. (B) Sequence of AP initiation to force generation for a representative cardiac beat. (C) Dynamics of underlying currents for a typical AP. Top panel illustrates a typical mouse AP as outputted by the computational model. Middle panel demonstrates the large currents shaping the AP, note the axis for I_{Na} is on the right. By convention, inward positive ion movement constitutes a negative current. Notice the rapid time course for I_{Na} and the balance between $I_{Ca,L}$ and outward going K^+ currents during the repolarization phase. Bottom panel shows smaller magnitude ion movements that are active both during AP firing and at rest. (Figures reproduced with permission from Bondarenko *et al,* 2004 and Mullins *et al, 2013.*[15, 16])

from murine myocytes. Since our experiments are based in mice, which are amendable to genetic modification and experimental manipulation, this mouse ventricular myocyte model serves as the basis of further computational modifications and study in this thesis as well.

1.4.1 Comparison of the Mouse vs. Human action potential

While the fundamental mechanism of excitation contraction coupling is similar in the mouse compared to the human heart, a number of differences are worth noting. In the mouse heart, the L-type Ca^{2+} current contributes less to the ventricular AP than in humans, and therefore the murine AP shows a gradual repolarization rather than a distinct plateau phase. In humans, the plateau phase ends when the balance shifts from the slowly inactivating $I_{Ca,L}$ to slowly activating potassium currents, giving rise to the final repolarization until the resting potential is restored. In human ventricular myocytes, $I_{to,f}$ is mainly involved in the first phase of repolarization and I_{Kr} and I_{Ks} are predominantly responsible for the late repolarization, whereas the much faster repolarization in murine ventricles is mediated by $I_{to,f}$, $I_{to,s}$, I_{Ks}, and a non-inactivating steady state K^+ current (I_{Kss}). The equivalent of the murine I_{Kss} has not been detected in human ventricles.[17] Ca^{2+} handling is somewhat different in mice, where up to 90% of Ca^{2+} is taken back up into the SR.[18, 19] In larger mammals, approximately 70% of Ca^{2+} is taken back into the SR and 30% is eliminated by the NCX and PMCA. Murine myocytes also have a higher cytoplasmic Na^+ concentration than larger mammals, which favors less extrusion of Ca^{2+} by the NCX, consistent with a higher fraction of SR Ca^{2+} reuptake.[20] While an increase in heart rate often leads to enhanced SR Ca^{2+} loading by decreasing the diastolic period for calcium extrusion, leading to greater contractile force at higher heart rates in larger mammals, the lower fraction of NCX-mediated Ca^{2+} extrusion in mice could explain why an increase in heart rate hardly affects SR Ca^{2+} load in mice. Combined with refractoriness of excitation contraction coupling, in which reduced fractional SR calcium release occurs at higher frequencies, a negative force-frequency relationship prevails in the mouse.[20] While important differences exist

between the mouse and larger mammals, transgenic mouse models are still a valuable tool for preclinical studies and results should be interpreted with these differences in mind.

1.5 Overview of Purinergic Receptors

Purinergic receptors were initially conceived to describe the likely existence of membrane receptors responding to ATP (P2 receptors) or its breakdown product adenosine (P1 receptors) in causing non-adrenergic, non-cholinergic relaxation of gut smooth muscle.[21] Cloning of these receptors has yielded insights into their properties and signaling mechanisms, allowing further P2 classification into sub-families of seven ionotropic (P2X) and eight metabotropic (P2Y) receptors based on structure.[22] P2X channels respond to ATP as their only endogenous ligand and are organized as homo- or hetero-trimers of two transmembrane domain subunits that form non-selective cation channels, though some channels have been demonstrated to allow passage of anions and large molecules.[23] The P2Y receptors are G-protein coupled receptors that have recently been shown to form hetero-oligomers as well.[24] In addition to endogenous ATP and ADP, P2Y receptors respond to the pyrimidines UTP and UDP. $P2Y_1$, $P2Y_2$, $P2Y_4$, and $P2Y_6$ are coupled to G_q to activate PLCβ, leading to IP_3-mediated mobilization of intracellular calcium storage, while $P2Y_{12}$, $P2Y_{13}$, and $P2Y_{14}$ couple to G_i and thus inhibit adenylyl cyclase. $P2Y_{11}$ uniquely couples to both G_q and G_s to increase calcium and cAMP (summarized in Figure 1.4).

Purinergic receptors are now associated with a number of important roles in normal and patho-physiology[25]. Adenosine has been employed extensively as a vasodilator and an anti-arrhythmic, and efforts to target each adenosine receptor subtype as novel therapies are ongoing.[26] $P2Y_{12}$ antagonists are also utilized as cardiovascular therapies[27] and pharmacological interest exists for a number of other P2 receptors for a wide range of clinical applications,[28, 29] with the P2X class most notably targeted for chronic pain treatment and

immunomodulation.[30] Here we focus our attention on P2 receptors in the heart, and more specifically on novel aspects of the $P2X_4$ receptor.

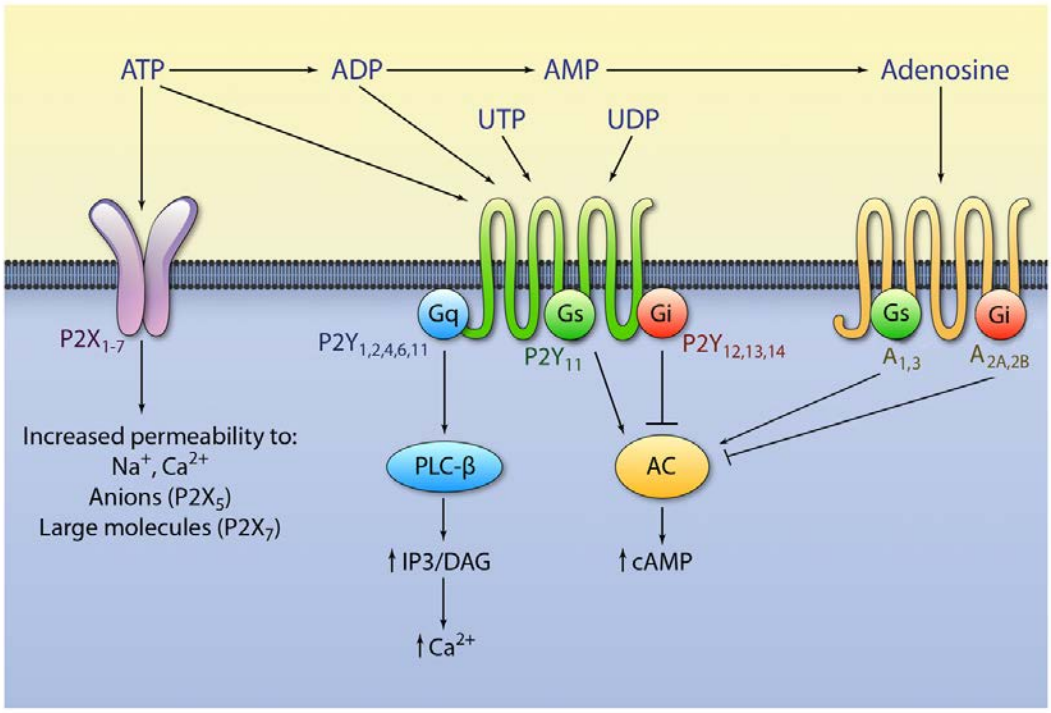

Figure 1.4 Summary of Purinergic Signaling.
Three broad categories of receptors respond to extracellular purines and pyrimidines. P2X refers to nonselective cation channels that respond to ATP, with some subtypes demonstrating the ability to pass anions and large molecules. P2Y receptors are G-protein coupled receptors that respond to endogenous ATP and ADP, as well as the pyrimidines UTP and UDP. Activation of $P2Y_1$, $P2Y_2$, $P2Y_4$, and $P2Y_6$ lead to G_q coupled PLCβ signaling, leading to IP_3-mediated mobilization of intracellular calcium storage. $P2Y_{12}$, $P2Y_{13}$, and $P2Y_{14}$ couple to G_i and thus inhibit adenylyl cyclase. $P2Y_{11}$ is uniquely coupled to both G_q and G_s and can increase calcium and cAMP. Further breakdown of ADP to AMP and adenosine can then lead to activation of adenosine receptors (also referred to as P1 receptors or A receptors), which are also G-protein couple receptors. Three subtypes have been identified, with A_1 and A_3 stimulating G_s while A_2 is coupled to G_i.

1.6 P2 receptors in the heart

Studies of ATP's effects on the heart predate the conception of purinergic receptors. While extracellular ATP concentration is typically in the nanomolar range, ischemic events can cause an increase up to hundreds of micromolars,[31] leading to the activation of the myriad of receptors described in Figure 1.4. Some of the earliest studies of extracellular ATP application were motivated by its large increase in injury/trauma,[32, 33] though it wasn't realized until later that

the cardiac muscle cells can also release ATP in response to hypoxia.[34] Many of the early identified effects on the heart have been shown to be mediated by adenosine due to the fast breakdown of ATP to adenosine by extracellular ectonucleotidases.[35] Adenosine is thought to be the main active compound responsible for the negative chronotropic, heart block, and vasodilatory effects seen with ATP administration, which is the basis for utilizing ATP bolus injections as an anti-arrhythmic to terminate supraventricular tachycardia.[36, 37] Additionally, adenine nucleotides given to isolated perfused mammalian hearts often caused a positive inotropic effect, in many cases shown to be exerted directly on the myocardium rather than through the vasodilatory effects of these compounds.[38] Increasing the phosphorylation status of adenosine (ATP> ADP> AMP) correlated well with an increasing effect on cardiac contractility, whereas adenosine itself had no direct effect on cardiac contractility,[38] suggesting P2 receptor mediated contractile enhancement. This effect has also been described in the human myocardium.[39] However, as the rate of degradation of these compounds *in vivo* is difficult to control and the large number of possible receptors lead to combinatorial complexity that is difficult to unravel, the effects of ATP on the heart and the mechanisms leading to them are still

Reference	**Species**	**Cardiac region**	**Disease**	**Receptors present**
Banfi C, *et al*. 2005	Human	LV	CHF & healthy	All at the mRNA level. Protein not confirmed for $P2X_5$ & $P2Y_2$ $P2X_6$ upregulated in CHF
Musa H, *et al.* 2009	Human	RA and SAN	Healthy	mRNA for $P2X_{4\text{-}7}$ and $P2Y_{1,2,4,6,12\text{-}14}$ P2X: $P2X_{4,7}$ most abundant P2Y: $P2Y_{1,2}$ most abundant in RA, $P2Y_{1,2,14}$ most abundant in SAN
	Rat	LV, RA, and SAN	Healthy vs. Coronary artery ligation	<u>Healthy</u> P2X: $P2X_5$ most abundant in all regions P2Y: $P2Y_{1,12,14}$ most abundant in LV $P2Y_{2,13}$ highest in RA & SAN <u>Coronary artery ligation</u> $P2X_4$ mRNA upregulated by 93% in the SAN, non-significant increase trend in the RA & LV

Table 1.2 Widespread P2 receptor expression in cardiac tissue.
Note regional and species differences. CHF= Congestive heart failure, LV = left ventricle, RA = right atrium, SAN = sinoatrial node.

debated. It is worth noting that transcripts for all P2 subtypes have been detected in the hearts of human and rodent,[40, 41] and additional changes and regulations can occur during pathological conditions (Table 1.2). Overall, a better understanding of the role of cardiac P2 receptors and their regulation in diseased hearts is likely to have implications for preventing and slowing the progression of disease.

In isolated cardiac cells, early experiments in adult rat myocytes showed that extracellular ATP evoked a transient increase in intracellular Ca^{2+} concentration in quiescent cells, and that extracellular Ca^{2+} influx was necessary for this change.[42-45] ATP stimulated the trans-sarcolemmal influx of Ca^{2+}, whereas ADP, AMP and adenosine were ineffective.[38, 45]. This was associated with an ATP-activated inward current that had a reversal potential near 0mV, suggesting the presence of ATP-gated cation channels in the cardiomyocyte, and was further accompanied by depolarization towards the threshold of AP firing in rat myocytes.[45] Under quiescent conditions, oscillatory contractions could be induced, in which the frequency but not the amplitude was regulated by the concentration of extracellular ATP.[46] Ca^{2+} release and uptake by the SR was necessary for the observed oscillations in intracellular Ca^{2+} concentration and contraction. During electrical stimulation, extracellular ATP activation of purinergic receptors was shown to both potentiate the amplitude of electrically stimulated contractions and induce spontaneous contractions.[42, 46]

The extracellular ATP induced inward current has been replicated in various species.[44, 47, 48] In adult ventricular myocytes from healthy wild type mice, P2 agonism caused an increase in a non-selective cation current.[49] An analogue of ATP with a methylthio group in place of hydrogen in position 2 of the adenine nucleobase: 2-methylthioadenosine-5'-o-triphosphate (2-meSATP), was used for its higher resistance to nucleotidase breakdown and its inability to activate P2Y receptors (thought at that time) and coronary vasodilatory (adenosine) effects [50] to limit the impact of confounding factors on the heart. The reversal potential of this current was similar to that of the cloned $P2X_4$ receptor.[47] Furthermore, the current induced by 2-meSATP

was partially insensitive to antagonism by suramin and pyridoxalphosphate-6-azophenyl-2′,4′-disulphonic acid (PPADS), which is also a characteristic of the $P2X_4$ receptor.[47, 49] The $P2X_4$ receptor, structurally similar to others in the P2X family, have EC50 for ATP similar to $P2X_{2,5,6}$, higher than $P2X_{1,3,}$ and approximately one order of magnitude lower than $P2X_7$. Its unique property of being potentiated by ivermectin also allows for its identification.

1.7 Cardiac specific manipulation of the $P2X_4$ gene in mice

A reductionist approach led to identification of the $P2X_4$ channel as a likely important endogenous component of the cardiac response to P2 agonism. To further understand the effects of this channel, a cardiac specific overexpression mouse model was created by subcloning the human $P2X_4$ cDNA into an expression vector carrying the alpha myosin heavy chain (α-MHC) promoter, which confers cardiac specific expression.[51] After sequence verification, the recombinant clone was purified and microinjected into the male pronucleus of the B6SJL/F1 mouse zygote, which was then implanted in pseudopregnant female mice. Founders and subsequent generations of transgenic mice were identified by PCR and immunoblotting for protein expression. Immunoblotting suggested an average of 20 fold overexpression over wildtype while electrophysiological data demonstrated an approximate doubling of inward current with 3μM of 2-meSATP treatment.[47]

2-meSATP induced a greater increase of contractility in cardiac myocytes isolated from these transgenic mice than in wild type myocytes,[51] further indicating that the $P2X_4$ receptor has a physiological effect in native murine myocytes and that the signal can be augmented with transgenic overexpression. Under basal control conditions, these mice with cardiac specific $P2X_4$ receptor overexpression ($P2X_4$ROE) were overtly normal without cardiac hypertrophy or failure as they age.[51] Their response to cardiac injury, however, proved more interesting. These mice were shown to be protected from a genetic model of calsequestrin (CSQ) overexpression-

induced heart failure (HF),[52, 53] in which CSQ binds to Ca^{2+} in the SR and impairs its release during cardiac cycles. The expression of the cardiac $P2X_4$ receptor was increased in the CSQ overexpressing model of hypertrophy and dilated cardiomyopathy, and the 2-meSATP-stimulated current was also greater in ventricular myocytes isolated from the CSQ mice as compared to WT mice. This indicated a possible role for the $P2X_4$ receptor in pathophysiology but also suggested a potentially compensatory mechanism, as $P2X_4$R OE/CSQ OE double transgenic mice had improved survival and cardiac function.[52] Moreover, in the more disease relevant model of left anterior descending coronary artery ligation to induce ischemia and consequent HF, the $P2X_4$R OE mice showed improved survival and better preserved cardiac function as compared to WT (Figure 1.5 and Table 1.3).[1] $P2X_4$R expression, as assessed by immunoblotting for protein, did not change in the remote non-infarcted region in post-infarct WT mouse hearts, though it has been shown to be up-regulated in the right ventricles of rats exposed to hypobaric hypoxia.[54] The downstream mechanism(s) by which this ATP-gated non-selective cation channel protects against myocardial functional deterioration is still incompletely understood, but the inotropic support offered by P2X activation may supply the needed functional enhancement during the critical period after ischemic injury.[1]

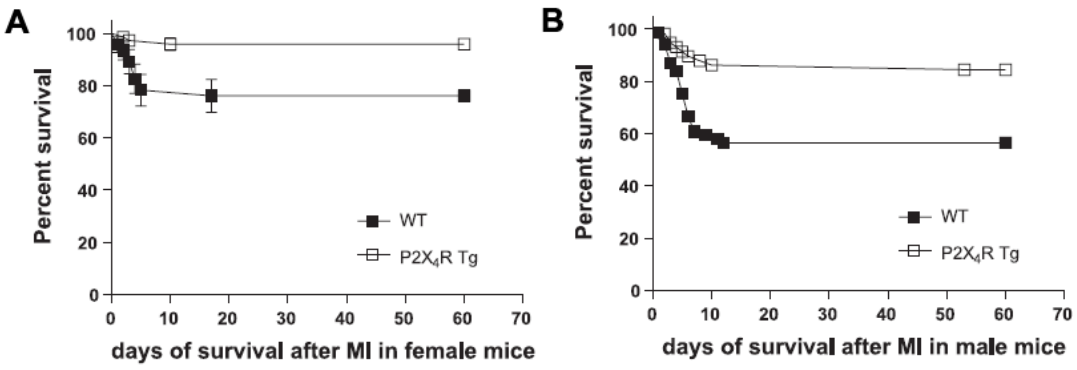

Figure 1.5 Improved Survival in $P2X_4$R overexpression mice after ischemia injury
$P2X_4$ receptor overexpression transgenic ($P2X_4$R Tg) mice demonstrated less mortality after myocardial infarction (MI) induced by left anterior descending coronary artery ligation in both (A) females and (B) males. Gender differences are consistent with known improved outcome in females. (Figure reproduced with permission from Sonin, *et al.* 2008.[1])

Table 1.3 Echocardiographic parameters in WT and $P2X_4ROE$ animals after Ischemic Injury

Females

Time After MI	*N*	FS, %	LVPW Thickening, mm	LVEDD, mm	LVESD, mm	MI Size, %
7 days						
WT	28	20.50±0.59†	0.059±0.0047†	3.87±0.0840†	3.08±0.0770†	40.4±4.02†
$P2X_4R$ OE	21	22.60±0.84*	0.079±0.0100*	3.91±0.0970†	3.05±0.0850†	38.3±3.37
1 month						
WT	19	18.80±0.59	0.053±0.0055	3.91±0.1100	3.18±0.0950	43.2±2.90
$P2X_4R$ OE	14	24.20±0.77*	0.080±0.0100*	4.19±0.1350	3.19±0.1220	40.5±3.14
2 months						
WT	22	18.49±0.56	0.040±0.0052	4.27±0.1600	3.51±0.1430	27.0±2.03
$P2X_4R$ OE	17	23.14±0.76*	0.102±0.0140*	4.39±0.1590	3.39±0.1370	30.5±3.20

Males

Time After MI	*N*	FS, %	LVPW Thickening, mm	LVEDD, mm	LVESD, mm	MI Size, %
7 days						
WT	28	17.65±0.49	0.051±0.0047	4.34±0.0870	3.53±0.10	44.8±3.67†
$P2X_4R$ Tg	21	24.50±0.95*†	0.090±0.0083*	3.98±0.1600*	3.14±0.13*	38.1±4.22
1 month						
WT	14	18.23±0.85	0.035±0.0056	4.33±0.1500	3.57±0.14	44.0±1.92
$P2X_4R$ Tg	10	22.72±1.14*	0.090±0.0160*	4.57±0.2190	3.55±0.21	42.3±1.83
2 months						
WT	23	17.15±0.88	0.053±0.0055	4.29±0.1600	3.53±0.15	31.9±1.73
$P2X_4R$ Tg	18	20.42±0.98*	0.087±0.0096*	4.62±0.2900	3.68±0.26	33.6±4.90

Values are means ± SE. At 7 days, 1 month, and 2 months after LAD ligation-induced myocardial infarction, WT and $P2X_4R$ OE mice of either sex were subjected to echocardiography evaluation of cardiac function. The various echocardiographic measurements were obtained as shown. FS=fractional shortening, LVPW=left ventricular posterior wall, LVEDD=left ventricular end diastolic dimension, LVESD=left ventricular end systolic dimension. MI size was determined by histology with Masson Trichrome staining. *$P < 0.05$ vs. WT mice at the same time point after MI. †$P < 0.05$ vs. the 2-month time point. (Table reproduced with permission from Sonin, *et al.* 2008.[1])

Further characterization of the effects of 2-mesATP in $P2X_4$ROE cardiac myocytes showed that the enhanced myocyte contractile response was not accompanied by any change in the L-type calcium channel current-voltage relationship. This observation, along with the lack of depolarization in response to 2-meSATP (re-examined in Chapter 3), indicated no Ca^{2+} influx via the L-type Ca^{2+} channel during P2X agonism.[55] However, increased SR calcium loading was seen in $P2X_4$R OE transgenic myocytes with exposure to agonist, providing a mechanism for $P2X_4$ receptor-mediated increase in contractility and suggesting that another source of Ca^{2+} may be involved. Among the P2X receptors, $P2X_4$ is one of the most Ca^{2+} permeable, though the majority of entering ions are still Na^{+}. Enhanced Na^{+} entry via overexpressed $P2X_4$ channel may act to further increase Ca^{2+} by affecting the NCX, which we further explore in the next chapter. Localized domains of Ca^{2+} increase at the plasma membrane may activate Ca^{2+}-dependent protein(s) in close vicinity of the receptor channel, after which diffusion of Ca^{2+} may reach the SR to enhance its loading.

Endothelial nitric oxide synthase (eNOS) is one possible interacting protein activated by Ca^{2+} and calmodulin. Studies on a global $P2X_4$R knockout mouse model have demonstrated that this receptor is an important mechano-transducer in endothelial cells, with $P2X_4$R knockout endothelial cells exhibiting abnormal shear responses. This was demonstrated to be due to a lack of force-induced Ca^{2+} influx and subsequent nitric oxide production.[56] This role in maintaining flow-induced vasodilation is important in physiological vascular homeostasis, as a single nucleotide polymorphism leading to decreased ATP binding was recently associated with increased pulse pressure in humans.[57] No cardiac performance observation has been mentioned about the $P2X_4$R knockouts, presumably due to a lack of significant basal phenotype change, though it would be of interest to see if exposing these animals to cardiac insult exposes a diseased phenotype. Given a possible link between $P2X_4$ receptors and eNOS, as well as the known cardioprotective effect of nitric

oxide and cGMP-dependent protein kinase (PKG),[58] it is intriguing to suspect a role for eNOS in mediating an anti-hypertrophic effect, offering protection from ischemia injury and development of heart failure in the $P2X_4R$ OE mice (Chapter 4).

1.8 Aims and Significance of this Research

By combining experiments with computational modeling, we sought to understand the effect of the $P2X_4$ channels on cardiac function in the integrated framework of excitation contraction coupling. In light of previous work on this channel, which demonstrated inotropic enhancement and protection in ischemic injury, a number of aims to assess the risks and feasibility of targeting these receptors in the treatment of cardiac disease were developed and the results are presented in the referred chapters.

AIM 1: To understand P2X impact on cardiomyocyte Na^+ handling and its possible involvement in contractile enhancement (Chapter 2)

We examine if Na^+ influx via the $P2X_4$ channel can modify activities of other important transporters in cardiac myocytes, namely the Na^+/K^+-ATPase pump and the NCX. Increased intracellular Na^+ concentration can favor the Ca^{2+} entry mode of the NCX, whereby Na^+ is pumped out in exchange for Ca^{2+} entry, thus enhancing the calcium transient and contraction. We quantify the level of intracellular Na^+ concentration change in response to purinergic activation and test whether the NCX may be involved in P2X-elicited enhancement of contraction.

AIM 2: To test cardiomocyte and whole heart excitability following P2 agonism (Chapter 3)

The flow of positive charge into the cell can induce depolarization, which in the context of a cardiomyocyte can alter AP generation and its propagation in the whole heart.

ATP has been suggested in some studies to cause spontaneous electrical activities and arrhythmias, though the mechanism is not entirely understood. We take advantage of our $P2X_4R$ overexpressing hearts to test whether cellular excitability and whole heart ectopic activity is increased with activation of these channels.

AIM 3: To examine if nitric oxide signaling is activated following P2 agonism and whether it has a role in $P2X_4R$-mediated protection (Chapter 4)

Nitric oxide signaling, particularly through eNOS, is one of the calcium dependent pathways known to be protective against injury and heart failure. $P2X_4$ receptor dependent eNOS activation has been suggested in vascular endothelial cells. We test if there is an interaction between $P2X_4R$ and eNOS in the cardiomyocyte and if this mediates $P2X_4R$ overexpression conferred cardioprotection.

The research presented here makes significant contributions to understanding how purinergic channels can affect heart function. Genetically modified animals allow us to further dissect mechanisms underlying ATP-mediated effects, which remain largely elusive due to challenges in pharmacology. We build upon findings from the cardiac specific $P2X_4R$ overexpression mouse and utilize additional genetic and pharmacological tools to derive new insight into the mechanisms that could underlie $P2X_4R$ overexpression mediated protection. Furthermore, with the computational framework of the cardiomyocyte in mind, we consider the dynamics of the P2X current in re-evaluating prior controversies in the field on ATP-induced arrhythmogenesis. Our results suggest that P2X receptors may be a viable target for cardiac treatment with transient effects on excitability.

Chapter 2

Cardiac P2X Purinergic Receptors as a New Pathway for Increasing Na^+ Entry in Cardiac Myocytes[b]

2. 1 INTRODUCTION

Intracellular Na^+ concentration and its homeostasis are important in regulating the contractile and electrical activity of the heart.[59] The sarcolemmal Na^+-K^+ ATPase (Na^+ pump) utilizes energy derived from the hydrolysis of ATP to generate an outward pump current carried by Na^+ at rest as well as during action potentials to maintain resting potential.[60] The Na^+/Ca^{2+} exchanger (NCX) is a major mechanism of Ca^{2+} extrusion in the cardiomyocyte, but through its Ca^{2+} entry mode can also extrude Na^+ from the cardiac myocytes.[61, 62] P2X receptors are ligand-gated ion channels which are permeable to Na^+, K^+ and Ca^{2+} with a reversal potential near 0 mV.[63, 64] Extracellular ATP, a P2X receptor ligand, can induce a nonselective cationic current in murine,[47] rat,[44] and guinea pig[48] cardiac ventricular myocytes. Under normal extracellular Ca^{2+} concentration (1.8mM), Ca^{2+} contributes about 8% of the total inward current induced by ATP via homotrimeric human $P2X_4R$ expressed in HEK cells.[65] However, most of the ATP-induced inward current is carried by Na^+.[47, 65] To confirm the functional importance of this Na^+ entry pathway, we examined the effects of Na^+ entry via P2X receptors on the activities of either Na^+-K^+ ATPase or NCX as each is sensitive to

[b] This chapter is adapted from a prior publication: Shen JB*, Yang R*, Pappano A, Liang BT. "Cardiac P2X purinergic receptors as a new pathway for increasing Na^+ entry in cardiac myocytes". Am J Physiol Heart Circ Physiol. 2014 Nov 15; 307 (10):H1469-77. *First 2 authors contributed equally.

J.B.S. and R.Y. performed experiments; J.B.S., R.Y., A.J.P., and B.T.L. analyzed data; R.Y. carried out mathematical simulations; J.B.S. and R.Y. prepared figures and drafted manuscript; J.B.S., R.Y., A.J.P., and B.T.L. approved final version of manuscript; R.Y., A.J.P., and B.T.L. interpreted results of experiments; A.J.P. and B.T.L. participated in conception and design of research; A.J.P. and B.T.L. edited and revised manuscript.

intracellular Na^+ changes. Myocyte contraction was also tested in the presence of Ca^{2+} entry mode NCX inhibitors, KB-R 7943 and YM-244769, to determine the role of the NCX in 2me-SATP-stimulated contraction. Studies were carried out in $P2X_4R$ overexpression cardiac ventricular myocytes to facilitate detection of an effect on Na^+-K^+ ATPase and NCX activities by P2X agonist. Current-voltage (I-V) relationships of the Na^+ pump and NCX were also simulated with mathematical modeling. Similar studies were carried out in ventricular myocytes of wild type (WT) mice to explore the physiologic relevance of this receptor in modulating Na^+ handling.

2. 2 MATERIALS AND METHODS

2.2.1 Isolation of Adult Cardiac Myocytes

$P2X_4$ receptor overexpression ($P2X_4R$ OE) mice were generated and bred as previously described.[51, 55, 66] Animals were maintained according to protocols approved by the Institutional Animal Care and Use Committee at the University of Connecticut Health Center and conform to the Guide for the Care and Use of Laboratory Animals from the United States National Institutes of Health. Cardiac ventricular myocytes were obtained from 3-month-old cardiac specific $P2X_4R$ OE or WT mice of either sex using an enzymatic dissociation procedure.[47] Briefly, the heart was rapidly excised from mice that had been adequately anesthetized using a mixture of ketamine (100 mg/kg) and xylazine (10 mg/kg). Animals were also anti-coagulated with 1000 U of intra-peritoneal heparin. The aorta was cannulated while visualized under a surgical microscope, then we perfused the heart on a Langendorff apparatus at 37°C with a calcium-free oxygenated buffer containing (in mM): 125 NaCl, 4.4 KCl, 1 $MgCl_2$, 4 HEPES, 18 $NaHCO_3$, 11 glucose, 3 2,3-butanedione monoxime, pH 7.3. After 2-3 min, the coronaries were free of blood, and the perfusion buffer was switched to the same buffer containing 0.08mg/mL Liberase Blendzyme 4 (Roche

Molecular Biochemicals) and 25μM $CaCl_2$ for 10 min. The left ventricles were minced and titurated to yield myocytes. Myocytes were then exposed ultimately to and kept at 1.0mM external $CaCl_2$ for studies. Myocytes that maintained a rod shape without blebs or blurred striation in light microscopy were studied. For contraction studies, myocytes also needed to meet the criteria of remaining quiescent without spontaneous contraction at baseline while capable of generating contractions when electrically paced. The experiments were carried out at room temperature (22 to 23°C) and were completed within 5 h after myocyte isolation.

2.2.2 Whole cell patch-clamp method

The whole cell patch-clamp technique was used for the experiments. Electrodes were prepared from borosilicate glass pipette (1.2 mm i.d.) with a two-step pulling procedure and filled with pipette solution (see below). Electrode resistances were 2–4 MΩ. The pipette was connected via an Ag-AgCl wire to the head stage of an amplifier (List EPC-7, Medical Systems, Greenvale, NY). After electrical contact was established for a few minutes, membrane capacitance was calculated from a -5 mV voltage step. Voltage commands and data acquisition were accomplished with Axon pClamp software version 9.0.

2.2.2.1 Na^+/Ca^{2+} exchange current (I_{NCX}) measurement

To measure I_{NCX}, electrodes were filled with a solution containing (mM): 135 cesium aspartate, 5 Na_2ATP, 3 $MgCl_2$, 10 HEPES, and 10 EGTA (pH 7.3 adjusted with CsOH). The outlet of the rapid solution changing device (SF-77B, Warner Instrument) was brought within 50 μm of the cell. Then the superfusion medium was changed to a modified Tyrode's solution (5.4 mM KCl was omitted and 10 mM CsCl, 10 μM nifedipine and 5 μM ouabain were added to Tyrode's solution) to block K^+ currents, L-type Ca^{2+} current (I_{CaL}) and the Na^+ pump current (I_p), respectively. The voltage protocol used to elicit I_{NCX} was as follows: from a holding potential of -80mV, a brief 10ms step to +80mV was followed by a 2 s repolarizing

ramp to -100mV. The ramp was applied to myocytes three times at one second intervals and then the superfusing fluid was rapidly changed to a solution containing 10 mM $NiCl_2$ for 10 s. At the end of the Ni^{2+} application, the same ramp protocol was applied again. Three Ni^{2+}-sensitive current traces from 60 mV to -100 mV were averaged to construct the I-V relationship of I_{NCX} under control conditions.[67, 68] Then, 3 μM 2-meSATP was added to the superfusion solution for 3-4 min while the myocyte was clamped at -80mV. The same procedures of ramp protocol and rapid solution change were applied again in the presence of 2-meSATP. The I-V relationship of I_{NCX}, taken as the Ni^{2+}-sensitive current, was compared in the absence and presence of 2-meSATP.

To measure only the Ca^{2+} entry mode of I_{NCX}, the current at +30mV was continuously recorded before and after rapid application of 10mM Ni^{2+}. During the subsequent 2-meSATP exposure, the myocyte was held at -80mV to promote Na^+ entry. After 3-4 min, the holding potential was changed to +30mV again and the Ni^{2+} was applied to block the Ca^{2+} entry mode of I_{NCX}.

2.2.2.2 Na^+-K^+ ATPase current (I_p) measurement

Myocytes were voltage-clamped with the same pipette solution as in I_{NCX} experiments. Pipette Na^+ was varied from 5-100 mM by equimolar adjustment of Cs^+ and Na^+ concentrations. After electrical contact was established and the membrane capacitance was obtained, the bath solution was then changed to a zero-K^+ Tyrode's solution to block I_p. The solution also contained 5mM $NiCl_2$ to block I_{NCX} and I_{CaL}.[69, 70] The holding potential was set to -80mV to promote the 2-meSATP-induced inward current. I_p was measured as the K^+-activated outward current elicited by rapidly changing the extracellular solution from zero-K^+ to 5.4 mM K^+-modified Tyrode's solution for 5 s. The holding potential was switched to -20mV to obtain the maximal activation of I_p. Peak I_p was selected to evaluate Na^+-K^+ATPase activity before and after 2-meSATP application, since the Na^+ changes sensed by Na^+-K^+

ATPase are more accurately reflected by peak I_p than the steady I_p.[69] The brief exposure to extracellular solution minimized the change of intracellular ion environment during 2-meSATP application. After the peak I_p was obtained at control, 3μM 2me-SATP was added to the superfusion solution for 3-4 min while the myocyte was clamped at -80mV and then the peak I_p was measured again. Peak I_p after 5 min washout was also obtained.

2.2.3 Cell shortening measurement

Cell shortening (CS) of ventricular myocytes was elicited by field stimulation at 0.5 Hz and was detected by a video edge-detector device (Crescent Electronics, Sandy, UT) as previously described.[66]

2.2.4 Data and Statistics

I_{NCX} and I_p (pA) were normalized to membrane capacitance (pF). All data are shown as mean± SEM. Student's t test for paired samples was used for statistical analysis, unless otherwise indicated.

2.2.5 Mathematical Simulation

Simulated current I-V relationships for I_{NCX} and I_p are based on previous formulations.[71] The equation for I_p is $I_p = \overline{I_p} \times f_p \times \frac{1}{1+(\frac{K_{m,Na_i}}{[Na^+]_i})^{1.5}} \times \frac{[K^+]_o}{[K^+]_o+K_{m,K_o}}$, where the last two terms describe pump dependence on $[Na^+]_i$ and $[K^+]_o$, and the f_p term defines the dependence of the pump current on voltage: $f_p = \frac{1}{1+0.1245 \times e^{-0.1\frac{VF}{RT}}+0.0365 \times \sigma \times e^{-\frac{VF}{RT}}}$. The factor σ is further defined by $\sigma=\frac{1}{7}(e^{\frac{[Na^+]_o}{67.3}} - 1)$, and shows that the voltage dependence can be further modified by extracellular Na^+ concentration. In our case, the maximum I_p current, $\overline{I_p}$, is set to 1.88 pA/pF based on the maximum calculated from our own I_p vs. $[Na^+]_i$ plot (Figure

1D), instead of the 1.5 pA/pF from the publication. All other parameter values are replicated from the original publication or given by experimental conditions: K_{m,Na_i}= 10mM, K_{m,K_o}=1.5mM, $[K^+]_o$ =5.4mM, $[Na^+]_o$=140mM, $[Na^+]_i$ is 10mM for the basal condition and set at 11.2mM to simulate effect of 2-meSATP treatment.

I_{NCX} is defined by the equation $I_{NCX} = k_{NCX} \times \frac{1}{K_{m,Na}^3+[Na^+]_o^3} \times \frac{1}{K_{m,Ca}+[Ca^{2+}]_o} \times \frac{1}{1+k_{sat}\times e^{[(\eta-1)V\frac{F}{RT}]}} \left\{ e^{(\eta V\frac{F}{RT})}[Na^+]_i^3[Ca^{2+}]_o - e^{[(\eta-1)V\frac{F}{RT}]}[Na^+]_o^3[Ca^{2+}]_i \right\}$. Keeping all appropriate concentration values, half saturation constants,[c] and the original values for η and k_{sat} (which are the voltage dependence and negative potential saturation factors for I_{NCX} respectively), an overall scaling factor k_{NCX} was estimated to fit our I_{NCX} data using a least squares fitting method in Excel.

2.2.6 Materials

KB-R7943, 2-[2-[4-(4-nitrobenzyloxyl)phenyl]ethyl]isothiourea, and 2me-SATP, 2 methylthio-ATP, were obtained from Sigma Aldrich, Corp (St. Louis, MO, U.S.A). YM-244769, N-(3-aminobenzyl)-6-{4-[(3-fluorobenzyl)oxyl]phenoxy} nicotinamide, was obtained from Tocris Bioscience (Bristol, United Kingdom).

---

[c] **Glossary of Equation Terms and Values**

F	Faraday constant, 96,500 coulombs/mol
f_p	voltage-dependence parameter of I_p
σ	$[Na^+]_o$-dependence parameter of f_p
η	Factor controlling voltage dependence of I_{NCX}, 0.35
k_{sat}	Saturation factor for I_{NCX} at very negative potentials, 0.1
$\bar{I}_p$	Maximum Na^+-K^+ ATPase current
K_{m,K_o}	K^+ half-saturation constant for I_p, 1.5mM
K_{m,Na_i}	Na^+ half-saturation constant for I_p, 10mM
$K_{m,Na}$	Na^+ half-saturation constant for I_{NCX}, 87.5mM
$K_{m,Ca}$	Ca^{2+} half-saturation constant for I_{NCX}, 1.38mM
k_{NCX}	Scaling factor of I_{NCX}
R	gas constant, 8.314 J/(°K×mol)
T	absolute temperature, °K

2. 3 RESULTS

2.3.1 Agonist activation of P2X$_4$R increased peak I$_p$

Na^+-K^+ ATPase activity was measured in $P2X_4R$ OE ventricular myocytes using the protocol described in Figure 1A. Thus, 3 µM 2-meSATP induced an inward current (1.4 ±0.36 pA/pF) in 11 of 17 $P2X_4R$ OE myocytes (from 9 $P2X_4R$ OE mice) confirming our previous results.[47] In these myocytes, the effect of P2X agonist on I_p was determined with 10 mM pipette [Na^+] (Figure 1B). In response to 3 µM 2-meSATP, I_p peak increased to 0.58±0.03 pA/pF from a

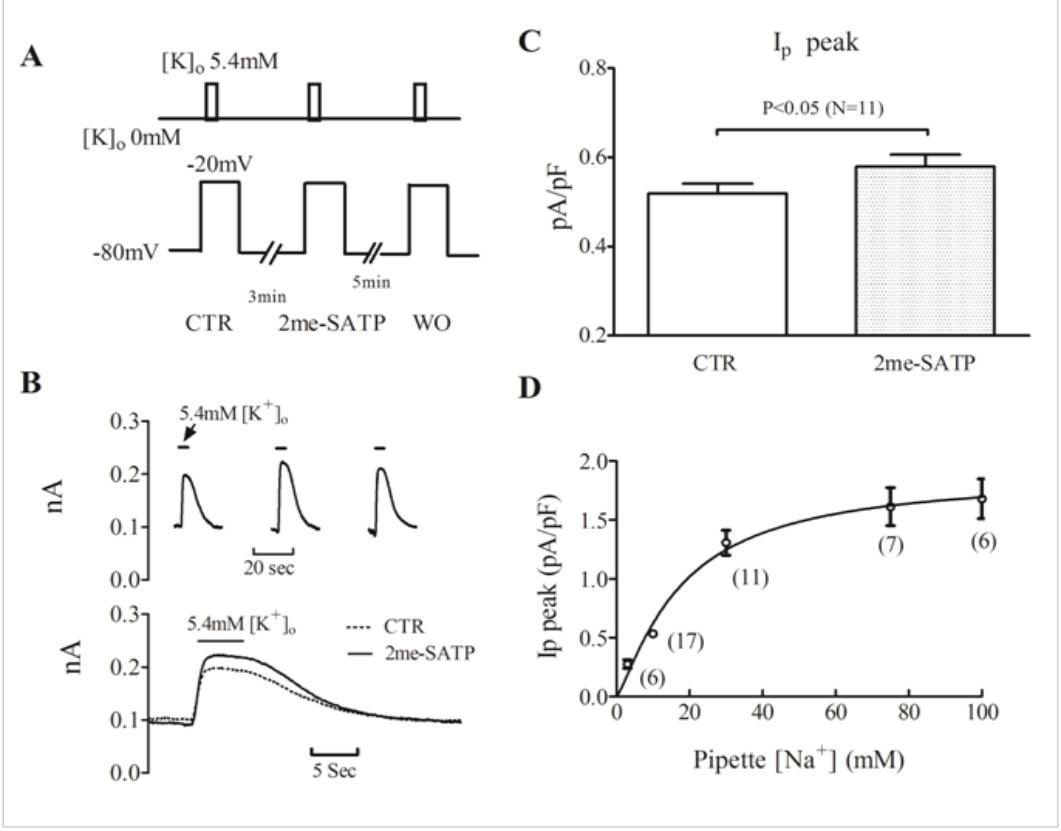

Figure 2.1 Peak Na^+-K^+ ATPase current increases after 2-meSATP application in $P2X_4$ receptor-overexpressing cardiac myocyte. (A) Upper panel shows rapid solution change protocol with 5.4mM $[K^+]_o$ to elicit K^+-activated I_p; lower panel is membrane voltage. I_p is recorded at -20mV and 2me-SATP was applied at -80mV. CTR: control; WO: washout. (B) upper panel: individual traces in a typical myocyte showing the increase of $[K^+]_o$ -activated I_p after 2me-SATP application; lower panel: superimposed traces of I_p in control and in 2me-SATP. (C) Peak I_p, normalized by cell capacitance, is presented as mean±SEM. The average control peak I_p differed from that with 2me-SATP. (D) Relationship between peak I_p and pipette [Na^+]. Peak I_p was elicited by switching $[K^+]_o$ from 0 to 5.4mM at -20mV; pipette Na^+ was varied as shown. Normalized peak I_p is presented as mean±SEM. The number of cells is indicated in the parentheses (from 18 $P2X_4R$ OE mice).

baseline value of 0.52 ±0.02 pA/pF ($P<0.05$, Figure 1C), consistent with increased K^+-activated Na^+ pump activity. We next estimated the increase in intracellular Na^+ that could result from the P2X agonist-mediated increase in I_p. To do this, stepwise increments of pipette $[Na^+]$ were made and increases in I_p determined (Figure 1D). The data describing the relationship between pipette $[Na^+]$ and I_p were fitted by the Hill equation where $I=I_{max} * [Na^+]_p^h/(K_d^h + [Na^+]_p^h)$ and $[Na^+]_p$ is Na^+ concentration in the pipette. The K_d value for $[Na^+]$ from the equation was 17.6mM, similar to the value obtained by others.[69] Accordingly, back calculating from this equation, the 0.06±0.01 pA/pF net increase in peak I_p would correspond to a 1.08±0.27mM increase of intracellular Na^+ during agonist application.

2.3.2 P2X agonist enhances Ca^{2+} entry mode of I_{NCX}

The NCX current is known to be Ni^{2+}-sensitive,[61] and was isolated in this manner after taking measures to block other large currents of the cell. After recording the baseline Ni^{2+}-sensitive current, 3μM 2me-SATP was applied to myocytes held at -80mV for 3-4 min. An inward current was observed in 10 of 15 $P2X_4R$ OE myocytes (1.3±0.41pA/pF, from 8 P2X4 OE mice, Figure 2A). These 10 myocytes were further tested for an effect of the P2X agonist on I_{NCX} by rapidly adding 10mM $NiCl_2$ to calculate the Ni^{2+}-sensitive current in the presence of 2me-SATP. Data in Figure 2 B and C show that 2-meSATP caused an increase in Ni^{2+}-sensitive current at positive potentials (0.55±0.09 pA/pF at control vs 0.82±0.14pA/pF with 2-meSATP at 50mV, $P<0.05$). The P2X agonist had minimal effect on I_{NCX} at the negative potentials (-0.46±0.06 pA/pF at control vs -0.45±0.05pA/pF with 2-meSATP at -80mV). These data indicate that 2-meSATP caused an increase of I_{NCX}, notably in its Ca^{2+} entry mode, helping extrude Na^+ in exchange for Ca^{2+}.

From the I-V relationships of Ni^{2+} -sensitive currents, the reversal potential of I_{NCX} shifted from -14±2.3mV under control condition to -25±4.1mV in response to 2-meSATP in

these myocytes. We next calculated the change of intracellular Na^+ that would cause such a shift of the I_{NCX} reversal potential from the following equations.

$$E_{Na-Ca} = 3*E_{Na}-2*E_{Ca}$$

$$E_{Na}= (RT/F)^{*}\ln[Na^+]_o/[Na^+]_i$$

$$E_{Ca}=(RT/2F)*\ln[Ca^{2+}]_o/[Ca^{2+}]_i$$

In the calculation, the intracellular resting Ca^{2+} was artificially kept at 100 nM. With a negative shift of approximately 11±3.52 mV in the reversal potential of I_{NCX} after 2-meSATP, intracellular Na^+ sensed by the NCX would need to increase by 1.28±0.42 mM, provided that $[Na^+]i$ before agonist treatment was 10mM as was provided in the pipette solution. If the resting Ca^{2+} were presumed to be 50 nM, the intracellular Na^+ sensed by the NCX would still increase by 1.0±0.34 mM. The subsarcolemmal $[Ca^{2+}]_i$ is difficult to estimate even if there is 10 mM EGTA in the pipette solution. This is due to the fact that EGTA is relatively ineffective in buffering Ca^{2+} within 20-100 nm of the pore [72]. Under the physiological condition of a living cardiac myocyte, 2-meSATP may cause an increase, even small, of intracellular Ca^{2+} level *via* a direct calcium entry through the $P2X_4R$. Under this circumstance, the estimated 1.28±0.42 mM increase of Na^+ in the subsarcolemmal space might be under-estimated. Overall, while we could not be certain of the exact subsarcolemmal Ca^{2+} level, whatever the presumed level of Ca^{2+}, $[Na^+]_i$ would have to increase to cause the observed shift of NCX reversal potential. The fact that this estimate from NCX measurements is remarkably similar to that obtained from Ip measurements provides additional confidence in the value obtained.

To verify that 2-meSATP increases Ca^{2+} entry mode I_{NCX}, the Ni^{2+}-sensitive current was measured at a holding potential of +30mV without running the ramp protocol before and after 3 μM 2me-SATP application (Figure 2D). At 30 mV, the Ni^{2+}-sensitive current increased from 0.28±0.04pA/pF in control condition to 0.48±0.06pA/pF ($P<0.05$) after 2me-SATP (Figure 2E). Thus, by either voltage ramp or step, P2X agonist elicited an increase in Ca^{2+} entry mode I_{NCX}.

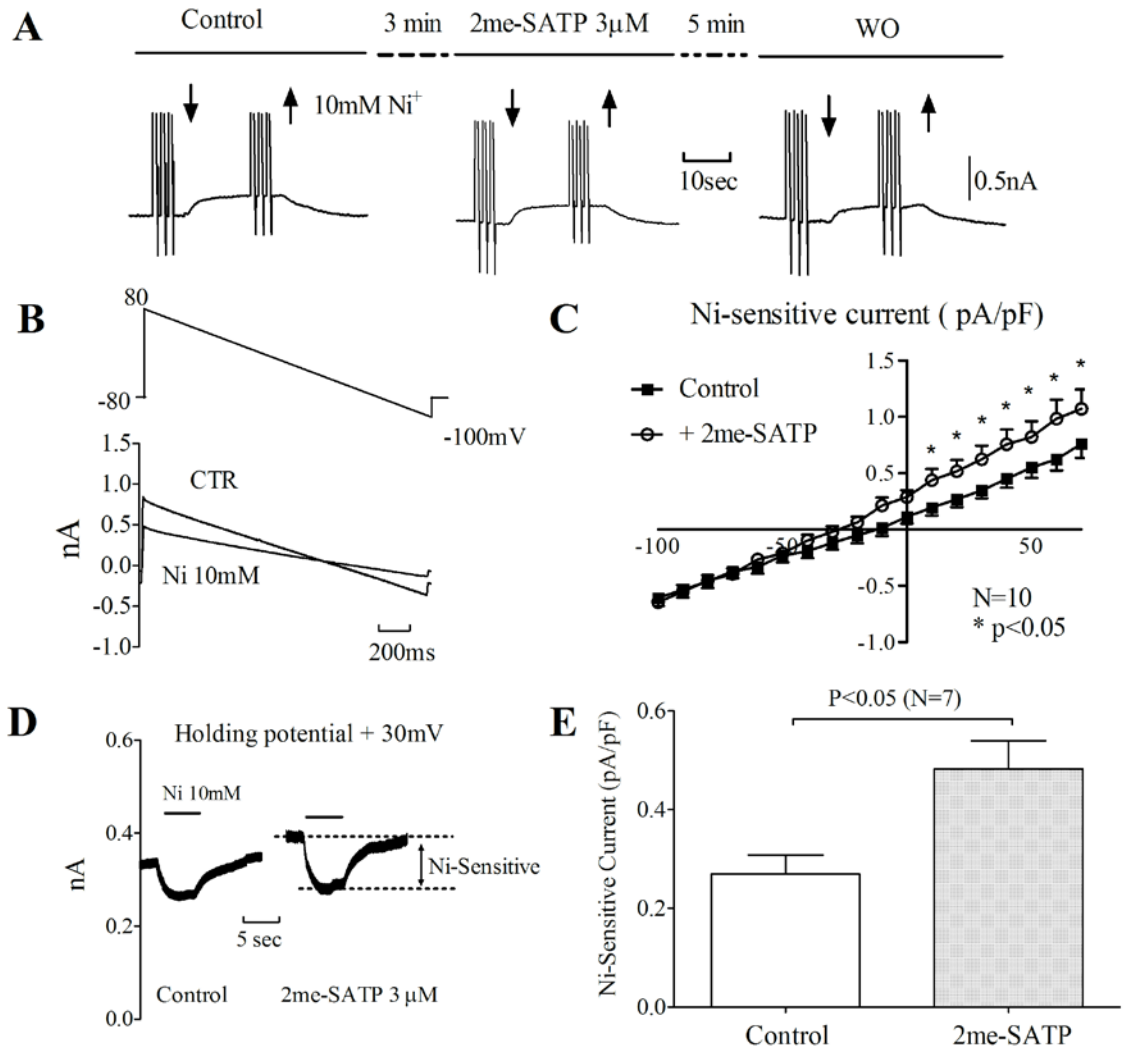

Figure 2.2 Calcium entry mode of Na^+-Ca^{2+} exchanger is increased with 2-meSATP. I_{NCX}, represented by Ni^{2+}-sensitive current, in $P2X_4R$ OE ventricular myocytes was determined. (A) Representive trace is shown for membrane current when 10mM Ni^{2+} was applied (time period bracketed by down and up arrows) under control conditions, during 2me-SATP application and after washout (WO). (B) Upper panel: descending voltage ramps from 80mV to -100mV were used to contruct the I-V relationship. Lower panel: typical traces of membrane currents are shown in control (CTR) and in the presence of Ni^{2+}. (C) Mean I-V relationships of the Ni^{2+}-sensitive current in control (filled squares) and in the presence of 2me-SATP (open circles). *P<0.05, N=10 from 8 $P2X_4R$ OE mice. (D) 2me-SATP increases Ca^{2+} entry mode I_{NCX}**.** Representative traces were shown for the Ni^{2+} -sensitive currents at +30mV before and after 2me-SATP application in a $P2X_4R$ OE myocyte. E: Plot of Ni^{2+}-sensitive current at +30mV at control and during 2me-SATP application (P<0.05 N=7 cells from 5 $P2X_4R$ OE mice)

2.3.3 Simulated I-V relationships

The experimental data indicate that elevation of $[Na^+]_i$ by $P2X_4R$ activation results in an increase of I_p and of I_{NCX}. We asked whether a simulated rise in $[Na^+]_i$ of the same magnitude can cause an increase of I_p and I_{NCX} like that observed experimentally in $P2X_4R$ overexpressing myocytes. In simulations (see Methods), when the cellular Na^+ was increased by 1.2 mM, a magnitude similar to that estimated by the experimentally measured stimulation of I_{NCX} or I_p by 2-me-SATP, the predicted I-V relationship of I_p matched closely the experimentally observed increase in I_p (Figure 3A). Similarly, the computationally derived I-V relationship of I_{NCX} agreed well with our experimental results (Figure 3B). Thus, based on established mathematical models for NCX and Na^+ pump,[71] the increase in $[Na^+]_i$ and its corresponding stimulation of I_{NCX} and I_p agreed well with our experimental results.

We modified the scaling factor from 1.5 pA/pF in the original equation for I_p model[71] to our experimentally measured maximum I_p current at 1.88 pA/pF. In the computerized model, I_p is outwardly directed over the entire test potential range (-80 to +50 mV) and is increased following a 1.2 mM increment of intracellular Na^+ (Figure 3A). At -20 mV, the predicted increase in I_p, 0.04 pA/pF, is similar to the experimentally determined increase of 0.06±0.01 pA/pF following stimulation by 2me-SATP.

In the modeling of I_{NCX}, the best fit for our experimental I_{NCX} data led us to use a k_{NCX} of 2606.64 pA/pF instead of 2000 pA/pF used by others.[71] The modeled I-V relationship of NCX shifted leftward upon the 1.2mM step increase of intracellular Na^+ from 10 mM to 11.2 mM. This leftward shift was not a parallel change since the primary effect was an increase in Ca^{2+} entry mode of I_{NCX} with little if any change of the Ca^{2+} exit mode. The computationally simulated shift of the I-V curve for I_{NCX} was similar to the experimentally observed shift by 2-meSATP (Figure 3B). At +50 mV, the modeled Ca^{2+} entry mode increased from 0.60 pA/pF at 10mM $[Na^+]_i$ to 0.86 pA/pF at 11.2mM $[Na^+]_i$ (0.26 pA/pF net increase). This modeled increase agrees well with that observed experimentally (0.27±0.10 pA/pF net increase,

Figure 2C). Overall, an elevated intracellular Na^+ level has a more detectable effect on the Ca^{2+} entry rather than the Ca^{2+} exit mode of I_{NCX}.

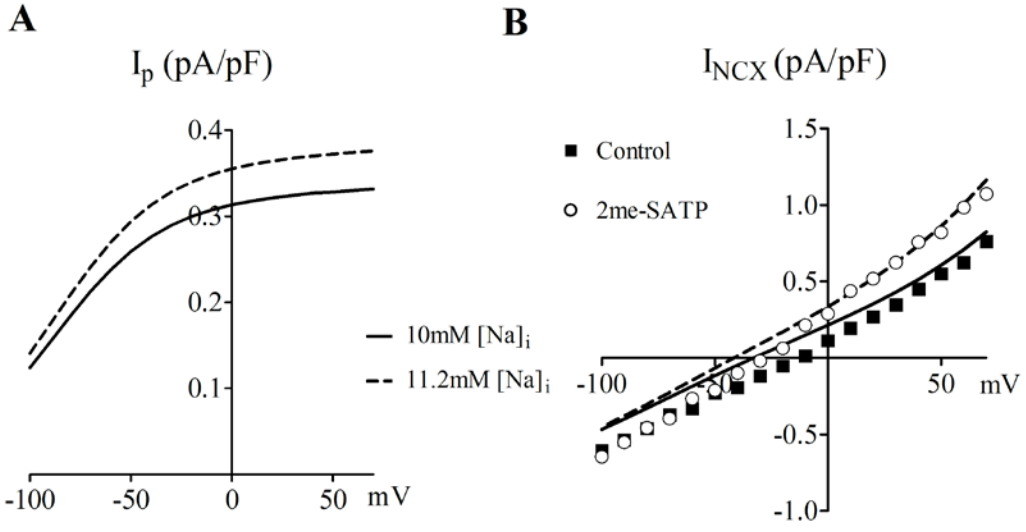

Figure 2.3 Simulated I-V relationships with intracellular [Na^+] change. (A) Simulation for I_p with $[Na^+]_i$ taken as cellular (pipette) Na^+ of 10 mM (solid line) and 11.2 mM (dotted). (B) Simulation for I_{NCX} with $[Ca^{2+}]_i$ kept constant at 100nM for cellular Na^+ of 10 mM (solid line) and 11.2 mM (dotted). The actual experimental data under control (solid squares) and after 2me-SATP application (open circles) were also plotted for comparison to the simulation.

2.3.4 KB-R7943 or YM 244769 inhibits 2me-SATP-induced increase of cell shortening

Extracellular 2-meSATP increases CS in $P2X_4R$ OE cardiac myocytes.[51] To explore if the Ca^{2+} entry mode of NCX contributes to the increase of CS by 2-meSATP in $P2X_4R$ OE cardiac myocytes, KB-R7943 and a structurally different NCX inhibitor YM 244769,[73] which preferentially oppose the Ca^{2+} entry mode, were tested in $P2X_4R$ OE myocytes. KB-R7943 at 5 µM or YM-244769 at 0.1 µM did not alter the basal cell shortenings of the $P2X_4R$ OE myocytes (total of 19 myocytes from 7 $P2X_4R$ OE mice, Figure 4B), similar to previous observation.[74] It was shown that while NCX-mediated Ca^{2+} influx could be blunted with 5µM KB-R794, baseline contraction remained unaffected.[74] Superfusion with 3 µM 2me-SATP increased CS by 29.2±3.7% above basal in 16 of 23 $P2X_4R$ OE cardiac myocytes paced at 0.5 Hz ($P<0.05$, from 10 $P2X_4R$ OE mice). When 5 µM KB-R7943 was added in the

continued presence of 2me-SATP, the increase of CS was reduced to 13.8±3.9% above basal (P<0.05, Figure 4A and 4C). In another set of similar experiments, we tested the effect on 2-me-SATP-stimulated CS by YM-244769. In these studies, 3 μM 2me-SATP increased CS by 31.4±7.1% in 10 of 15 $P2X_4R$ OE cardiac myocytes paced at 0.5 Hz (P<0.05, from 6 $P2X_4R$ OE mice). At 0.1 μM, YM-244769 reduced the 3 μM 2me-SATP-stimulated CS to 17.3±7.4% above basal (P<0.05, Figure 4D). Thus, either KB-R7943 or YM-244769 could inhibit the 2me-SATP-induced increase of CS, indicating a role of NCX Ca^{2+} entry mode in

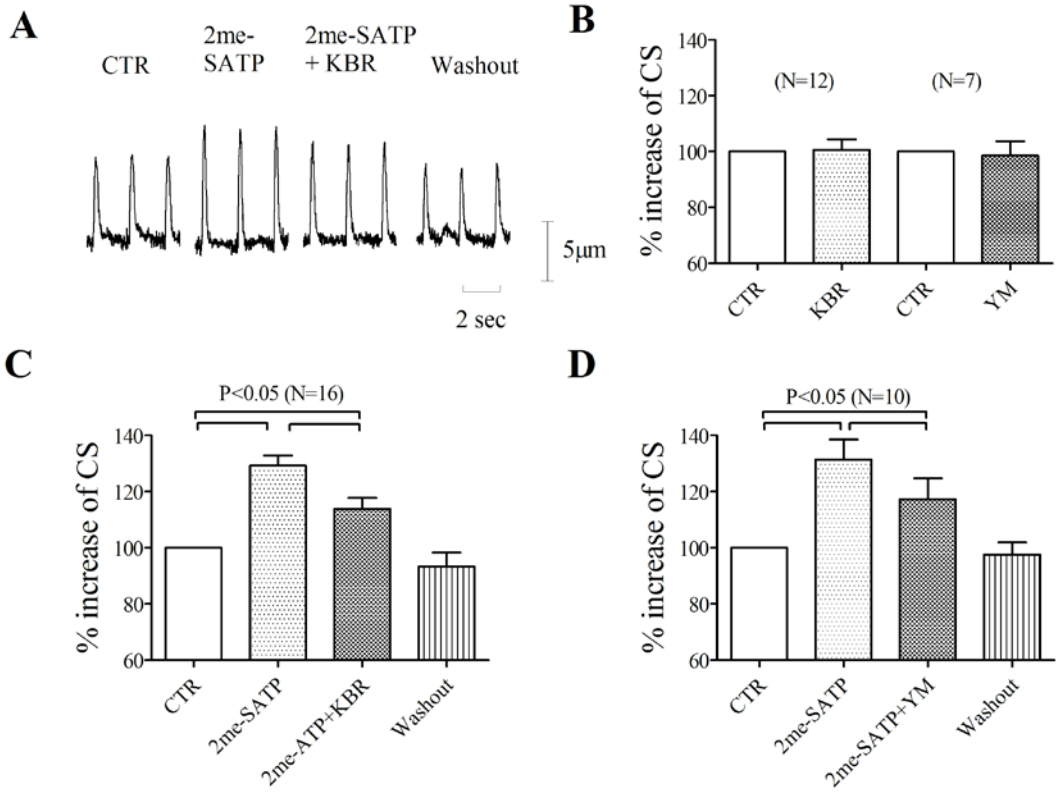

Figure 2.4 Preferential calcium entry mode blockers of the Na^+-Ca^{2+} exchanger inhibits 2me-SATP-induced increase of cell shortening. (A) Representative traces of cell shortening (CS) in $P2X_4R$ OE myocytes paced at 0.5 Hz are shown for cells exposed to 2me-SATP and then to 2me-SATP plus KB-R7943 (KBR), followed by washout. (B) Basal CS did not change after application of KB-R7943 (N=12) or YM-244769 (N=7). (C) Percent increases of CS above basal during application of 2me-SATP alone (N=16 cells, 10 $P2X_4R$ OE mice) was blunted during addition of KB-R7943 plus 2me-SATP. (D) Percent increases of CS above basal during application of 2me-SATP alone (N=10 cells, 6 $P2X_4R$ OE mice) was higher than that during exposure of YM-244769 (YM) plus 2me-SATP. P<0.05 for all bar indicated pair comparisons in panels C & D.

mediating the P2X agonist effect on myocyte contractility in these $P2X_4R$ OE myocytes.

2.3.5 P2X agonist can stimulate I_{NCX} in WT ventricular myocytes

To explore the physiologic relevance of this receptor in modulating Na^+ handling, the effect of P2X agonist on I_{NCX} and myocyte contraction were tested in cardiac ventricular myocytes from WT mice. Application of 10 μM 2me-SATP induced an inward current at -80mV (0.68±0.26pA/pF) in 8 of 34 WT ventricular myocytes (from 7 WT mice), similar to our previous findings.[47] These P2X agonist-responsive myocytes were then tested for changes in I_{NCX}. 2me-SATP increased Ni^{2+}-sensitive current at positive potentials (0.46±0.05 pA/pF at baseline vs 0.59±0.06pA/pF with 2me-SATP at +50mV, $P<0.05$, Figure 5A). There was no significant change induced by 2me-SATP in Ni^{2+}-sensitive current at negative potentials (-0.40±0.09 pA/pF at control vs -0.42±0.09pA/pF with agonist at -80mV, $P>0.05$). The primary effect on the Ca^{2+} entry but not the exit mode of NCX in WT myocytes is essentially the same as that found in myocytes from $P2X_4R$ OE hearts. The reversal potential of I_{NCX} shifted from -13.25 ±1.72 mV to -17.5±1.29 mV in response to 2me-SATP ($P<0.05$). These data demonstrate that P2X agonist can also elicit an increase in NCX Ca^{2+} entry mode in some WT myocytes.

As further evidence for a physiological role of cardiac $P2X_4$ receptors, the effect of KB-R7943 on the P2X agonist-induced increase of CS was tested in WT murine cardiac myocytes. In WT myocytes, P2X agonist has little or no effect on basal contraction. To facilitate detection of an agonist-stimulated effect on CS in WT myocytes, 3 μM ivermectin, which selectively potentiates the $P2X_4$ effect,[63] was combined with 10 μM 2me-SATP. The combined presence of 2me-SATP and ivermectin increased CS by 14.8±3.1% above basal in 8 of 32 WT paced at 0.5 Hz ($P<0.05$, from 7 WT mice). Adding 5 μM KB-R7943 to 2me-SATP plus ivermectin reduced the CS to 7.2±2.3% above basal (Figure 5B, $P<0.05$), similar to the response elicited by KB-R7943 in the $P2X_4R$ OE myocytes. The data support a role of

Ca^{2+} entry NCX mode in mediating the $P2X_4$ receptor-induced increase of CS in WT myocytes.

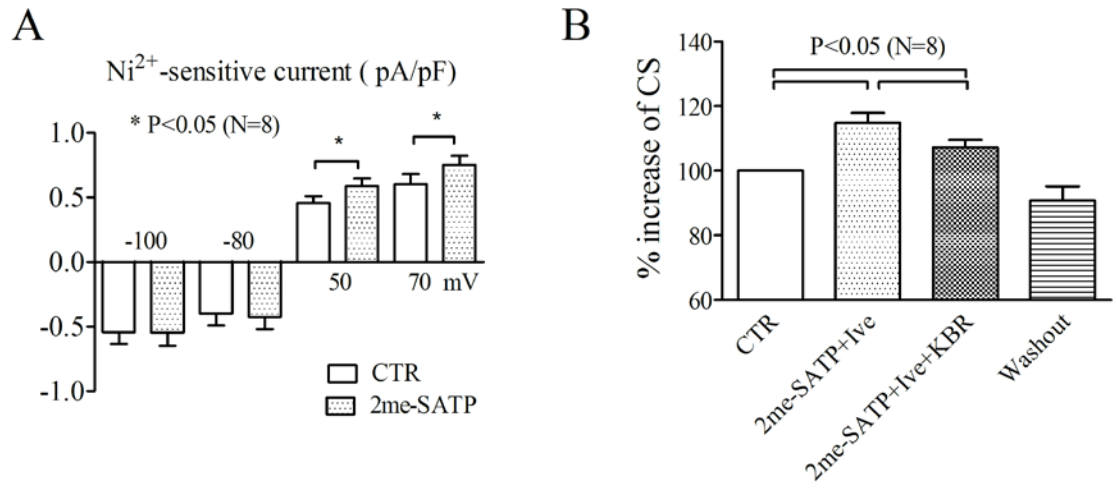

Figure 2.5 The link between P2X receptors and NCX in WT myocytes. (A) 2me-SATP-induced increase of I_{NCX} in WT myocytes. Ni^{2+}-sensitive currents before and after 2me-SATP application are presented at membrane potentials of -100, -80 , 50 and 70mV. I_{NCX} at +50 mV and +70mV were significantly larger in the presence of 2me-SATP than in control (*P<0.05, N=8 cells, 7 WT mice). (B) Percent increases of CS above basal were shown during application of 2me-SATP plus ivermectin (Ive) (N=8 cells, 7 WT mice) and during the subsequent exposure of KB-R7943 (KBR) plus 2me-SATP and Ive (% above basal with KBR plus 2me-SATP and Ive *vs* that by 2me-SATP plus Ive, P<0.05).

2.4 DISCUSSION

Belonging to a family of ligand-gated ion channels, $P2X_4$ receptors are an important subtype of the endogenous P2X receptor channel in the cardiac myocyte. When activated by extracellular ATP, these channels conduct cations in a voltage-dependent manner with a reversal potential near 0 mV.[63, 64] As a Na^+ entry pathway, these channels may have a physiological role in regulating cellular Na^+ levels in cardiac myocytes. The objective here was to test the hypothesis that activation of these channels by extracellular ATP causes an increased cellular Na^+ level in cardiac myocytes. We further determined whether the P2X receptor-induced stimulation of NCX has a role in modulating the contractile state of cardiac myocytes.

In the present study, we used myocytes from both $P2X_4R$ OE and WT mice to test these concepts, which are supported by the following lines of evidence. First, the P2X receptor-mediated increase in Na^+ entry into the myocyte[47] should stimulate I_p because the pump functions to extrude intracellular Na^+. Indeed, activation of the $P2X_4R$ by its agonist 2-meSATP was able to increase I_p in $P2X_4R$ OE cardiac myocytes. Second, P2X agonist should stimulate I_{NCX}, another cellular mechanism for Na^+ extrusion. We found that in both WT and $P2X_4R$ OE cardiac myocytes, 2-meSATP could stimulate the Ca^{2+} entry mode of NCX. Third, an increase in $[Na^+]_i$ due to P2X receptor-mediated Na^+ entry can be estimated in $P2X_4R$ OE myocytes. For I_p, which was only measured in $P2X_4R$ OE myocytes, the magnitude of $[Na^+]_i$ increase, 1.08±0.27 mM, was calculated based on responses calibrated to concentration changes in pipette and hence in cytosolic Na^+. For I_{NCX}, the receptor-mediated shift of reversal potential yielded a 1.28±0.42 mM Na^+ increase, assuming a constant intracellular $[Ca^{2+}]$. These data provided experimental evidence under voltage clamp condition that stimulation of P2X receptors can result in measurable cellular Na^+ increases. Fourth, computational modeling, assuming an increment of $[Na^+]_i$ like that observed experimentally, replicated the experimental findings and permitted estimation of the pattern and magnitude of increases in I_p and I_{NCX}. The simulated effects on I_p and I_{NCX} from the increase in $[Na^+]_i$ were similar to previously established dependencies of these currents on ionic concentrations and voltage. Experimentally, the activation of the $P2X_4$ channel primarily increased the Ca^{2+} entry mode of NCX. Computationally simulated I_{NCX} I-V relationship in response to a similarly increased cellular $[Na^+]$ also showed an increase in only the Ca^{2+} entry mode. There was minimal effect on Ca^{2+} exit mode of NCX in the simulation. Overall, the computer simulation agreed with experimental data regarding the cellular ionic effects on I_p and I_{NCX}. P2X agonist also induced a similar pattern of increase in Ca^{2+} entry mode of NCX in cardiac ventricular myocytes of WT animals, supporting a physiological role of the cardiac P2X receptor in regulating Na^+ handling.

We attempted to measure directly the $[Na^+]_i$ in $P2X_4R$ OE myocytes using the fluorescent Na^+ indicator SBFI. We could not detect any change in the intracellular Na^+ concentration after 2me-SATP application in $P2X_4R$ myocytes (data not shown). This is not surprising given that the amount of cellular Na^+ increase is below the sensitivity of this Na^+-sensitive dye, the K_d of which is 3.8mM in the absence of K^+ and 11.3 mM in the presence of physiological concentrations of K^+ (Molecular Probe website). Swift et al observed that a low concentration of ouabain (0.3 μM) increased contractility by 40% via its selective inhibition of the α_2-isoform of Na^+ pump but they could not detect an increase in global $[Na^+]_i$ by SBFI in rat cardiac myocytes.[75] They concluded that the increased contractility in response to 0.3 μM ouabain could not be explained by a substantial global rise in $[Na^+]_i$. Similar to our finding of a P2X agonist-induced stimulation of NCX, a local accumulation of $[Na^+]_i$ after ouabain was detectable by I_{NCX} measurements.[75] It is thought that the Na^+ concentration in the subsarcolemmal space is sensed by the Na^+ pump, NCX, and other membrane transport mechanisms.[76-78] It is possible that the increase in I_{NCX} or I_p measured during cardiac $P2X_4R$ activation reflects an increase in the subsarcolemmal Na^+ concentrations.

In studying the role of NCX in mediating the P2X receptor-induced effect on contraction, we used $P2X_4R$-overexpressing cardiac myocytes. The $P2X_4R$ OE myocytes displayed a greater magnitude of P2X receptor-mediated increase in contraction and were a better model to determine the mechanism of contractile effect of P2X agonist. We postulated that Ca^{2+} entry mode of NCX, stimulated by intracellular Na^+ elevation, contributes to contraction increase by P2X agonist. This postulate is supported by our finding that P2X agonist was able to enhance sarcoplasmic reticulum Ca^{2+} content in $P2X_4R$ OE myocytes.[55] In the present study, KB-R7943 could inhibit the 2me-SATP-induced increase in CS in $P2X_4R$ OE myocytes. KB-R7943, at 5 μM, can serve as a selective Ca^{2+} entry mode inhibitor.[74, 79] Another structurally different selective inhibitor of the Ca^{2+} entry mode, YM-

244769,[73] was also able to inhibit the 2me-SATP stimulation of CS in the $P2X_4R$ OE cells. Neither KB-R7943 nor YM-244769 affected the basal CS in these cardiac myocytes.

Several considerations deserve to be mentioned. Ca^{2+} may enter directly through the $P2X_4R$, and could contribute as much as 8% of the total inward current induced by ATP via the human homotrimeric $P2X_4R$.[65] Direct Ca^{2+} entry via the P2X receptor may impact dynamically the cellular Na^+ by further increasing the accumulation of Na^+ that enters through the receptor under physiological condition in myocytes. We could not exclude that P2X agonist increases subsarcolemmal $[Ca^{2+}]_i$ *via* direct calcium entry through the receptor channel. A direct measurement of subsarcolemmal $[Ca^{2+}]_i$ during P2X agonist stimulation was not feasible in the present study.

Another implication of P2X receptor activation merits further consideration. That both I_{NCX} and I_p can extrude the P2X receptor-mediated Na^+ entry distinguishes the P2X effect from the contractile and pro-arrhythmic effects of digitalis. Digitalis, by inhibiting the Na^+-K^+ ATPase and thus causing an increase in intracellular Na^+, results in NCX as the only Na^+ extruding mechanism in digitalis-treated cardiac myocytes. Since both I_{NCX} and I_p can operate to extrude P2X receptor-conducted Na^+ entry, the cell is less likely to be overloaded by intracellular Na^+ and Ca^{2+} during stimulation of P2X receptors. Finally, the physiological relevance of cardiac myocyte P2X receptor is supported by the demonstration in WT cardiac myocytes that P2X agonist can stimulate NCX and that inhibition of Ca^{2+} entry mode of NCX could reduce $P2X_4$ receptor-induced contraction in these cells.

Chapter 3

P2X Agonism leads to Limited Cardiac Myocyte Excitability

3.1 INTRODUCTION

As discussed earlier and demonstrated in the previous chapter, P2X receptors allow passage of cations, the majority of which are Na^+, into cells. They are thus capable of causing depolarization and calcium increase in many cell types to initiate signaling. The consequence of this seemingly simple event becomes more difficult to envision when imposed on a cardiac myocyte, whose function uniquely relies on tightly regulated cycles of action potential (AP) firing and calcium transients. How these highly dynamic cycles are affected by the relatively slower changing P2X current is not well characterized.

We have shown that P2X driven electrophysiological changes can underlie an enhancement of contraction in cardiac myocytes, and this may be important in maintaining cardiac pump function during ischemic injury and in the critical period after injury. Overexpression of $P2X_4R$ protects against calsequestrin overexpression-induced and post-infarct heart failure.[1, 52] On the other hand, inward cation passage can increase cellular excitability and lead to spontaneous activity that is undesirable for the controlled rhythm of the heart. There exists a conceptual gap regarding how inotropic enhancement may occur without significant electric disturbance. Here we consider the dynamics of P2X activation and study its impact on cardiac function in an integrated framework of excitation contraction coupling.

3.2 MATERIALS AND METHODS

3.2.1 Computational Simulation of the P2X current in the context of a Single Cardiac Myocyte

An ordinary differential equation-based model of the mouse cardiac myocyte, previously developed by Bondarenko, et al[15] was implemented in the Virtual Cell simulation software[80] and modified to include an additional flux representing the P2X channel. The simulated P2X current follows the general shape of the previously determined I-V relationship[47] (Figure 3.1A) and is desensitized with an exponential function with modifiable time constant. Simulations were run for 1000s with 1Hz pacing for values to reach relative steady state, and the end results were copied into new simulations as initial values. VCell outputs for select model parameters were exported and plotted.

3.2.2 Animals

$P2X_4$ receptor overexpression ($P2X_4R$ OE) mice were generated and bred as previously described.[51, 55, 66] All animal handling protocols have been approved by the Institutional Animal Care and Use Committee at the University of Connecticut Health Center.

3.2.2.1 $P2X_4R$ Knockout Animals

The Cre-Lox recombination technology was employed for $P2X_4R$ gene targeting.[81] The first loxP site was inserted into intron 4 and the second loxP site together with the Frt-PGKneo-Frt cassette was inserted in intron 1, in a direction opposite to the transcription of $P2X_4R$. The targeting vector was electroporated into embryonic stem cells, which were derived from F1 (129Sv/C57BL6J) blastocysts. Chimeric animals were generated by aggregating targeted ES cells with CD1 morula. The PGKneo cassette was removed by breeding chimeric males with ROSA26-Flpe females (Jax stock no: 009086) to generate $P2X_4^{floxed/+}$ F1 pups. F1 mice were

backcrossed with C57BL6 mice for over ten generations to produce $P2X_4^{floxed/floxed}$ mice in the C57BL6 background.

Homozygous $P2X_4^{floxed/floxed}$ males were then bred with heterozygous females with widespread expression of the Cre recombinase, including in the unfertilized egg (129S1/Sv-$Hprt^{tm1(cre)Mnn}$/J; Jax stock no. 004302 bred to the C57BL6 background) to produce $P2X_4^{floxed/+}$ F1 pups with Cre-excised floxed gene, which were crossed together to generate homozygous global $P2X_4R$ knockouts. Genotyping was carried out using primers listed in Appendix A Table 1, and immunoblotting confirmed protein decrease.

3.2.3 Measuring Voltage with Single Cell Patch Clamp

Myocytes from 8-16 week old WT and $P2X_4R$ OE mice were obtained and placed in a small superfusion chamber on the stage of an inverted microscope. For isolation procedure, refer to Section 2.2.1. Rod-shaped myocytes with clear striations and without spontaneous contraction are considered healthy cells for experimentation. Whole-cell patch clamp was established with a K^+-based pipette solution (in mM: 120 potassium aspartate, 30 KCl, 5 Na_2ATP, 1 $MgCl_2$, 10 HEPES, and 10 EGTA, pH 7.3 adjusted with KOH) to maintain physiological internal conditions for subsequent voltage examination. 2-meSATP or control buffer solution was given via rapid perfusion (SF-77B, Warner Instrument) to quiescent or stimulated (action potentials elicited with current injection) cardiac myocytes in current-clamp mode. Generation of protocols and acquisition of data were carried out in pCLAMP10 (Axon Instruments). For characterizing initial depolarization in response to P2 agonism, each cell was only exposed to 2-meSATP once to avoid desensitization effects. In a subset of experiments, 2-meSATP was withdrawn after some time to establish washout of drug, where as in other experiments 2-meSATP was delivered continuously for 10 minutes to examine natural desensitization.

3.2.4 Ex Vivo Working Heart for monitoring Whole Heart Function

Mice 8-16 weeks in age from both sexes were anesthetized with a ketamine/xylazine mixture before the chest was opened and the heart, with all major vessels and lungs attached, excised for immediate cannulation of the aorta. The viability of the heart was maintained with oxygenated Krebs-Henseleit bicarbonate buffer (in mM: 119 NaCl, 25 $NaHCO_3$, 4 KCl, 1.2 KH_2PO_4, 1 $MgCl_2$, 1.8 $CaCl_2$, 10 glucose and 2 Na-pyruvate; pH adjusted to 7.4 by bubbling with 95% O_2 and 5% CO_2) in the Langendorff mode while the pulmonary vein was cannulated and a pressure transducer was inserted into the left ventricle. After the heart was stably mounted, retrograde perfusion through the aorta was switched to antegrade perfusion via the pulmonary vein, establishing the working heart mode. The afterload against which the perfusate is ejected from the left ventricle was set to be constant with a column of buffer connected to the aorta. Hemodynamic parameters were derived from digitized pressure traces and analyzed in LabChart Pro (ADInstrument). In a number of experiments, electrodes were placed at the right atrium and left ventricle for a 2-lead electrical rhythm recording. After a stabilizing period with drug-free perfusate, 2-meSATP of a given concentration between 10nM to 100uM was administered for 10 minutes. Hearts were allowed to beat at their intrinsic pace. Those with baseline heart rate under 250 beats per minute were excluded from further experimentation. Additional experiments were performed on $P2X_4R$ KO hearts at 1µM of 2meSATP to further test differences seen between WT and $P2X_4R$ OE animals.

3.2.5 Quantification of Ectopic Activity

Abnormal beats were detected using the heart rate variability module of LabChart Pro. Deviations from normal heart rate are easily visualized using the tachogram, which plots successive R-R intervals over time. Ectopic beat detection was confirmed with visual inspection of the tachogram and the raw recording trace. The numbers of ectopic beats 10 minutes before

and after drug application were recorded. Hearts with greater than 5% of its baseline beats classified as abnormal were excluded from further analysis.

3.2.6 Data Analysis and Statistics

Patch-clamp data were analyzed using Clampfit 10.0 (Molecular Devices, CA, USA) and exported to GraphPad Prism for graphs. Pressure traces from isolated working hearts were analyzed in LabChart Pro. Pressure parameters from beat cycles were averaged every 5 seconds, and data were normalized to 4 minutes before drug application for percent change from baseline. Data are reported as mean ± standard error of the mean (SEM). Paired t-test was used to compare drug effects, and differences between genotypes were compared with two tailed, unpaired t-tests. The level of significance is taken as being $P<0.05$.

3. 3 RESULTS

3.3.1 Computational modeling predicts enhanced cardiac myocyte excitability with P2X activation

Simulations demonstrated that P2X activation can evoke a spectrum of outcomes for calcium transients that result in its eventual enhancement, consistent with the suggestion that P2X activation can enhance contraction in cardiac myocytes. However, the initial cellular response can be variable, depending on P2X current characteristics and other cellular factors. Select simulation outputs are displayed in Figure 3.1. The P2X current was assumed to be 90% carried by Na^+ and 10% by Ca^{2+} ions, and the desensitization constant was assumed to be 60 seconds in these simulations. Mimicking turning on the P2X current at 150 seconds into the simulation in WT cardiac myocytes (Figure 3.1A open circles showing previous experimental data for WT, and solid data illustrating simulated I-V relationship for a representative WT myocytes), AP generation was not significantly altered except for a slight initial depolarization,

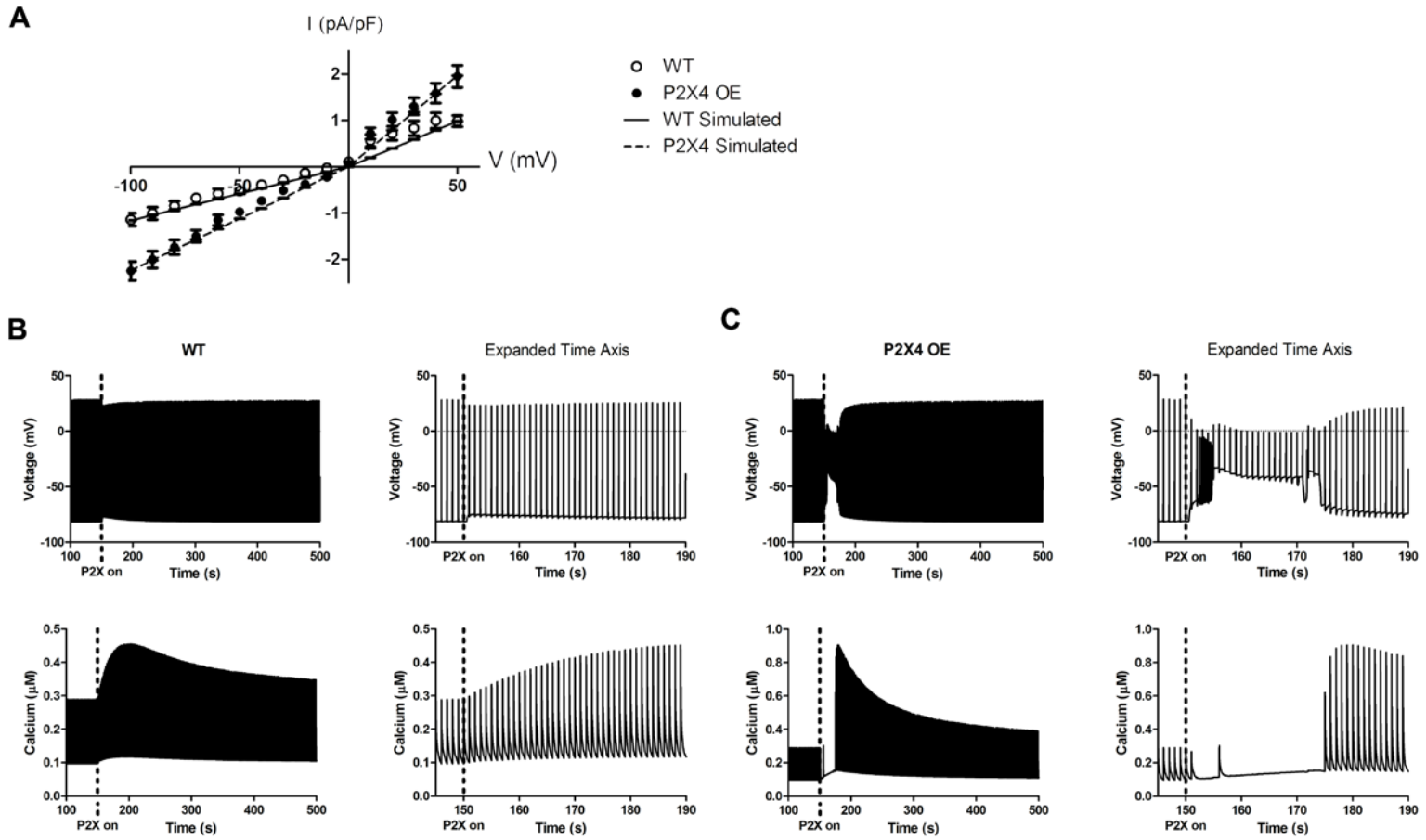

Figure 3.1 Computational predictions of P2X induced action potential and calcium changes. (A) Simulated I-V curves as compared to previously experimental data from WT (open circles, simulated results in solid line) and $P2X_4R$ OE (closed circles, simulated results in dashed line) cardiac myocytes. (B) Simulated cardiac myocyte response to activation of P2X current in WT cardiac myocyte showing slight resting membrane depolarization that does not disrupt action potential generation and gradual enhancement in calcium transients. (C) Simulated voltage and calcium response to activation of current in $P2X_4R$ OE cardiac myocyte. Membrane depolarization is large enough to initially blunt normal AP generation and calcium cycling, but normalizes over time.

while corresponding calcium transient trace demonstrate increase over baseline (Figure 3.2B). At a conductance level similar to what we measured previously in the $P2X_4R$ OE cardiac myocytes (Figure 3.1A closed circles and dashed line), opening of the P2X channel can lead to an initially large depolarization from rest, temporarily attenuating stimulated APs and beat-to-beat calcium cycling (Figure 3.1C). A number of ectopic action potentials are seen in the simulation data, due to partial opening of fast Na^+ channels. But given that the P2X receptor desensitizes, these disruptions are transient and enhanced calcium transients were observed when APs normalized. These results are in contrast to our earlier conclusion that activation of the $P2X_4$ current does not alter cellular excitability, which was based on observations that $P2X_4R$ OE myocytes exposed to 3 minutes of 3μM of 2-mesATP bath perfusion had no significant change in action potential characteristics at that time point.[55] Simulation results thus prompted us to re-examine our previous protocol and to retest cardiac myocyte excitability and the propensity of arrhythmogenesis in the intact heart in response to P2X activation.

3.3.2 $P2X_4R$ OE myocytes display transient depolarization in response to activation

We performed current clamp experiments with K^+-based pipette solutions in order to investigate whether inward current activated by 2-meSATP were able to induce changes in resting membrane potentials and modulate the excitability of ventricular myocytes. Rather than using gravity based bath application of 2-meSATP, we employed a fast switch system that allowed us to pinpoint the drug application to a sub-second scale. In resting $P2X_4R$ OE myocytes, we observed prompt depolarization responses to pulses of 2-meSATP (Figure 3.2A). Note that none of the subsequent depolarizations were larger than the initial depolarization, suggesting that desensitization is observed with each pulse of agonist application, which is further supported by the observation that a longer off time between two pulses led to greater recovery. More prolonged 2-meSATP application caused immediate

membrane depolarization that slowly normalized over minutes (Figure 3.2B).

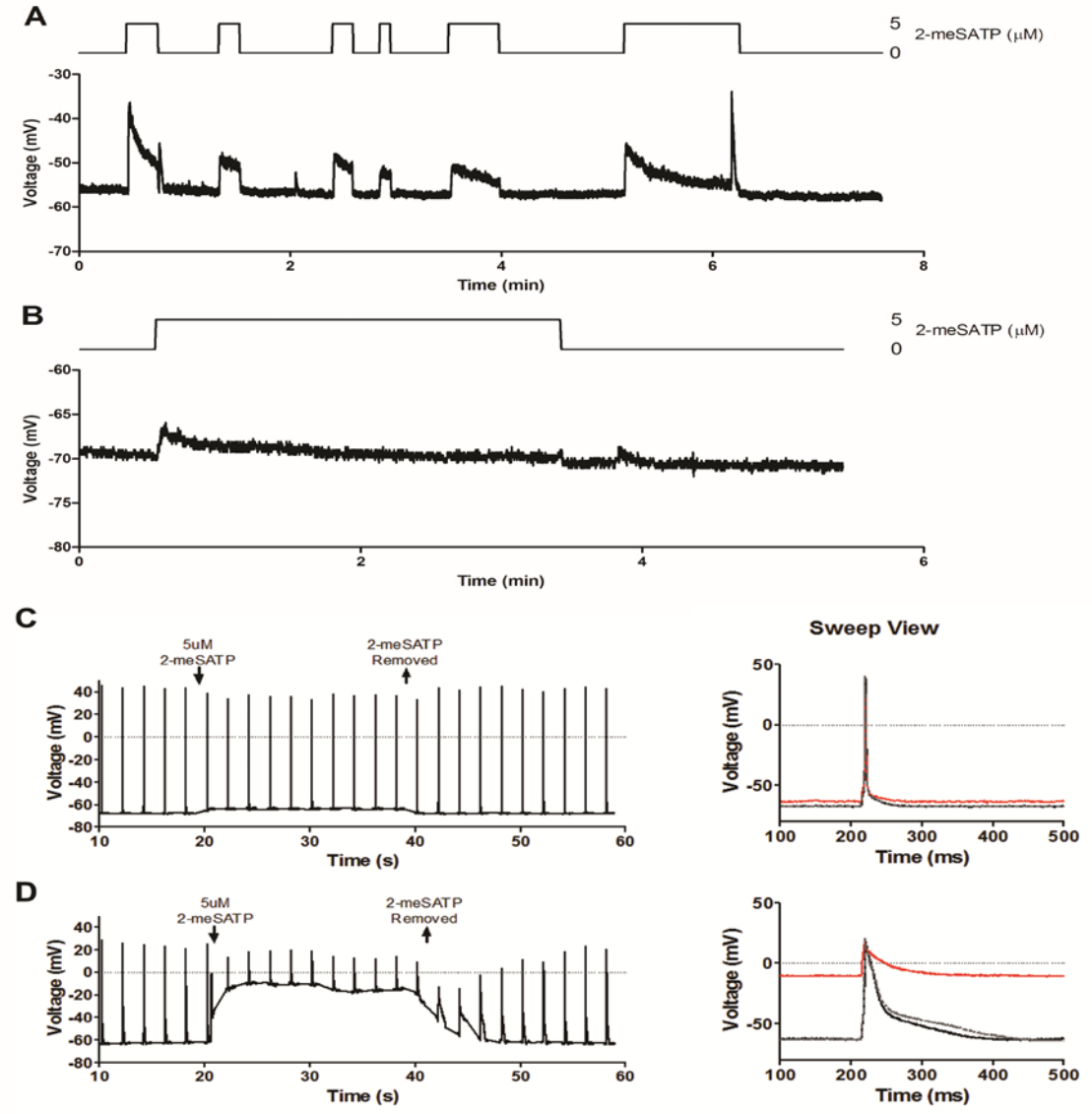

Figure 3.2 2-meSATP elicits membrane depolarization in P2X$_4$R OE cardiac myocytes. (A) Example quiescent myocyte in current clamp mode, measuring resting membrane potential and depolarization caused by 5μM 2-meSATP pulses. (B) More sustained 2-meSATP delivery demonstrating normalizing membrane potential in another quiescent myocyte over 3 minutes. (C) and (D) Examples of myocytes, stimulated every 2s to fire an action potential. 5μM 2meSATP is administered during action potentials 11 to 20. The myocyte in (C) experienced less resting membrane depolarization and action potential alteration than the myocyte in (D). Spikes observed during 2-meSATP application in (D) likely reflect stimulus current. Overlapped sweep views to the right show difference in action potential duration between the two cells, pointing to a likely difference in repolarizing capacities. Black line is pre-drug baseline, red corresponds to maximum depolarization, and grey line shows recovery.

To better understand the effect of $P2X_4$ channel mediated depolarization on beating cardiac myocytes, a 0.5ms current of sufficient magnitude to elicit an action potential (0.5-2nA) was injected every 2 seconds. Myocytes were recorded for 30 cycles of AP, with 5µM 2-meSATP applied during AP numbers 11-20. The responses of two myocytes are shown in Figure 3.2 C and D, illustrating the variability in the magnitude of resting membrane depolarization and effects on action potential generation. While some cells experienced small depolarizations, others experienced large (>40mV) depolarizations, which then rendered the cell unable to fire APs in response to subsequent current injections. These results demonstrate that the purinergic agonist 2-meSATP can trigger immediate depolarizations in both quiescent and stimulated cardiac myocytes isolated from cardiac specific $P2X_4R$ OE hearts. The general features mimic what would be expected from the activation of a $P2X_4$ current, namely, fast activation followed by slow desensitization.

There was a clear difference between the response of $P2X_4R$ OE cardiac myocytes and that of the WT cardiac myocytes to stimulation with 2-meSATP (Figure 3.3). A concentration dependent shift in the proportion of cardiac myocytes that experienced large depolarizations in response to the agonist was evident in $P2X_4R$ OE myocytes. Out of the ten cells exposed to 5µM 2-meSATP, three experienced >40mV depolarizations. The average depolarization of these three cells was 49.91±2.05 mV, while the seven cells that had smaller responses was 4.20 ±0.98 mV, combining for a total average of 17.92±8.63 mV for 5µM 2-meSATP induced depolarization in $P2X_4R$ OE myocytes. A closer examination of the data suggests that baseline action potential duration may impact myocyte responses to purinergic agonism, offering insight into the variable cellular response at this lower concentration of agonist. Myocytes that took longer for action potentials to reach 90% repolarization (APD90) before drug was added showed greater depolarization in response to P2X activation, which may reflect relatively blunted repolarization mechanisms in these cells

(Figure 3.3B). When 100µM 2-meSATP was applied, all tested $P2X_4R$ OE cardiac myocytes displayed large depolarizations, which averaged 51.67±3.34 mV. The mean magnitude of depolarization and the proportion of cells experiencing large depolarization increased with increasing concentration of 2-meSATP in the $P2X_4R$ OE animals, while the majority WT myocytes did not experience an immediate depolarization even at 100µM of 2meSATP (0.74±0.53 mV, n=11, p>0.05 against buffer control; individual data points displayed in

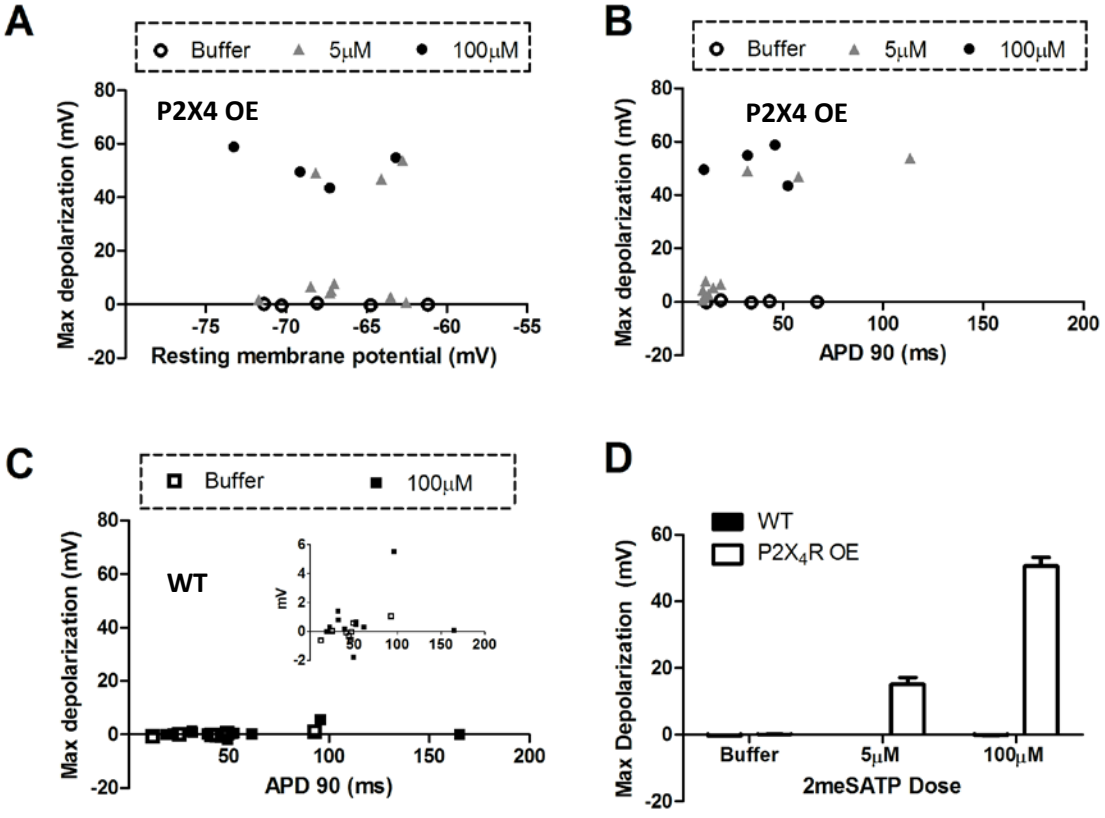

Figure 3.3 Summary of maximum depolarization in response to 2-meSATP
2-meSATP elicited depolarization in $P2X_4R$ OE cardiac myocytes. Maximum resting membrane depolarization in response to 2-meSATP are plotted against baseline AP characteristics that may reflect K^+ channel activity: (A) Resting membrane potential, and (B) the time for action potential to recover 90% (APD90). 3 out of 10 cells experienced large depolarizations in response to 5µM 2-meSATP and APD90 may be a good predictor of this response. All cells exposed to 100µM 2-meSATP experience large depolarizations. (C) WT cardiac myocytes did not significantly depolarize in response to 100µM 2-meSATP. (D) Summary of WT and $P2X_4R$ OE immediate cellular depolarization in response to P2 agonism.

Figure 3.3C, with insert showing magnified voltage scale). However, 8/11 of the WT cells exposed to 100µM of 2meSATP experienced spontaneous activity at a later point during the treatment. Buffer control did not elicit significant depolarization in either $P2X_4R$ OE (0.05±0.15 mV, n=5) or WT (0.01±0.20 mV, n=8) cardiac myocytes. These results support a $P2X_4$ channel mediated depolarization response to 2-meSATP, with concentration dependent change in the population response.

After establishing that the depolarization response is specific to agonist stimulation of the $P2X_4$ receptor, we next asked what would happen in the continued presence of agonist. As predicted by the computational model, desensitization of the P2X current would lead to normalization of action potential in the continued presence of 2-meSATP, and this was corroborated by patch clamp data. In 3 of the 4 $P2X_4R$ OE myocytes exposed to 100µM of 2-meSATP, current injection stimulated action potential firing resumed after 18, 21 and 34 seconds (example cell shown in Figure 3.4B; refer to simulation result in Figure 3.1C expanded AP graph for comparison). In the other cell where membrane potential did not recover, the seal was confirmed to be lost after 3 minute. It should be noted that these

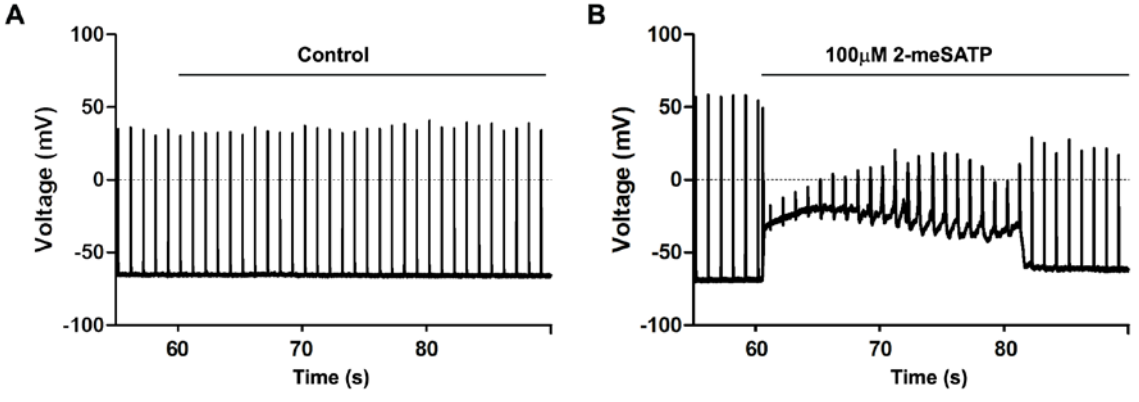

Figure 3.4 $P2X_4R$ mediated membrane depolarization is transient
(A) Buffer control had no effect on cardiac myocyte APs. (B) $P2X_4R$ activation led to membrane depolarization that initially blunted current injection stimulated AP firing but recovered over time, with resumption of stimulated APs. Bars indicate presence of treatment solutions, which were continually applied for 10 minutes. While the recovered APs shown in (B) are of smaller amplitude compared to baseline, this is not representative of the APs later

in time as the P2X current continued to desensitize. A full recovery comparable to baseline would be seen later.
experiments were performed with 10mM EGTA in the pipette solution to buffer intracellular Ca^{2+}. These findings reveal that while 2-meSATP-evoked inward cationic current via the $P2X_4$ channel can lead to cellular excitability, direct depolarization effects are temporary.

3.3.3 P2X activation does not increase arrhythmogenesis in Intact Hearts

Because cellular electrophysiological data confirmed that $P2X_4$ channel activation can rapidly modify myocyte membrane excitability and since others have suggested that P2 agonism can induce serious ventricular arrhythmias, we sought to more carefully examine this arrhythmogenic potential in intact hearts. Isolated hearts were mounted in the working heart configuration and allowed to beat at their intrinsic pace. Baseline heart rates were similar, at 393.4±6.64 (n=64) and 390.7±6.95 (n=53) beats per minute for WT and $P2X_4$R OE hearts, respectively. We did not observe significant arrhythmic activity in $P2X_4$R OE hearts as compared to WT at baseline. Eight WT and one $P2X_4$R OE hearts had greater than 5% of their baseline beats classified as abnormal, and were excluded from analysis of agonist treatment effect. Most ectopic activities took the form of premature ventricular beats (Figure 3.5A). Paired t-test comparisons of the effect of 2-meSATP application indicated that there was a significant increase in the number of ectopic beats in WT hearts at 10μM and 100μM of 2-meSATP (Figure 3.5B). There was a trend towards increased ectopic activity at the highest concentrations of 2-meSATP in $P2X_4$R OE hearts as well, mainly driven by 3 hearts that had a noticeable increase (>5%) in the number of abnormal beats, but this increase remains statistically insignificant. These data suggest that 2-meSATP at high concentrations can increase ectopic action potentials in WT hearts, but $P2X_4$ channel overexpression in cardiac myocytes does not increase baseline and agonist-induced arrhythmic activity.

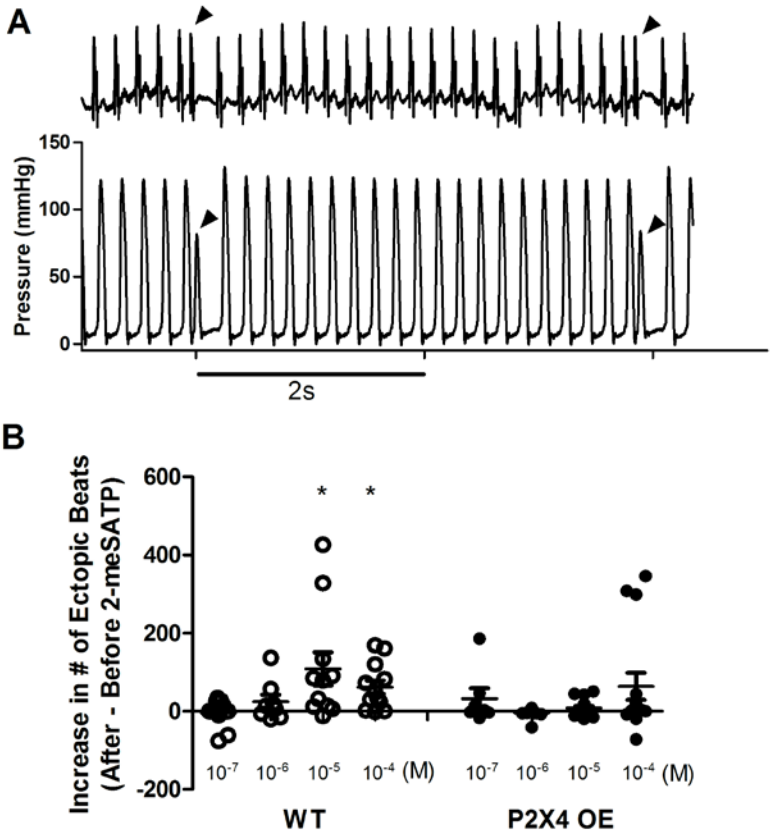

Figure 3.5 Summary of Ectopic Activity in Intact Hearts
(A) Example electrical and pressure trace from a $P2X_4R$ OE heart treated with 100μM 2-meSATP. Arrows mark ectopic events. (B) Summary of the increase in the number of ectopic beats after 2-meSATP application for each individual heart. * denotes significant increase by paired t-test in WT with 10μM and 100μM of 2-meSATP.

3.3.4 A novel biphasic contractile response to 2-meSATP in murine hearts

In addition to close examination of possible arrhythmic sequelae induced by altered cardiac myocyte excitability in whole hearts, the working heart setup allowed us to quantify additional parameters associated with pressure development in the left ventricle. Continuous 2-meSATP treatment led to a surprising, previously undescribed, biphasic response in both WT and $P2X_4R$ OE hearts (Figure 3.6). Control perfusion did not elicit significant change, and 2-meSATP below 1μM had minimal effect. In response to doses of 2-mesATP 1μM and

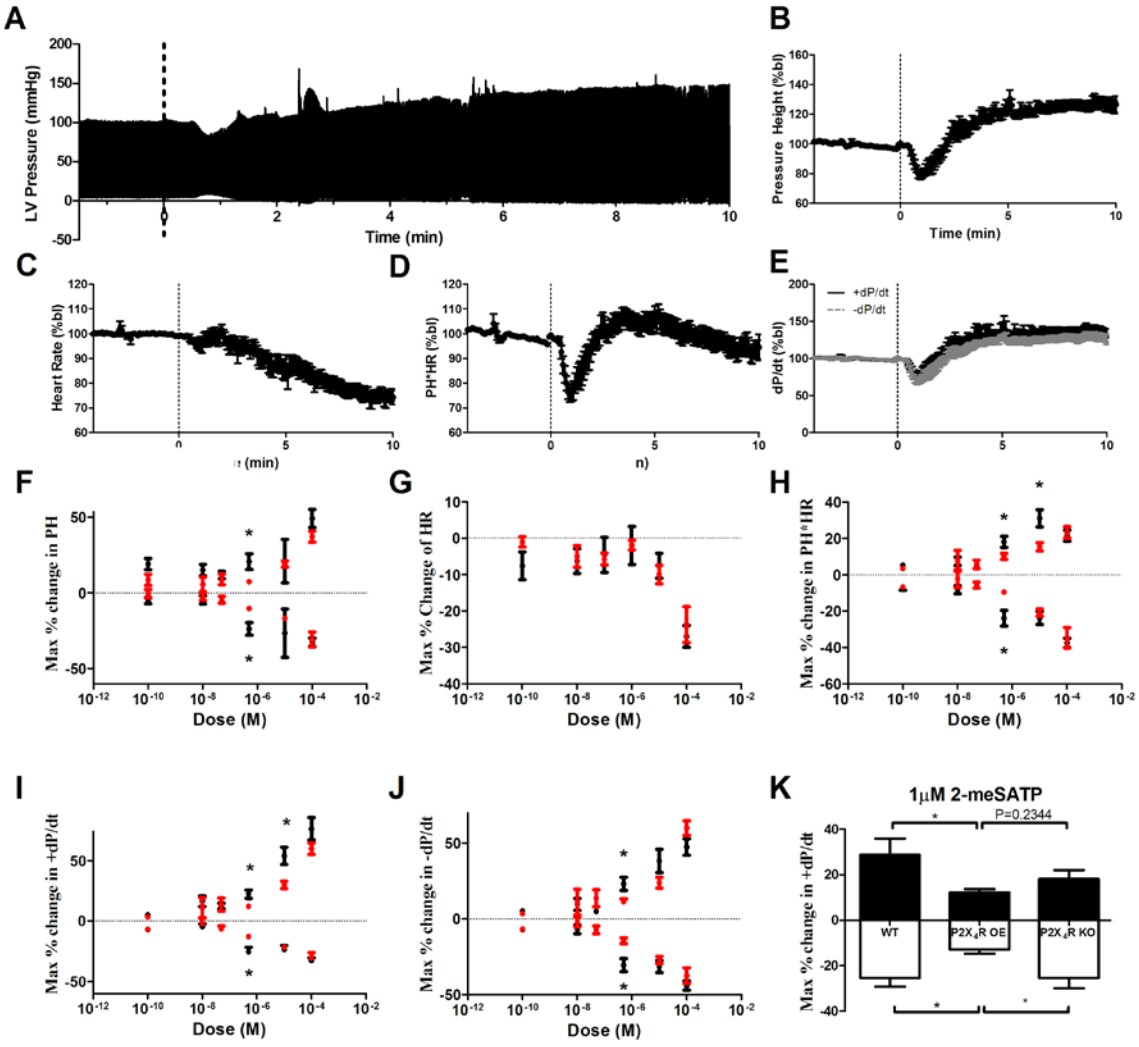

Figure 3.6 2-meSATP leads to dose-dependent biphasic response in the murine heart. (A) Raw data trace from an example WT heart, treated with 100μM 2-meSATP. Corresponding 5 second averages recorded for WT hearts exposed to 100μM 2-meSATP showing percent changes from baseline (bl) in terms of (B) left ventricular pressure height and (C) heart rate. (D) The pressure and heart rate product (PH*HR) and (E) the maximum rate of pressure development (+dP/dt, black solid line) and maximum rate of relaxation (-dP/dt, gray dashed line) are shown as surrogates for overall cardiac output. (F-J) Summary of biphasic response showing maximum depression and enhancement changes from baseline after various doses of 2-meSATP in both WT and $P2X_4R$ OE hearts (black circles for WT, red circles for $P2X_4R$ OE; n=15 for each group exposed to 1μM to 100μM; WT hearts treated with 10nM and 100nM had n=10 per group; $P2X_4R$ OE hearts at 10nM and 100nM had n=2 and 7 respectively). (K) Summary of +dP/dt maximum changes from baseline at 1μM across hearts of all three genotypes (n=11 for $P2X_4R$ KO). *P<0.05 indicates significant difference between WT and $P2X_4R$ OE for F-J and for the indicated pairs in K.

greater, an initial drop in pressure was evident, usually occurring within one minute. The pressure then recovered and rose higher than the baseline pressure in most cases. Wash out of drug returned measures to baseline levels or slightly below baseline due to a natural decline of function over time. Both the depressive and enhancement phases were dose dependent, and a slowing of heart rate was significant at 100μM of 2-meSATP in both WT and $P2X_4R$ OE hearts (Figure 3.6 C and G). There was no sign of loss of sinus rhythm.

A significant difference between WT and $P2X_4R$ OE hearts was consistently observed at 1μM 2-meSATP, where both the depressive and enhancement phases were greater in the WT (Figure 3.6F, H, I, J). Further experimentation on $P2X_4R$ KO hearts at this concentration of agonist showed that the biphasic response is persistent in $P2X_4R$ knockout hearts (Figure 3.6K) and was not different from WT response. 1μM 2-meSATP treatment of $P2X_4R$ knockout hearts led to an initial depression in LV pressure followed by recovery and enhancement in a similar time course and to comparable magnitudes as WT hearts. Baseline parameters were also not significantly different from WT littermates. The baseline PH for $P2X_4R$ KO hearts was 90.87±3.66 mmHg (vs. 92.85±2.46 mmHg in WT, n=6) and the HR was 379.5±14.35 beats per minute (vs. 374.6±23.55 in WT, n=6).

3.4 DISCUSSION

Extracellular ATP-activated purinergic receptors have been implicated in different physiological and pathophysiological events such as platelet aggregation, hypoxia, pain, and vascular diseases. With increasing interest in targeting these receptors for treating various aspects of cardiovascular disease, it is important to clarify their effects on cardiac excitability. While many studies have described the cardiac effects of ATP, reviewed in [82], results are mixed and remain controversial due to differences in methodology and fast breakdown of the extracellular nucleotide. It is difficult to ascertain both the composition and concentration of ATP and its metabolites that reach the heart after bolus injections and *in vivo* data can be

complicated by nerve terminal release of ATP as co-transmitters[83, 84] and reflexive responses to sympathetic afferents.[85] In this study, in addition to examining P2 agonism in WT animals, we took advantage of our $P2X_4R$ OE transgenic animals to further clarify the effects of activating these receptors.

At the cellular level, we along with other groups have previously demonstrated enhanced contraction after 2-meSATP application in a number of studies.[42, 49] Others have observed spontaneous contractions in quiescent myocytes and ectopic beats in electrically stimulated myocytes in response to P2 agonist that suggest altered cellular excitability.[46, 86] Earlier data from our laboratory also established a current-voltage (I-V) relationship caused by 3μM of 2-mesATP after 3 minutes of bath perfusion and suggested no significant change in action potential at that time point.[55] When we incorporated the previously obtained I-V relationship into an established murine cardiomyocyte computational model, we observed immediate depolarization that, in the case of the current magnitude representing $P2X_4R$ OE myocytes, was large enough to blunt subsequent action potential firing. Therefore we revisited the question of cellular excitability in the $P2X_4R$ OE cardiomyocytes with a modified protocol. Instead of bath application of agonist, as is done in most studies, we employed a rapid perfusion technique that allowed us to precisely determine the timing of drug stimulation. With this improved technique we saw immediate depolarization in $P2X_4R$ OE cardiomyocytes that desensitized with prolonged agonist presence both in quiescent and stimulated myocytes (Figure 3.2B and 3.4B). The EC50 and current desensitization/resensitization rates of P2X currents in more pure expression systems have been reported.[63] Comparing the range of these values to our data suggests that our observation is $P2X_4R$-specific. $P2X_1$ and $P2X_3$ are desensitized at a much faster rate, while $P2X_5$ and $P2X_6$ are thought to have low membrane expression and thus contribute little to overall agonist-induced current. $P2X_7$ is uniquely stimulated at higher concentrations of agonist and does not desensitize significantly on the minute time scale. $P2X_2$ has similar

characteristics as $P2X_4$, and heterotrimeric combinations of P2X subtypes (P2X1/2, 1/4, 1/5, 2/3, 2/6, 4/6, 4/7) are plausible contributors as well, as many have a similarly slow rate of desensitization or remain uncharacterized.[87] However, the lack of response in WT cardiomyocytes further suggest that the immediate excitation seen in $P2X_4R$ OE myocytes were specific to the activation of the $P2X_4R$ channel. Considering the desensitization characteristics observed in these experiments, it is not surprising that we previously did not see changes in action potential characteristics after 3 minutes of treatment. Additionally, the previous experiments were performed with 3μM 2-meSATP, which would stimulate a smaller population of cells to have large depolarization responses that would significantly affect electrically stimulated APs. It is of interest to note that 8 out of 11 WT cells that were exposed to 100μM of 2-meSATP spontaneously depolarized at later times during treatment, somewhat consistent to findings in other studies.[46] The significance and mechanism of these ectopic events are unclear.

After observing that high concentration 2-meSATP stimulation of $P2X_4$ receptors resulted in robust immediate depolarizations, we questioned its effects on action potential propagation in intact hearts. Somewhat to our surprise, we did not observe increased arrhythmic activity in $P2X_4R$ OE hearts, even with high concentration 2-meSATP treatment. In the WT intact hearts, however, we observed a significant increase in the number of ectopic beats after high concentration 2-meSATP treatment. This may be consistent with observations from others. Monophasic action potential recording in Langendorff-perfused mouse hearts showed that high concentrations of ATP (10μM and 100μM) can induce delayed after-depolarization (DAD) and ectopic APs, which can be blocked with 100μM suramin or 30μM PPADS, but not with 10μM nifedipine.[86] As nifedipine blocks the L-type Ca^{2+} channel and in turn deplete SR Ca^{2+} storage, it was suggested that the ATP-induced arrhythmic events likely involved Ca^{2+} influx via purinergic receptors. Ventricular tachycardia (VT) was reported in 3 out of 7 spontaneous beating hearts and in 6 out of 7 hearts that were

perfused with ATP for 20 minutes before being provoked with programmed electrical stimulation.[86] It is difficult to ascertain the severity of VT in this report given the relatively loose definition of VT as three or more successive ectopic beats, but we did not observe any sustained VT in our experiments. It is possible that 2-meSATP is less potent than ATP in stimulating the subset of P2 receptors responsible for the proarrhythmic activities observed. For example, 2-meSATP is a partial agonist of $P2X_4R$ receptors with an EC50 of 10 to 100μM, as opposed to ATP, which has an EC50 of 1 to 10μM.[23] Given that the $P2X_4R$ is not blocked by suramin or PPADS at the concentrations used to prevent ATP-induced arrhythmias,[23] combined with the fact that we did not observe increased propensity for arrythmogenesis in our $P2X_4R$ OE hearts, it is unlikely that the $P2X_4$ receptor played a role in the arrhythmias elicited in the earlier report. ADP has also been shown to be proarrhythmogenic to a lesser extent, while UTP and adenosine had no effect. This agonist profile suggests that in the WT murine heart, $P2Y_1$ and $P2Y_{11}$ receptors may be involved in the increased arrhythmogenesis, as they are linked to phospholipase C and cAMP pathways that could increase mobilization of intracellular calcium.[88] The $P2Y_{11}$ receptor has also been implicated to be responsible for ATP-induced inotropic increase in murine cardiac myocytes.[89] Phospholipase related IP3 production can activate IP3 receptors in the SR membrane and nuclear envelope, which can modulate excitation contraction coupling by sensitizing nearby ryanodine receptors, leading to positive inotropic but also pro-arrhythmic effects.[90] Since significant overexpression of a P2X channel in the $P2X_4R$ OE hearts did not show an increased propensity to develop serious arrhythmias even at high concentrations of the agonist, it is difficult to imagine how other P2X receptors would be proarrhythmogenic, as they would operate similarly in terms of electrophysiology and most others are even faster desensitizing or less Ca^{2+} permeant (except for $P2X_7$ at high concentration agonist). However, their involvement in the WT heart is not entirely ruled out, as localization is also important and it is unknown if any of these channels are localized to the T-tubule

invaginations. Staining for CaV1.2, the α1 subunit of cardiac dihydropyridine-sensitive L-type Ca^{2+} channels, shows a characteristic striated pattern reflecting their localization in the T-tubular system,[91] which acts as the basis of calcium-induced calcium release. Staining for $P2X_4$ receptors in the $P2X_4R$ OE cardiomyocytes demonstrate clusters in the cell periphery (Figure 4.1C in the following chapter), thus Ca^{2+} influx via this channel is unlikely to induce spontaneous SR mobilization. Whether other P2X channels are juxtapositioned to calcium release units on the SR remains to be studied. Overall, despite significant membrane excitation due to $P2X_4R$ activation in the $P2X_4R$ OE single cardiomyocytes, we did not observe increased propensity for these hearts to be more arrhythmic. Proarrhythmic mechanisms active in single myocytes in many cases do not lead to a propagated response in the intact tissue, because the current generated by a myocyte will leak away to its neighbors without reaching the action potential threshold. The occurrence of a proarrhythmic event will have to be synchronized in a sufficiently large group of myocytes in order to reach the threshold for propagation away from that area. The transient nature of the P2X induced depolarization also makes sustained arrhythmic activity unlikely in the whole heart.

We initially hypothesized that this transient depolarization due to P2X activation could form a basis for the biphasic contractile phenotype seen in the whole heart. That is, a portion of cardiomyocytes would initially have arrested APs and attenuated calcium transients that reflect the initial depression in the whole heart, which, when followed by a subsequent desensitization of the P2X current, would then lead to AP normalization and an enhanced calcium transient in the later phase of enhanced contractions. Complementary to altering agonist concentration, we hypothesized that increased myocyte surface $P2X_4R$ expression would augment initial conductance and possibly prolong desensitization kinetics, leading to an exaggerated biphasic response at a given concentration of agonist in the $P2X_4R$ OE animals and ultimately to a left-shifted dose response curve as compared to WT. Our data, however, did not indicate an obvious difference between WT and $P2X_4R$ OE hearts in terms

of left ventricular pressure development in response to 2-meSATP. A biphasic contractile response was observed in both, suggesting that depolarization at the cellular level is not essential to the initial depressive phase of 2-meSATP induced biphasic response, as no significant depolarization was seen in the WT cardiomyocytes. 2-meSATP, with the hydrogen in position 2 of ATP replaced with a methylthio group, is thought to be more resistant to nucleotidase breakdown and to lack coronary vasodilatory effects (adenosine effect),[50] however, some evidence suggest it is also prone to degradation by ectonucleotidase enzymes.[92] In the whole heart setting, the activity of these enzymes are better preserved than in the isolated myocytes preparations, and thus the specificity of 2-meSATP for P2X receptors in the whole heart is less clear and may explain the lack of significant difference between WT and $P2X_4R$ OE heart. A small but significant difference was observed between WT and $P2X_4R$ OE hearts at 1μM 2-meSATP, but additional study in a global $P2X_4R$ KO line showed a response similar to WT. The persistence of the biphasic response in the knockout animals further suggests that this response was not $P2X_4R$ specific.

The biphasic cardiac contractile response to purinergic agonism has been observed in a few studies,[39, 93, 94] however, this is the first observation in a working mouse heart model looking at ventricular function with 2-meSATP as the agonist. The eventual enhancement of cardiac function is consistent with previous observations,[39, 49, 82] though the mechanism by which this is achieved is still debated. It is encouraging that the biphasic contractile response has previously been demonstrated in human atrial muscle strips,[39] suggesting that the cardiac functional responses of P2 agonism may be similar between rodents and human, and that it is mediated directly by affecting force generating cells rather than indirectly impacting other hemodynamic parameters such as HR. We did observe that with 100μM of 2-meSATP the heart rate progressively slowed down. This slowing could be a sign of agonist breakdown and stimulation of adenosine receptors and/or other G_i coupled P2Y receptors, as previous studies have indicated that ATP-induced slowed sinus pacemaker activity can

be blocked by theophylline and pertussis toxin.[95] Similar to previous work, in some cases an initial HR acceleration was seen before it slowed, which could be related to release of prostaglandins with purinergic activation.[95, 96] The existence of multiple subtypes of P2 receptors in the native heart and additional release of soluble factors complicate interpretation, but the crosstalks involved in these signaling pathways may be advantageous as P2 agonist-induced positive inotropic effect did not entail a rate related increase in myocardial oxygen consumption, as many current inotropes do.

The decrease in heart rate at the highest concentrations of 2-meSATP can partially contribute to the higher pressure development. We also cannot rule out involvement of the Frank-Starling mechanism in the later phase of the biphasic response. In the Frank-Starling phenomena, stretched muscle fibers can generate larger forces, as it is thought that stretching optimizes the overlap and interaction of myosin and actin filaments, and possibly also increases the sensitivity of the myofilaments to Ca^{2+}, which further augments force development.[97] In our experiment, the initial drop in pressure development can lead to incomplete chamber emptying and a backlog of volume that accumulates in the ventricle during diastole (bulging of the left atrium was sometimes visibly noticeable). This can increase stretch on the myofibers and via the Frank-Starling mechanism induce greater stroke volume on subsequent contractions. This, however, is unlikely the sole mechanism involved as the enhancement can be sustained. While the interpretation of contractile response in the whole heart is complicated by a number of considerations and not $P2X_4R$ specific, we demonstrate that $P2X_4R$ induced cardiomyocyte depolarization is transient and unlikely increases propensity for arrhythmia development.

Chapter 4

$P2X_4$ receptor-eNOS pathway in cardiac myocytes as a novel protective mechanism in heart failure[d]

4.1 INTRODUCTION

In previous experiments we have demonstrated that mice with $P2X_4R$ overexpression are protected from heart failure progression in surgically induced and genetically altered disease models. While an acute inotropic increase due to P2X activation can be explained by its electrophysiological effects, other changes potentially responsible for more chronic modulation of cardiac function are unknown. Since the $P2X_4R$ is calcium permeable and can alter calcium handling inside a cell, a multitude of downstream effects could ensue. One such possibility is the interaction with calcium-dependent nitric oxide synthases (NOS). $P2X_4R$ mediated endothelial nitric oxide synthase (eNOS) activation has been shown previously in endothelial cells, [56] with $P2X_4R$ deficient $P2X_4R^{-/-}$ mice exhibiting aberrant endothelial cell flow responses due to a blunting of flow mediated influx of Ca^{2+} and subsequent production of nitric

[d] This chapter has been adapted from two publications:

1. Yang T, Shen JB, Yang R, Redden J, Dodge-Kafka K, Grady J, Jacobson KA, Liang BT. "A Novel Protective Role of Endogenous Cardiac Myocyte P2X4 Receptors in Heart Failure." Circ Heart Fail. 03/2013.
2. Yang R, Beqiri D, Shen JB, Redden JM, Dodge-Kafka K, Jacobson KA, Liang BT. "P2X4 receptor-eNOS signaling pathway in cardiac myocytes as a novel protective mechanism in heart failure." *Comput Struct Biotechnol J.* 13:1-7. 11/2014; Review.

R.Y. performed immunoblotting, immunostaining, cGMP and S-nitrosylation measurements, and some NO imaging experiments. Dr. Shen and Dardan Beqiri also contributed significantly to NO dye imaging. Drs. Redden and Dodge-Kafka provided the Co-IP data. Long-term characterizations of animal function after injury involved many other members of the Liang lab. Dr. Tiehong Yang performed most *ex vivo* characterizations, and we also thank Carol McGuiness for care of animals and echocardiography, Dr. Chunxia Cronin for performing surgeries, and Dr. Ruibo Wang for additional technical assistance.

oxide (NO). These deficits were rescued with adenoviral $P2X_4R$ gene transfer. Additionally, the $P2X_4R^{-/-}$ animals were shown to have higher blood pressure and to excrete smaller amounts of NO products in their urine when compared to WT mice, and vessel dilation induced by acute increases in blood flow was markedly suppressed.[56]

Cardiomyocytes also constitutively express eNOS and neuronal nitric oxide synthase (nNOS),[98] and regulation of these enzymes have significant impact on cardiac function.[99, 100] The protective effect of eNOS and its stimulated second messenger, cGMP, against heart failure development is widely confirmed.[99, 101] We further examined a possible link between the $P2X_4R$ and eNOS and considered the existence of a physical interaction. To test for functional significance, NO and its downstream readouts were assayed and moreover, inhibition of eNOS by pharmacology or genetic knockout was carried out in $P2X_4R$ OE transgenic mice subjected to postinfarction and pressure overload HF.

4.2 MATERIALS AND METHODS

4.2.1 Determination of nitric oxide formation

NO formation inside isolated cardiomyocytes was first measured by real-time imaging with diaminofluorescein-FM diacetate (DAF-FM DA, Molecular Probes, Eugene, OR). Cardiomyocytes were loaded with 5μM of DAF-FM DA for 30min at 37°C before imaging on a confocal microscope (Zeiss LSM510meta). Rod shaped striated myocytes were randomly selected. Fluorescence was excited at 488nM and emission was filtered through a 525nm long pass filter. Fluorescence intensities were quantified using MetaMorph (Molecular Devices, Inc, Sunnyvale, CA). Myocytes were incubated with vehicle normal saline or 2-meSATP and fluorescence determined at baseline and at each minute for 10 minutes.

In addition to time-series imaging with DAF-FM DA, we utilize a newly commercially available NO-sensitive fluorescent dye, 2-[4,5-bis[6-(2-ethoxy-2-oxoethoxy)-2-

methylquinolin-8-ylamino]methyl]-6-hydroxy-3-oxo-3H-xanthen-9-yl}benzoic acid (FL2E) in its copper complex form [Cu_2(FL2E)] (Strem Chemicals, Inc., Newburyport, MA), to image NO formation in living cardiac myocytes.[102-104] The Cu_2(FL2E) NO dye was prepared and stored according to manufacturer instructions. Before experiments, myocytes were loaded with 5 µM Cu_2(FL2E) NO dye for 1 h in Tyrode's solution, then plated onto glass bottom dishes for epifluorescence imaging with a Nikon Eclipse TE2000-S. Fluorescence was captured with a 480/40 excitation filter and a 535/50 emission filter. Given the observation that Cu_2(FL2E) demonstrates increased fluorescence with light exposure alone, we minimized data acquisition to pre- and 10 minutes post treatment, thus limiting view field exposure to light. Random 40× fields rich in rod shaped striated myocytes were selected and recorded with a CCD camera. Myocytes were incubated with buffer vehicle or 10 µM 2-meSATP (Sigma). 100 µM S-nitroso-N-acetyl-D,L-penicillamine (SNAP, Molecular Probes, Life Technologies, Grand Island, NY), a NO donor, was used as a positive control. Fluorescence intensities from individual rod shaped myocytes were quantified using ImageJ (NIH). Twenty to sixty myocytes were counted from each plate before and after treatment for each mouse.

4.2.2 Immunoprecipitation, Immunoblotting, and Immunostaining

To test whether there is a physical interaction between $P2X_4R$ and eNOS, we performed co-immunoprecipitation on cardiomyocyte lysates using mouse monoclonal eNOS (BD Transduction; 1-3 µg) and rabbit polyclonal $P2X_4R$ (Alomone; 2µg). Cells were lysed in HSE buffer (20mM HEPES, 150mM NaCl, 5mM EDTA, 1% Triton X-100 and protease inhibitors (leupeptin, pepstatin, benzamidine and ARBSF), pH 7.4). Supernatants were incubated at 4°C overnight with the indicated antibody and 15µL of prewashed Protein A/G-agarose. Following extensive washing, captured proteins were solubilized in sample buffer and analyzed by immunoblot.

For immunostaining of isolated cardiac myocytes to evaluate co-localization of $P2X_4R$ and eNOS, cardiomyocytes were fixed with 4% paraformaldehyde in PBS for 20 minutes. Cells were then cytospun onto slides for staining. Cardiomyocytes were permeabilized with 0.5% Triton, and then blocked with 10% normal goat serum plus 3% BSA in PBS for 1 hour at room temperature or 4°C overnight. Primary antibodies to eNOS and $P2X_4R$ (same as used in co-immunoprecipitation) were applied both at 1:150 dilution for 1 hour, followed by incubation with secondary antibodies (goat-anti-mouse-FITC from Santa Cruz and goat-anti-rabbit-Texas Red from Invitrogen) at 1:500 for 45 minutes at room temperature. Confocal fluorescence images were acquired on a Carl Zeiss LSM 780 with 488nm and 561nm laser excitation using a 63X oil lens (Carl Zeiss Microscopy, LLC, Thornwood, NY).

Antibodies specific for eNOS phosphorylation sites Ser1177 (Cell Signaling #9571) and Thr495 (Cell Signaling #9574 and Millipore #04-811) were used to assess eNOS activation in WT and P2X4R overexpression heart homogenates. Antibodies from Cell Signaling against all three NOS isoforms: eNOS (#9572), nNOS (#4236), and inducible NOS (#2982) were also used to examine expression differences.

4.2.3 Determination of cGMP levels

NO can lead to soluble guanylate cyclase production of cyclic guanosine monophosphate (cGMP). We measured cGMP levels in left ventricular homogenates of $P2X_4R$ OE and WT animals, following the manufacturer's acetylated protocol (cGMP determination kit, GE Healthcare). Isolated hearts were perfused with buffer, NO donor S-nitroso-N-acetylpenicillamine (SNAP, 100µM), or 2-meSATP (10µM) for 10 minutes in the working heart mode before they were flash frozen in liquid nitrogen and stored at -80°C for further processing.

4.2.4 Biotin Switch for S-nitrosylated Proteins

Heart tissues were obtained from $P2X_4R$ OE and WT animals (n=5 per group). 8 µm thick tissue sections were subjected to biotin switch staining following the manufacturer's protocol (S-Nitrosylated Protein Detection Kit, Cayman Chemicals, Ann Arbor, MI). The biotin switch method is based on the conversion of nitrosylated cysteines to biotinylated cysteines to allow for detection of the NO-mediated modification of cysteine residues (addition of a nitrosothiol). Slides were visualized on a confocal microscope (Zeiss LSM 510 meta) at 20X magnification. Five 12-bit images of non-overlapping, tissue rich regions were acquired for each slide. Images were segmented for positive staining areas, which were summed across five images to produce a total area for each slide.

4.2.5 Surgical Models of Heart Failure

Animals with similar age (8-10 week old) and body weights were used. Mice were anesthetized with ketamine (100mg/kg) and xylazine (10mg/kg) intraperitoneally. After endotracheal intubation under a dissecting microscope at 37°C, the cannula was connected to a small rodent ventilator (Hugo Sachs-Harvard Apparatus, Minivent Type 845, Holliston, MA) on room air with a stroke volume of 0.3mL at a rate of 150 per minute. All animal procedures were performed according to protocols approved by the University of Connecticut School of Medicine Animal Use and Care Committee.

4.2.5.1 Left Anterior Descending (LAD) Ligation as a model of Myocardial Infarction

Permanent LAD ligation was performed to induce myocardial infarction (MI) related heart failure as previously described.[1] After anesthesia and intubation, a left intercostals thoracotomy was performed. MI was produced by ligating the LAD with an 8-0 nylon suture within 2mm below the edge of the left atrium, near the origin of the coronary artery. Echocardiography was performed at 7 and 30 days after ligation to examine heart function *in*

vivo. Cardiac function was also assessed *ex vivo* at 30 days after ligation, using the working heart preparation (detailed in Section 3.2.4), in which equal loading conditions provide a controlled environment to compare contractile performance, complementing echocardiography measures.

4.2.5.2 Transverse aortic Constriction (TAC) as a model of Pressure Overload Heart Failure

This model is distinct from ischemic injury leading to cardiac tissue death, but represents a state of chronic afterload which the heart must work harder against to deliver sufficient blood. The same opening steps as described above are followed. After left intercostals thoracotomy, the thymus was carefully separated to expose the aortic issues below it and surrounding tissues were carefully dissected to expose the aortic arch. TAC was created by placing a 27-gauge needle on the transverse aorta between innominate and left carotid arteries. A ligature of 7-0 Ethilon nylon suture was tied around the needle and the aorta, after which the needle was removed. The increase in pressure proximal to the constriction was confirmed by an increased Doppler jet velocity across the aortic banding site. After euthanasia, the integrity of the banding was confirmed by inspection of the surgical constriction and by visualization of differences in the caliber of the right and left carotid arteries. All groups of mice had similar pressure gradients across their aortic band. Echocardiography was performed at 7 days and 3 weeks after TAC.

4.2.6 Ablating eNOS activity in WT and $P2X_4R$ OE animals

The NOS inhibitor L-N5-(1-iminoethyl)ornithine hydrochloride (L-NIO; Sigma-Aldrich) was administered via intraperitoneal injection at 40 mg/kg per day[105] beginning at 3 days before LAD or TAC until cardiac function determination at 7 days post surgery. Phosphate buffer saline injections served as vehicle controls.

Mice globally deficient in eNOS (B6.129P2-Nos3^{tm1Unc}/J) were purchased from the Jackson Laboratory (Bar Harbor, Maine) and bred with cardiac-specific $P2X_4R$ OE animals to obtain $P2X_4R$ OE/eNOS KO mice.

4.2.7 Statistics

Statistical differences were mostly assessed by two-tailed Student's t-test. Two-way ANOVA was used to test cGMP content differences across genotype and agonist treatment. Data presented as mean ± SEM. We considered P values less than 0.05 to be statistically significant.

4. 3 RESULTS

4.3.1 $P2X_4R$ can induce NO formation and associates with eNOS

Since the $P2X_4R$ receptor is calcium permeant, it is possible that this receptor can interact with and activate the calcium-dependent endothelial nitric oxide synthase (eNOS). We investigated whether stimulation of P2X receptors in cardiac myocytes can lead to formation of nitric oxide molecules. Using the traditional 4-amino-5-methylamino-2',7'-difluorofluorescein (DAF-FM) diacetate dye for imaging nitric oxide (NO) in $P2X_4R$ OE

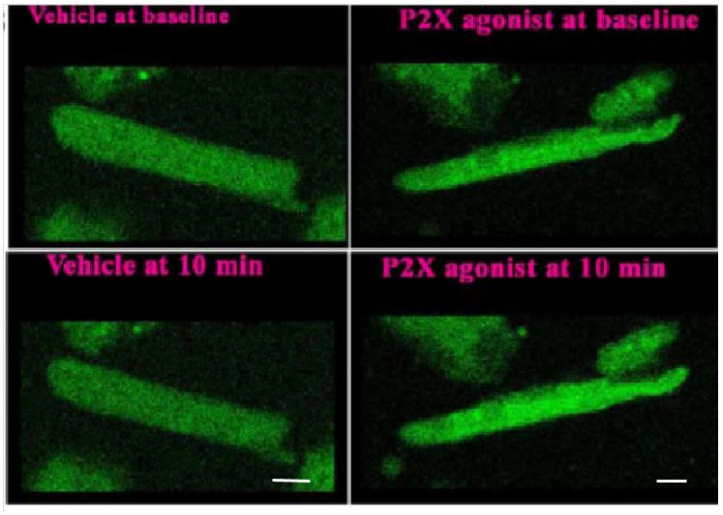

Figure 4.1 Example of change in DAF-FM intensity at baseline vs. after exposure to P2X agonist or vehicle. Note the declined intensity in vehicle-treated cells due to photobleaching of fluorescein. Bars indicate 10μm.

cardiomyocytes, increased fluorescence was observed over baseline or vehicle-treatment following 2-meSATP treatment (Figure 4.1). After 10 minutes, mean intensity with agonist normalized to those with vehicle was 109.3±2.6% (n=33 cells for vehicle-treatment and n=43 cells for 2-meSATP, P<0.05). As evident from vehicle treatment, DAF-FM has the drawback of photobleaching. Thus we repeated NO formation measurements with a newer NO-sensitive fluorescent dye, Cu_2(FL2E), which has been used to image NO formation in a

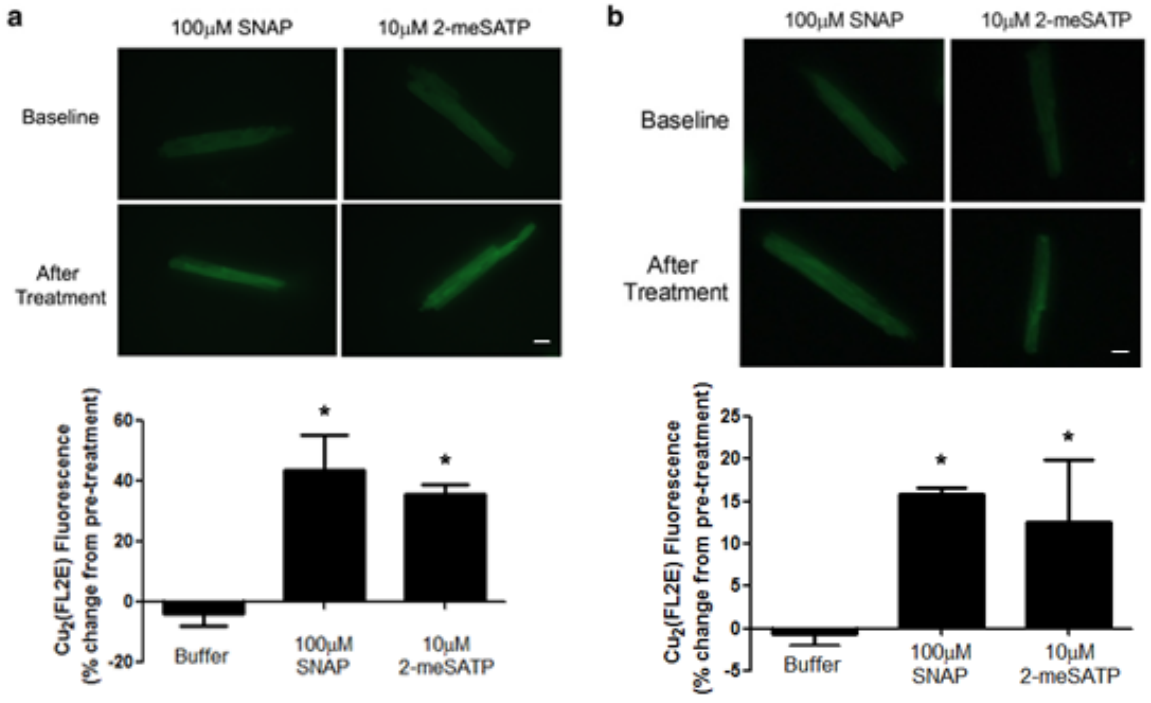

Figure 4.2 2-meSATP stimulated NO formation in $P2X_4R$ OE and WT cardiac myocytes imaged with Cu_2(FL2E) (a) Upper panel: Representative fluorescence images of Cu_2(FL2E) loaded $P2X_4R$ OE cardiac ventricular myocytes before and after SNAP or 2-meSATP treatment are shown. Lower figure: Quantification of fluorescence change normalized to pre-treatment, *P<0.05 using paired t-test for average fluorescence intensity before and after treatment with SNAP (n=4 mice) or 2-meSATP (n = 3 mice) from P2X4R OE animals. (b) Similar studies were carried out in cardiac ventricular myocytes from WT animals (n = 2 mice). Upper and lower panels show typical fluorescence imaging and average fluorescence intensity for treatment with SNAP and with 2-meSATP. *P<0.05 using paired t-test for SNAP or 2-meSATP treatment. 20-80 cells were counted from each mouse for each treatment condition. Bars indicate 10μm.

variety of biological systems, including intact living cardiomyocytes. Cu_2(FL2E) data confirmed NO formation following 2-meSATP stimulation in $P2X_4R$ OE myocytes (Figure 4.2a), as well as in WT myocytes (Figure 4.2b), with the former exhibiting greater NO formation. Thus, using two structurally distinct dyes specific for NO, we demonstrate that NO is increased within cardiac myocytes as a result of P2X receptor stimulation in both $P2X_4R$ OE transgenic myocytes and WT cardiac myocytes.

In considering a mechanism for NO production following $P2X_4R$ stimulation, the $P2X_4$ receptor was found to be present in eNOS immunoprecipitates obtained from cardiac myocytes of both WT (Figure 4.3a) and $P2X_4R$ OE (Figure 4.3b) hearts. The specificity of this physical interaction was supported by the absence of $P2X_4R$ in immunocomplexes captured using an IgG matched control antibody. $P2X_4R$ and eNOS were both more concentrated in sarcolemmal regions as assessed by immunostaining, and appear in close proximity in specific areas along the sarcolemma (Figure 4.3c). Both proteins also showed sarcolemmal staining in WT myocytes, although $P2X_4R$ staining was considerably fainter. The increased NO production in $P2X_4R$ OE hearts was not due to an up-regulation of eNOS protein expression or increased catalytic activity via phosphorylation of the serine 1177 residue (Figure 4.3d). There was no discernible band on immunoblots of WT and $P2X_4R$ OE heart homogenates for phospho-eNOS Thr495, nor for iNOS. No difference was seen in nNOS expression between the two genotypes (blot not shown). These data support the activation of eNOS to produce NO following $P2X_4$ channel activation.

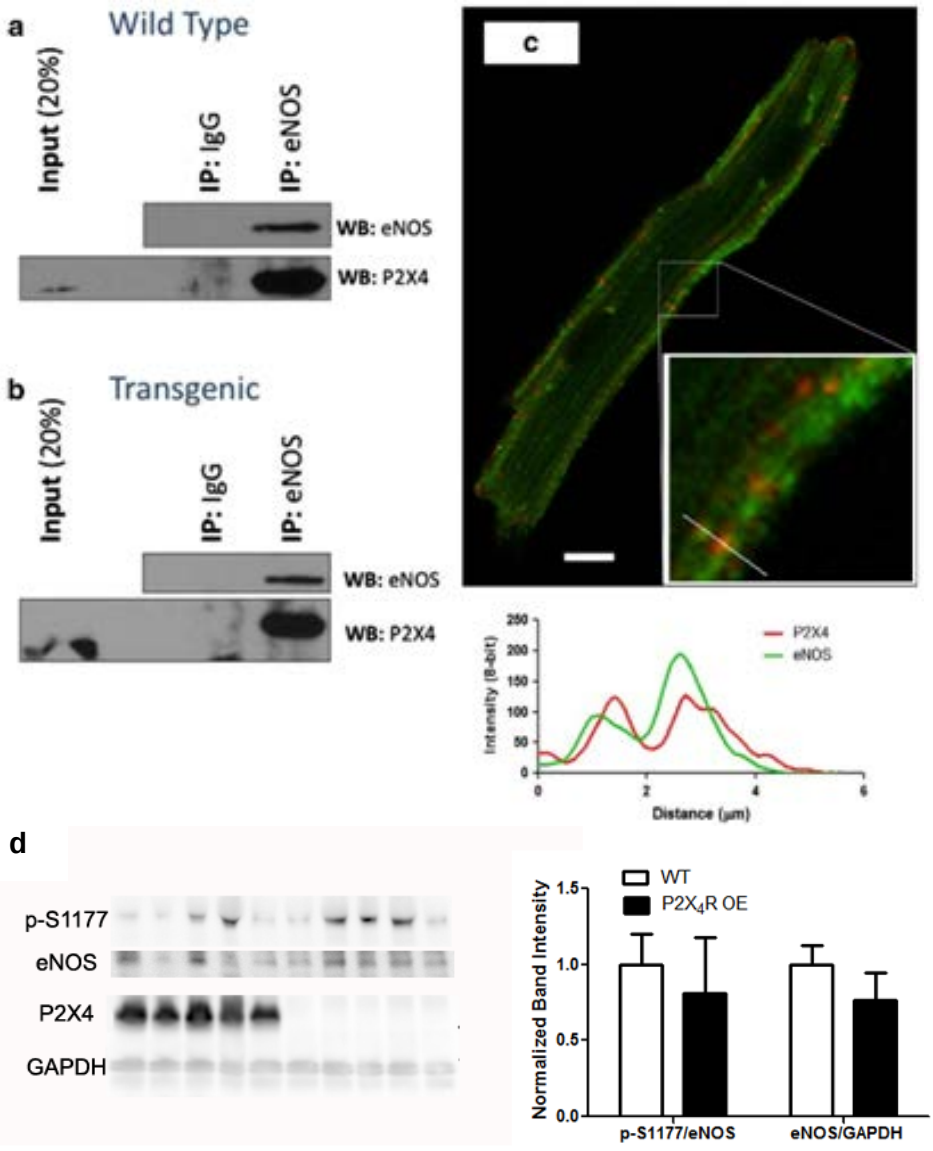

Figure 4.3 $P2X_4R$ and eNOS are co-immunoprecipitated and can exist in close proximity in cardiac ventricular myocytes (a) WT myocyte lysates were incubated with anti-eNOS antibody or with non-specific IgG as control. The isolated complex was probed with eNOS (top panel) and $P2X_4R$ (bottom panel) antibodies. $P2X_4R$ co-immunoprecipitated with eNOS antibody (lane 3) but not with control IgG (lane 2) and self-precipitation by eNOS also served as a control. (b) Same experiment as in (a) conducted in $P2X_4R$ OE transgenic myocytes. (c) Immunostaining of eNOS (green), $P2X_4R$ (red), with merged image shown for a $P2X_4R$ OE cardiac myocyte. Bar indicates 10μm. (d) Protein expression of eNOS did not differ between $P2X_4R$ OE and WT hearts and neither did phosphorylation of Serine 1177 (p-S1177) on eNOS. Blots are shown on the left and lane quantifications shown on the right (n = 5 each, P=0.32 for comparison of eNOS expression as normalized to GAPDH, and P=0.66 for p-S1177 as normalized to eNOS).

4.3.2 $P2X_4R$ stimulated NO formation leads to downstream signaling

NO can induce further downstream signaling activity, likely through stimulation of soluble guanylyl cyclase activation and 3′,5′-cyclic GMP (cGMP) formation, as well as through the more recently discovered S-nitrosylation of cellular proteins. Indeed there was an increased level of myocardial S-nitrosylation in P2X4R OE hearts as compared to WT hearts (Figure 4.4a), in agreement with enhanced endogenous NO production. To assay potential changes in cGMP, isolated hearts were perfused with buffer, 10μM 2-meSATP, or 100μM NO donor SNAP. SNAP caused a large increase in cGMP levels (buffer-perfused $P2X_4R$ OE: 2.61±0.33 fmol/mg, n=5 vs. SNAP-perfused $P2X_4R$ OE: 5.61±0.40 fmol/mg, n=5, $P<0.05$). The cGMP level was also higher in $P2X_4R$ OE hearts than in WT hearts after 2-meSATP treatment, with similar drug responses in both genotypes (WT+buffer: 2.36±0.21 fmol/mg, n= 15; WT+2-meSATP: 2.83±0.26 fmol/mg, n=12; $P2X_4R$ OE+buffer: 2.76±0.19 fmol/mg, n=18; $P2X_4R$ OE+2-meSATP: 3.39±0.20 fmol/mg, n=16; two-way ANOVA $p<0.05$ for both $P2X_4R$ OE and 10μM 2-meSATP treatment with no

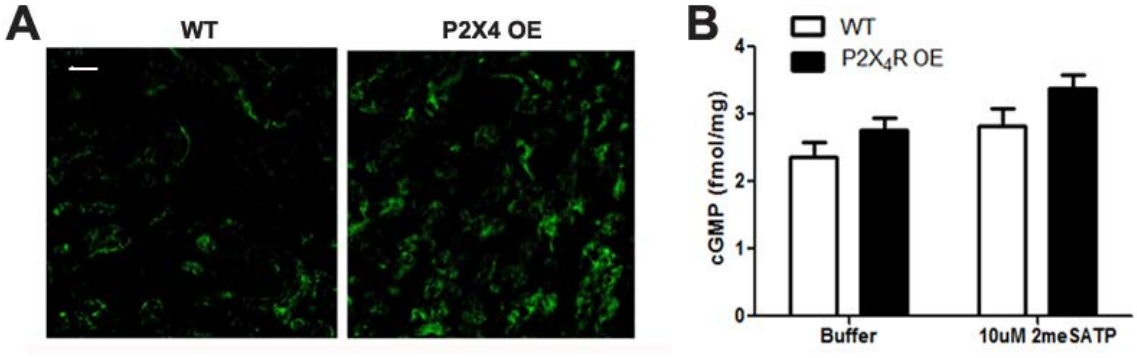

Figure 4.4 Increased cardiac protein S-nitrosylation and cGMP content in $P2X_4R$ OE animals. (A) Typical examples of S-nitrosylated proteins in $P2X_4R$ OE and WT hearts (n = 5 for each) as determined using the biotin switch method. Bar indicates 30μm. Summed positive areas from 5 images per heart produced one total area for each heart, with $P2X_4R$ OE hearts showing a significantly greater area of positive staining compared to WT (58563±9603 pixels for $P2X_4R$ OE vs. 31589±3771 pixels for WT, P=0.03). (B) Cardiac tissue cGMP content is overall significantly higher in $P2X_4R$ OE hearts vs. WT and in hearts that have been perfused with 10μM 2-meSATP vs. buffer (n= 15 for WT + buffer, n=12 for WT + 2-meSATP, n=18 for P2X4R OE + buffer, and n=16 for $P2X_4R$ OE+ 2-meSATP).

significant interaction, summarized in Figure 4.4B). These data are consistent with stimulation of the overexpressed cardiac $P2X_4R$ by endogenous extracellular ATP leading to S-nitrosylation of proteins and cGMP formation in $P2X_4R$ OE hearts. Overall, multiple lines of evidence point to $P2X_4$ receptor-induced intra-myocyte NO production with downstream functional consequences.

4.3.3 Cardiac $P2X_4R$ OE improved function after Pressure Overload

In addition to the previously demonstrated salutary effect of $P2X_4R$ OE against ischemia cardiac injury, $P2X_4R$ OE mice were also protected against pressure overload induced HF. The differences between $P2X_4R$ OE and WT manifested early. As early as 7 days after TAC, echocardiographic assessment demonstrated a significant difference between WT and $P2X_4R$ OE mice, and better preserved function in $P2X_4R$ OE mice continued to be evident at 3 weeks (Figure 4.5). 3 weeks after TAC, we observed moderate left ventricular hypertrophy with reduced cardiac fractional shortening in most animals but no overt HF or arrhythmias. $P2X_4R$ OE hearts also showed less fibrosis than WT hearts (n=16 for $P2X_4R$ OE, n=11 for WT, $P<0.05$ with both Picrosirius Red and Trichrome staining).

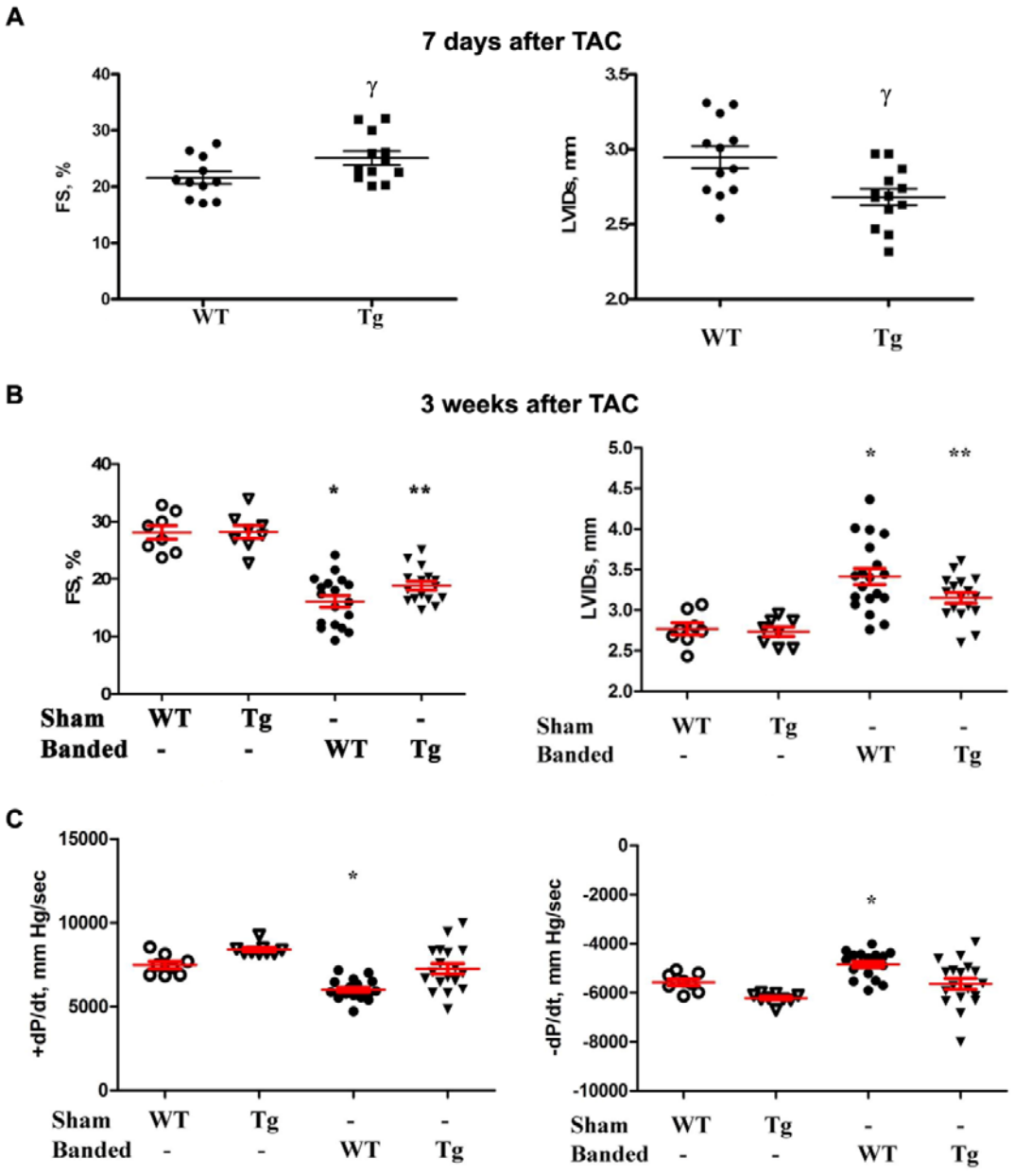

Figure 4.5 P2X$_4$R OE hearts have better cardiac function after transverse aortic constriction. (A) P2X$_4$R transgenic (Tg) mice (n=12) had better preserved fractional shortening (FS) and greater ejection as marked by smaller left ventricular internal diameter at end systole (LVIDs) compared to WT (n=11) at 7 days after TAC. (B) Echocardiographic parameters again demonstrated higher FS and smaller LVIDs in P2X$_4$R Tg (n=16) than WT (n=18) 3 weeks after TAC. (C) Examining heart function *ex vivo* showed greater +dP/dt and –dP/dt in Tg (n=18) than WT (n=18) hearts. $^{\gamma}$ P<0.05 P2X$_4$R Tg vs. WT after 7 days of aortic banding; *P<0.05 WT subjected to TAC was lower vs. sham WT (n=8), sham Tg (n=8 and 9) or Tg subjected to TAC; ** P<0.05 Tg subjected to TAC was different from sham Tg or sham WT.

4.3.4 Role of eNOS in mediating the protective effect of $P2X_4R$ in Heart Failure

In order to examine the role of eNOS in mediating $P2X_4R$ protection, we used a pharmacological inhibitor of NOS, L-NIO, as well as gene ablation of eNOS in $P2X_4R$ OE mice during heart failure (summarized in Figure 4.6). In one set of studies, we used the ischemic heart failure model involving permanent ligation of the LAD coronary artery to cause post-infarct heart failure. $P2X_4R$ OE led to a higher cardiac left ventricular fractional shortening (FS) after infarction, but no infarct size difference was observed in mice of various genotypes that were subjected to the ligation. Daily injection with L-NIO, which has been used to demonstrate eNOS function *in vivo*,[105] abrogated the improved cardiac performance of $P2X_4R$ OE mice during ischemic HF when compared to WT, as determined by both *in vivo* echocardiography and by *ex vivo* working heart examination.

To further confirm the role of eNOS in mediating the protective effect of the $P2X_4R$ during HF, eNOS KO mice were crossed with $P2X_4R$ OE mice ($P2X_4R$ OE/eNOS KO). KO of eNOS abrogated the protected phenotype conferred by the $P2X_4R$ OE genotype in postinfarction HF. Both the improved + dP/dt and FS in $P2X_4R$ OE mice during HF were lost in $P2X_4R$ OE/eNOS KO mice. To ascertain whether the protective effect of $P2X_4R$–eNOS is applicable to another form of HF, we tested the effects of $P2X_4R$-induced protection by pharmacological inhibition of eNOS on pressure overload HF. Pressure overload was produced by aortic banding in $P2X_4R$ OE and WT mice. $P2X_4R$ OE hearts showed better cardiac function as determined by echocardiography- derived FS after aortic banding. L-NIO blocked the increased FS in these animals. KO of eNOS in Tg animals also abrogated the improved FS in these Tg mice after aortic banding. These data provide functional evidence for a $P2X_4R$–eNOS interaction and support a key role of eNOS as a mediator of cardiac $P2X_4R$-induced protection in HF.

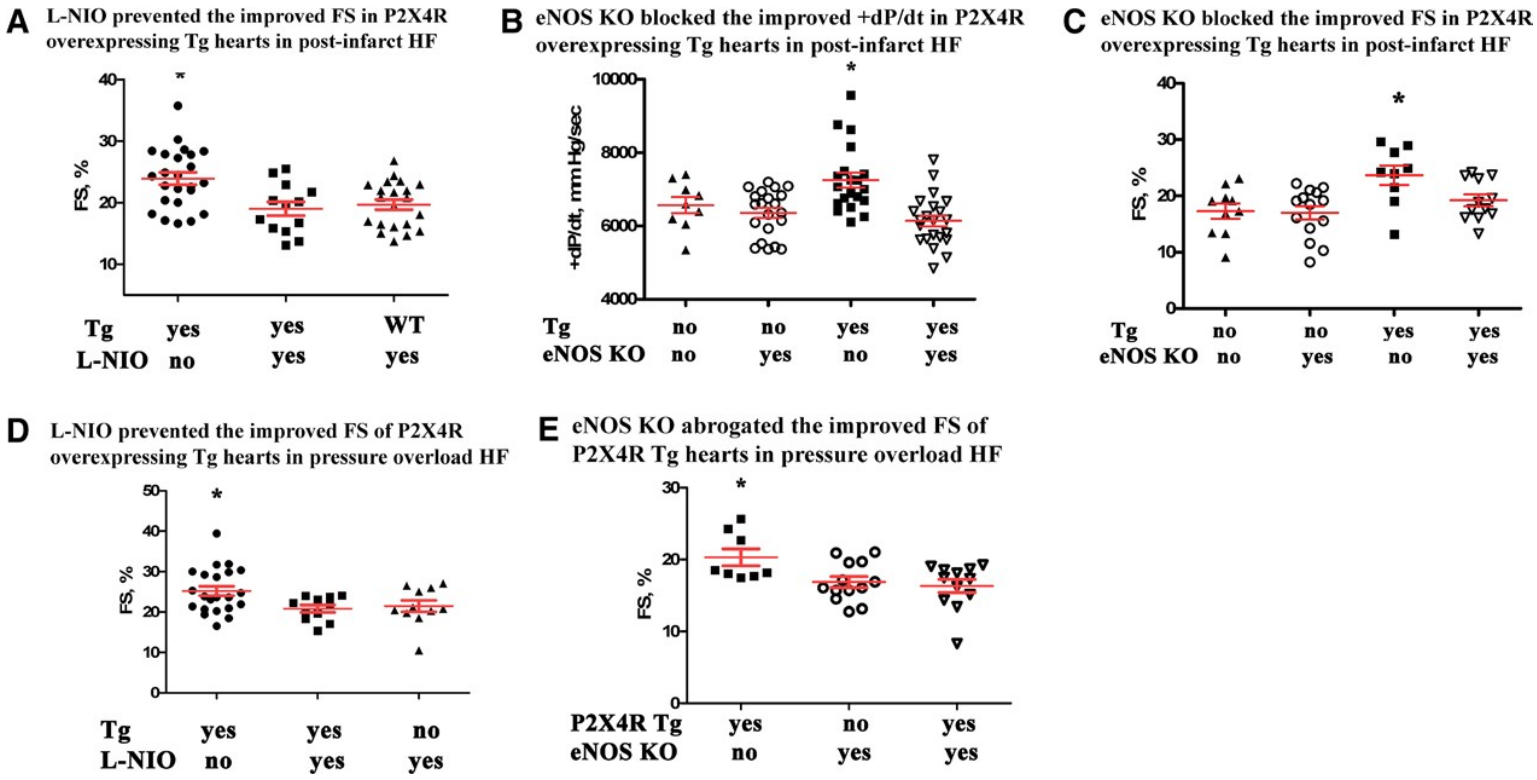

Figure 4.6 eNOS activity inhibition abrogated the improved cardiac function by $P2X_4R$ overexpression in heart failure. (A) Daily injection of L-NIO 3 days before and 7 days after LAD coronary artery ligation in $P2X_4R$ OE transgenic (Tg) mice (n=13) resulted in a reduced FS compared with $P2X_4R$ OE mice not receiving drug (n=24). $P2X_4R$ OE mice receiving L-NIO had similar FS as WT receiving the drug (n=21). (B) KO of eNOS in $P2X_4R$ OE mice blocked the improved +dP/dt and (C) FS by $P2X_4R$ overexpression in postinfarct heart failure thirty days after LAD ligation. $P2X_4R$ OE mice (n=20) showed better +dP/dt compared with $P2X_4R$ OE/eNOS KO (n=22), WT (n=9), or eNOS KO mice (n=21). Similarly, $P2X_4R$ OE mice (n=9) had greater FS than any other genotype at 30d after ligation. WT (n=10), eNOS KO (n=14), $P2X_4R$ Tg/eNOS KO mice (n=12) did not differ in FS (ANOVA and post-test comparison). 3 weeks after TAC, (D) $P2X_4R$ Tg mice treated with vehicle subjected to TAC (n=22) had higher FS compared with Tg animals that had received L-NIO injections (n=11); WT (n=11) and $P2X_4R$ Tg mice treated with L-NIO had similar FS. (E) $P2X_4R$ OE mice (n=8) showed better FS compared with $P2X_4R$ Tg/eNOS KO (n=12) or eNOS KO mice (n=13). *P<0.05 vs any other group on the same graph. P>0.05 among groups not marked.

4.4 DISCUSSION

In adult murine ventricular myocytes, the P2X agonist 2-meSATP induced a nonselective cation current with reversal potential similar to that of the cloned $P2X_4$ receptor.[47] Transgenic mice with cardiac-specific overexpression of the human $P2X_4R$ have previously been shown to be protected from ischemic HF induced by LAD ligation and from a genetic model of dilated cardiomyopathy from the overexpression of calsequestrin.[1, 52] Previous evidence suggested that activation of cardiac P2X receptors can elicit a cyclic AMP-independent increase in cardiac contraction[106] and as we discussed in the previous chapters, an electrophysiological basis exists for increasing myocardial calcium transients and contraction.[47, 107] However, the mechanisms by which these ligand-gated channels protect against HF remain incompletely understood. Here we demonstrated that eNOS is an effector in $P2X_4R$-mediated cardioprotection.

Direct measurement of NO production was made in $P2X_4R$ OE and WT cardiac myocytes after 2-meSATP stimulation. DAF-FM demonstrated a greater stimulated increase in NO level in $P2X_4R$ OE over WT myocytes. The newer NO-sensitive dye Cu_2(FL2E) corroborated the finding, showing enhanced fluorescence in both WT and $P2X_4R$ OE cardiac myocytes after treatment with the agonist, and a larger magnitude of change in the $P2X_4R$ OE myocytes. Furthermore, the level of S-nitrosylated proteins and cGMP were higher in transgenic than in WT hearts, consistent with a greater stimulation of endogenous NO production by the overexpressed $P2X_4$ receptors in transgenic hearts. These findings provide functional evidence for the activation of eNOS downstream of cardiac $P2X_4$ receptors. The expression of eNOS in cardiac myocytes is relatively low,[108] but a modest increase in DAF fluorescence by a synthetic nitrone in murine cardiac myocytes had a functionally significant impact in reversing contractile dysfunction,[109] and our data showed a similar degree of increase in DAF fluorescence after P2X agonist stimulation. The $P2X_4$ receptor coimmunoprecipitated with eNOS in isolated cardiac myocyte lysates from both $P2X_4R$ OE and WT animals. Co-immunostaining of $P2X_4R$ and eNOS in the

sarcolemma of $P2X_4R$ OE transgenic cardiac myocytes further supports an interaction of these two proteins. In considering other aspects of eNOS activation, phospho-eNOS Ser1177 normalized by total eNOS expression was unchanged in $P2X_4R$ OE vs. WT hearts. Phosphorylation of Ser1177 increases eNOS catalytic activity, representing a mechanism of eNOS activation different from that achieved by calmodulin binding.[110] We postulate that the mechanism of eNOS activation by $P2X_4$ receptors is from Ca^{2+} increase and subsequent calmodulin binding and may not involve Ser1177 phosphorylation. A close proximity between $P2X_4$ receptor and eNOS may prime for a confined domain of calcium to activate calmodulin and subsequently eNOS. In endothelial cells where eNOS is more abundant, $P2X_4R$ has also been implicated in stimulating eNOS,[56] though the physical interaction between $P2X_4$ receptor and eNOS remains unstudied in the endothelium.

If the interaction of eNOS with cardiac $P2X_4$ receptor is important in mediating the protective effect seen in $P2X_4R$ OE animals, one would expect that the inhibition of eNOS could block the cardiac $P2X_4$ receptor protective effect, and we indeed found this. Either pharmacological inhibition of eNOS by L-NIO or genetic KO of eNOS abrogated the HF protective effect of cardiac $P2X_4R$ OE. Cardiac $P2X_4R$ OE ameliorated both ischemic and pressure overload forms of HF. The cardioprotective effect of eNOS in ischemia/reperfusion injury and in post-infarct HF has been demonstrated in eNOS-overexpressing transgenic animals [111-113]. Upregulating eNOS by H_2S has also been shown to protect against pressure overload HF.[114] Although eNOS overexpression or upregulation is cardioprotective, eNOS KO has been reported to increase, decrease, or cause no change in ischemia/reperfusion injury.[111] The reason for these variable findings may have to do with the presence or absence of a compensatory upregulation of inducible NOS in some of the eNOS KO mice. The $eNOS^{-/-}$ line used in the present study, developed at the University of North Carolina and now available from the Jackson Laboratory, has been shown to have upregulated iNOS.[111] We did not observe a more severe HF phenotype after infarction in these eNOS knockouts, consistent with their

compensated phenotype. Nonetheless, protection provided by the $P2X_4R$-eNOS interaction in the $P2X_4R$ OE hearts was abrogated by eNOS knockout.

Additional caution was exercised when interpreting the data from L-NIO and eNOS KO mice. While L-arginine analogues such as L-NIO are believed to be NOS inhibitors, they may have other actions that secondarily affect remodeling after pressure overload or infarction as a consequence of its inhibition of eNOS in the endothelium, such as inducing hypertension and vasoconstriction. The eNOS KO animals exhibit mild hypertension and LV hypertrophy that could in turn confound the salutary effect of cardiac myocyte-specific $P2X_4R$ OE. A more severe HF could potentially result from pressure overload in eNOS KO animals, which may in turn abrogate the beneficial effect of cardiac $P2X_4R$ OE. However, when the same eNOS KO mice as used here were subjected to abdominal aortic banding, they did not show LV dilation when compared with WT controls.[115] In fact, ejection fraction was greater in eNOS KO than in WT mice after abdominal banding. This apparent protection against abdominal banding may be because of the compensatory upregulation of iNOS. However, in our postinfarct hearts, eNOS KO was not protective because cardiac function was similarly depressed in both eNOS KO and WT mice (Figure 4.6B).

The present data are consistent with previously reported protection by eNOS via the T-type calcium channel in pressure overload HF.[105] Although eNOS is cardioprotective, the downstream effectors mediating eNOS activity are not entirely clear. Possible candidates include cGMP, protein kinase G, and cellar protein S-nitrosylation.[58, 116] Cardiac-specific activation of eNOS may be more cardioprotective than an increased activity of global systemic eNOS[113] and intra-myocyte formation of nitric oxide may be more advantageous over nitric oxide derived externally from a donor. Overall, new evidences support a $P2X_4R$-eNOS interaction and its functional significance in HF protection, pointing to a novel sarcolemmal receptor-enzyme pathway in the heart.

Chapter 5

Conclusions[e]

5.1 SUMMARY OF FINDINGS

P2X receptors are ligand-gated ion channels that regulate various physiological processes and have emerged as promising therapeutic candidates for treatment of several pathophysiological conditions such as heart failure. The transition from experimental validation to clinical use necessitates a detailed mechanistic understanding of P2X mediated cardiac effects, as well as potential side-effects of targeting these receptors. In the studies presented in this dissertation, the downstream effects of activating these extracellular ATP responsive receptors in cardiac myocytes were examined in a transgenic mouse model with cardiac specific overexpression of the $P2X_4$ subtype ($P2X_4R$ OE), as compared to wildtype (WT) and other animals with relevant genetic modifications. We focused on electrophysiological consequences that are of paramount importance to the cardiomyocyte and also uncovered a novel protein interaction that has functional implications downstream of altered ion handling. First, in Chapter 2 we confirmed the hypothesis that cardiac P2X receptors can modulate the cardiac contractile state by adjusting Na^+ handling. Measurements of Na^+-K^+ ATPase (I_p) and Na^+/Ca^{2+} exchanger (I_{NCX}) currents in ventricular myocytes isolated from $P2X_4R$ OE mice indicated that the agonist, 2-methylthio adenosine-5-triphosphate (2-meSATP), increased peak I_p and the Ca^{2+} entry mode of I_{NCX}. These results were supported by simulation and showed that 2-meSATP caused an estimated $[Na^+]_i$ increase of around 1mM. Inhibitors that preferentially oppose the Ca^{2+} entry mode of NCX, KB-R7943 or a structurally different agent YM-244769, blunted the 2-meSATP-induced increase in cell shortening in $P2X_4R$ OE myocytes, suggesting that the Ca^{2+} entry mode

[e] Part of this chapter exists in print: Yang R, Liang BT. "Cardiac P2X4 Receptors: Targets in Ischemia and Heart Failure?" Circ Res. 111:397-401. 08/2012.

of I_{NCX} participates in the P2X agonist-stimulated enhancement in contraction. In ventricular myocytes from WT mice, despite a limited responsive subpopulation, P2X agonist also increased I_{NCX} and KB-R7943 was able to inhibit contractile effects elicited by the agonist. These data demonstrate a novel Na^+ entry pathway through ligand-gated $P2X_4R$ in cardiomyocytes that can subsequently modify contractile responses via the NCX.

In Chapter 3, we described experiments designed to better understand the potential balance between arrhythmogenic effects versus anti-ischemic and heart failure protection benefits of $P2X_4$ receptor activation. Again utilizing cardiac specific $P2X_4R$ OE animals, we found that activation of these receptors could lead to a brief period of membrane disturbance lasting around half a minute, which can be mimicked with a computational model based on known $P2X_4$ current kinetics. This transient excitability of the $P2X_4R$ OE cardiomyocytes did not translate to enhanced automaticity in the whole heart, and supports the notion of targeting P2X subtypes for cardiac inotropic support with transient effects on excitability. Previous conflicting results reflect measurements at different time points in the dynamic response and could also result from different agonists and doses used in the studies. Low concentrations of P2X agonist may be able to elicit an increase in contraction but not induce sufficient depolarization to cause ectopic beats and diastolic calcium buildup, which were only observed at >10μM of ATP and likely involve mechanisms other than P2X activation. Additionally, we unveiled a previously unreported biphasic response to P2 agonism in the mouse heart, which was present in WT and $P2X_4R$ KO animals as well. This substantiates the existence of multiple subtypes of P2 receptors in the native heart and emphasizes the importance of understanding the actions of specific P2 subtypes.

Lastly, in Chapter 4 we reported a novel feature of the $P2X_4R$ in that the receptor is not just an ion channel, but can associate with the enzyme endothelial nitric oxide synthase (eNOS). In the cardiac myocyte, we showed that $P2X_4$ receptor stimulation causes activation of eNOS,

as demonstrated by increased NO formation with two structurally distinct NO-sensitive fluorescent dyes. Cardiac tissue from $P2X_4R$ OE mice also showed enhanced S-

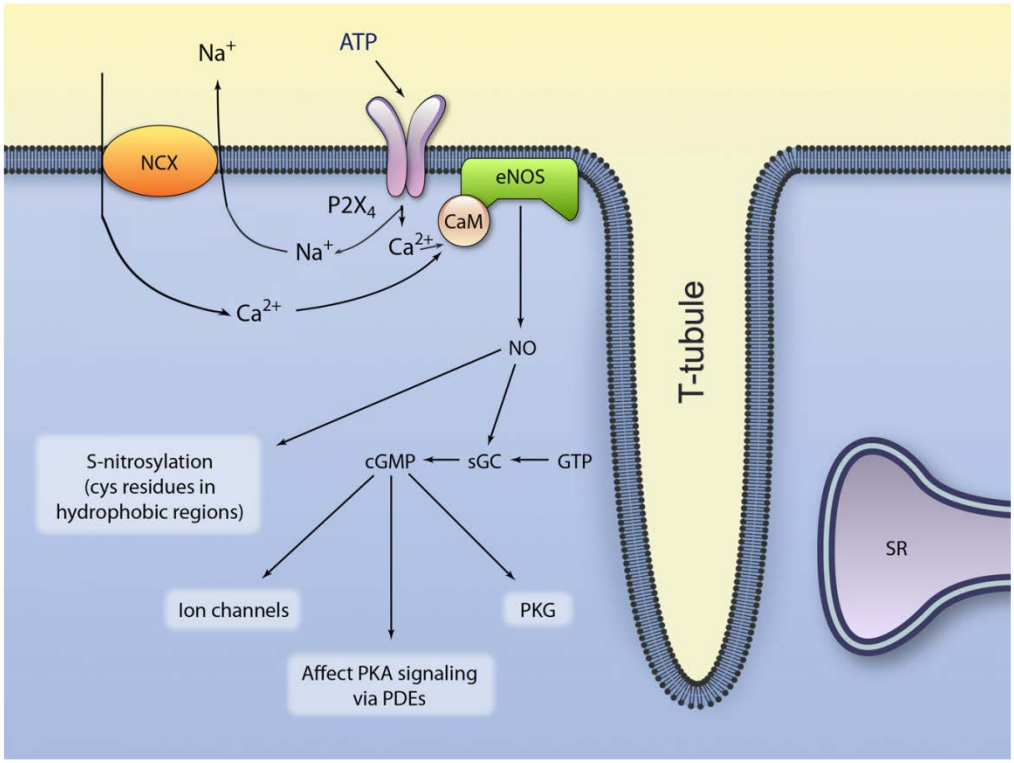

Figure 5.1 Model of the mechanism of action of P2X receptors in cardiac myocytes Ionic influx due to activation of the $P2X_4$ receptor can lead to intracellular Na^+ and Ca^{2+} concentration changes, partly by affecting the NCX. A localized increase in Ca^{2+} near eNOS can increase eNOS activity via calmodulin dependent activation. Some of the increase in calcium is taken up by the sarcoplasmic reticulum (SR). NO production can lead to stimulation of soluble guanylyl cyclase (sGC) with cyclic GMP accumulation as well as S-nitrosylation of myocardial proteins. The NO pathway is known to exert a salutary effect in heart failure and in ischemic injury.

nitrosylation and cGMP content. Blunting eNOS activity in $P2X_4R$ OE animals abrogated the protective effect seen in these animals after surgically induced cardiac injury, consistent with a functional significance for the $P2X_4R$–eNOS pathway in mediating cardioprotection in heart failure.

Overall, we propose the model summarized in Figure 5.1, where Na^+ entry via the $P2X_4$ receptor enables further ion exchange through the NCX to enhance calcium retention inside the cell. It is conceivable that $P2X_4$ flux exerts a primarily localized control over calcium mediated signaling with minimal or no effect on Ca^{2+} influx in the dyadic space. Diffusion of Ca^{2+} ions allows them to reach and enter the SR for enhanced loading and inotropic enhancement. The close physical distance between the $P2X_4R$ and eNOS primes NO production, which is beneficial in the setting of ischemic injury and heart failure.

5.2 FUTURE DIRECTIONS

5.2.1 Additional $P2X_4R$ considerations for Regulating Cardiac Function

In addition to directly modulating cardiomyocyte ion handling in the classical excitation contraction paradigm, the $P2X_4$ receptor has been implicated in a number of physiological processes that could indirectly modify cardiac function. Another possible mechanism by which $P2X_4R$ may be of benefit in the diseased heart may lie with its mechanosensitive properties. It is structurally similar to members of the mechanosensitive epithelial Na^+ channel (ENaC) family, and it has been shown that $P2X_4$ receptor desensitization to repeated ATP stimulation is prevented by applying shear stress to $P2X_4$ expressing Xenopus oocytes.[117] While this open-channel stabilizing mechanism is conceptually different from that of mechano-induced ATP release and subsequent channel activation,[56] they both support an important role for $P2X_4R$ in cellular response to mechanical force. In the remodeling heart experiencing increased mechanical stress, it is possible that enhanced $P2X_4R$ stimulation/opening may serve to enhance cardiac contractility. Detailed examination of $P2X_4$ activation and kinetics in myocytes under mechanical loading may be feasible with recently developed techniques.[118] Additionally, the $P2X_4R$ has recently been demonstrated to exist on lysosome-related exocytotic vesicles. Fusion of these vesicles to the plasma membrane leads to localized calcium increase that further induces Ca^{2+}-dependent vesicular fusion, promoting compound exocytosis.[119] While the

molecular exocytotic machinery in the heart is not well understood, it is tempting to speculate that enhanced $P2X_4R$ signaling in ischemia or heart failure may augment cardiac release of vesicular contents, which could contain cytokines and/or cardioprotective factors. Secretion of natriuretic pepetides and vascular endothelial growth factor (VEGF) are known to be stimulated under a number of conditions that involve hypoxia and mechanical stretch;[120, 121] and $P2X_4R$-mediated release of inflammatory mediators such as the known cardioprotectant brain-derived neutrophic factor (BDNF)[122] and $P2X_4R$ involvement in NLRP1 inflammasome signaling have been demonstrated in spinal cord and peripheral nerve injuries.[123] These scenarios are also pertinent to myocardial injury, in which inflammatory responses are necessary for tissue repair but need to be controlled and weighed against compensatory mechanisms to improve cardiac function. The $P2X_4R$ receptor may be a novel participant in the regulation of this process.

In response to peripheral inflammatory challenges, mice lacking the $P2X_4R$ show a complete absence of inflammatory prostaglandin E2 (PGE2) in tissue exudates and consequently do not develop pain hypersensitivity due to the lack of PGE2 promotion of sensory neuron hyperexcitability. PGE2 synthesis involves the activation of a multi-step enzymatic cascade that includes cyclooxygenases (COXs), the targets of nonsteroidal anti-inflammatory drugs. COX-2 inhibitors are used as anti-inflammatory and pain medication worldwide, though they have been associated with elevated cardiovascular risk.[124, 125] While a $P2X_4R$ antagonist may be useful as a new therapy to treat neuropathic pain,[126] our current data suggest that its antagonism may be deleterious to those individuals under cardiac stress as well, including heart failure. Modulating inflammatory responses has been considered a potential therapeutic approach to preserve and recover heart function after myocardial infarction as well,[127, 128] and the role of the $P2X_4R$ in this setting remains to be clarified. A number of mouse models with cell type specific knockout of the $P2X_4R$ are currently under development in our lab to permit determination of the function of each component (cardiac myocytes, endothelial cells, and monocytes) without confounding influence from other tissues and will together serve to

illuminate a better systemic view of targeting this receptor in cardiac treatment. Recent data on cardiac specific $P2X_4R$ knockouts showed worse outcome after ischemic and pressure overload injuries,[129] consistently with myocyte $P2X_4$ receptors being cardioprotective in disease.

5.2.2 Understanding Human Polymorphisms in P2X receptors

Genetic variants in the human population can be quite informative about the mechanisms of disease. In two Australian cohorts of healthy human subjects, containing 430 and 2874 subjects, a common allele with a non-synonymous single nucleotide (Tyr315→ Cys) polymorphic variant of the $P2X_4R$ gene was found to occur at a frequency of 1.1 and 1.4% respectively. This loss-of-function genetic variant in humans is associated with increased blood pulse pressure,[57] consistent with the role of $P2X_4R$ in regulating vascular tone.[56, 130] It has also been found, along with another polymorphism in the $P2X_7R$ gene, to form a haplotype that increases the risk of age-related macular degeneration in a cohort of 744 patients vs. 557 controls, likely due to impaired monocyte phagocytosis.[131] These observations are consistent with important roles for the $P2X_4R$ in processes that could impact cardiac function and remodeling after injury and it would be of interest to test if this variant occurs with a higher prevalence in heart failure. Complementary to the tissue specific knockout models, global and tissue specific knockins of this polymorphic variant can serve as more relevant study models for human disease.

5.2.3 Calcium and Nitrosative Signaling in Heart Failure

Electrophysiological remodeling in HF is complex and evolves over time as HF progresses. In the early stages of HF, Ca^{2+} transients can be increased, likely due to elevated intracellular Na^+ concentration and relatively normal SR function at this time point.[132] In the late stages of HF, SERCA down-regulation and RyR leakiness depress SR storage, and along with modifications of sarcolemmal channels and T-tubule disruption, contribute to dyssynchronous

calcium release and impaired contraction.[133] The cause and sequence of these changes remain mostly unclear. Oxidative and nitrosative balance is also disturbed in heart failure. In healthy tissue, superoxide is produced by xanthine oxidase, mitochondria, and NADPH oxidase, and becomes rapidly buffered by glutathione and broken down by superoxide dismutase.[109] The diseased myocardium has elevated superoxide levels, along with a nitroso-redox imbalance, can alter the function of a variety of excitation-contraction coupling proteins leading to contractile dysfunction.[133, 134] Dysfunctional NOS activity has been shown to lead to hyponitrosylation of the RyR receptor, contributing to SR calcium leak and enhanced xanthine oxidase activity.[135, 136] Antioxidant treatments have been shown to increase contractile function and promote cardioprotection in failing hearts,[137, 138] with success possibly incumbent on NO bioavailability.[139] Therapies aimed at increasing endogenous NO bioavailability may also be beneficial.[140] Whether P2X dependent enhancement in contraction and NO production can function with significant late alterations in the failing cardiomyocyte remain to be examined, as timing of therapy will likely impact outcome. Early intervention may be necessary to observe optimal $P2X_4$-mediated protection.

5.2.4 Developing pharmacological tools and therapeutic drugs

In addition to P2X-mediated contractile enhancement and cardioprotection, recent studies have also suggested differential roles played by various P2 receptors. $P2Y_{11}$ receptors may be largely responsible for ATP-induced inotropic increase, acting through cAMP and PLC dependent pathways.[89] The $P2Y_2$ receptor has been suggested to mediate UTP-conferred protection against myocardial damage after myocardial infarct,[141] though the existence of this receptor at the protein level has not been confirmed in the human heart.[41] In $P2Y_2$ knockout mice, the UTP-conferred reduction in infarct size and improvement in cardiac function were abrogated.[141] Additional evidence supports stimulation of $P2Y_2$ receptors as a protective

mechanism to decrease angiotensin type 1 receptor density in cardiac fibroblasts through inducible NOS-mediated S-nitrosylation of the p65 subunit of NF-kB, thus negatively regulating angiotensin II-mediated inflammatory responses in the heart.[142] The $P2X_7$ receptor has also been implicated in mediating effects of ischemic preconditioning and postconditioning, by interacting with pannexin-I hemichannels to release multiple cardioprotectants in Landendorff *ex vivo* rat hearts,[143] which could be interesting given the functional haplotype with $P2X_4R$. However, another study exposing HL-1 atrial cells to hypoxic stress in culture detected an early rise in ATP in culture, followed by increased release of cytoplasmic histone-associated DNA-fragments, indicating cell death that was thought to be directly induced by $P2Y_2$ and $P2X_7$ receptor subtypes, whereas the $P2Y_4$ receptor was thought to exert a protective effect.[144] Addition of apyrase to degrade extracellular ATP, or adding GAP26 or 18aGA to inhibit connexin hemichannels, also abolished hypoxic stress-associated apoptosis.[144] The implications of these results warrant further characterization and studies across different model systems. Understanding the physiological roles of individual P2 receptors in the heart will be imperative as interest grows in targeting purinergic receptor signaling in treating heart failure and ischemia. The many permutations of subtype combinations and the paucity of highly selective agonists and antagonists have made it difficult to ascertain the specific role of each P2 receptor in the heart. Additional pharmacological tools, accompanied by genetic modifications and our increasing ability to differentiate cells into specific lineages, may prove efficient at elucidating cell type-specific molecular and cellular mechanisms.

Coronary heart disease and myocardial infarction are disorders of high prevalence and incidence. According to the American Heart Association, a heart attack occurs every 34 seconds. Our results indicate that a small molecule drug stimulating or gene therapy-mediated overexpression of the $P2X_4R$ in cardiac myocytes may represent a new therapy for both ischemic and pressure overloaded HF. In light of the recent crystal structure obtained from zebrafish $P2X_4R$ in the open state with ATP binding,[145] new information on the conformational

changes associated with P2X channel gating will enable guided design of new pharmacological agents. Crystal structure and site-specific mutagenesis of $P2X_4R$ have elucidated the ATP-binding pocket, which resides at each pair of subunit interfaces in the trimeric channel. Four positively charged lysine and arginine residues line the binding pocket for ATP, whose phosphate groups mediate ligand specificity (ATP>ADP, AMP). Lys70 and Thr189 (Lys67 and Thr186 in human homologue) are important in maintaining specificity over CTP, GTP, and UTP.[145] The human Tyr315Cys mutation that disrupts agonist binding is located within this pocket. Additionally, the open state of the receptor leaves relatively large gaps that could be filled in by lipids and allosteric modulators such as ivermectin.[145] Detailed mechanisms of how the open state can be stabilized by such modulators, and more intriguingly by mechanical forces,[117] would be of interest in future investigations. Additional challenges in drug design include rapid adenine nucleotide degradation by extracellular nucleotidases and the negative charges on nucleotides preventing oral absorption. Development of nucleotidase-resistant ligands[146] and prodrugs at $P2X_4$ receptors with masked charges that can be restored after oral absorption are additional goals for clinical application.

5.2.5 Computational Modeling of the Cardiac System

Quantitative modeling has served to enhance our understanding of AP generation and excitation contraction coupling for more than half a century, reaching an advanced level allowing accurate predictions for experimental studies. In our case, simulation results prompted studies that helped to explain prior experimental disagreements and confirmed the notion that P2X activation can achieve inotropic enhancement. While some improvements can be made to incorporate more detailed descriptions of cardiac ion channels and proteins involved in EC coupling, such as incorporating Markovian models of the Na^+/K^+ ATPase[147] and SERCA[148], more interesting areas for future modeling investigations will involve channel modulation by cell signaling pathways. Beta-adrenergic receptor and calcium/calmodulin-dependent protein kinase

type II signaling pathway models in the heart have been under development,[132, 149, 150] and nitric oxide signaling would be another area of major interest. Models of myocardial energetics are also being pursued,[151, 152] which would serve as a crucial link to understand mismatched energy supply and demand in heart failure and to understand the interactions between metabolism and intracellular redox and nitrosative regulations.[153] The actions of signaling proteins on their molecular targets and the dynamics of the signaling pathway need to be incorporated, along with spatial considerations and information transfer between organelles, for a holistic understanding of the cellular system's interactions. While significant challenges will need to be overcome, tissue and organ level models are also useful for understanding AP propagation and structure-related functional changes that occur in myocardial injury and failure, and may be potentially useful in the clinical environment as tools to aid in the prevention, diagnosis and treatment of cardiac diseases.[154]

5.3 FINAL THOUGHTS

This dissertation characterized the effects downstream of $P2X_4R$ activation in the cardiomyocyte, and our results have pointed to a potentially rewarding translational outcome on treatment of myocardial injury and failure. In addition to contributing to the purinergic field, the mechanisms by which the $P2X_4R$ confer cardioprotection touch upon many important and active areas in cardiobiology research, and continued progress in these fields, with synergistic developments in experimental and computational arenas, will enhance our understanding of and ability to manage and treat the complex disease that is heart failure.

Appendix A

The human $P2X_4R$ gene is located on the q arm of chromosome 12 and the mouse gene is located on chromosome 5. The gene contains 12 exons. Figure 1 demonstrates genetic targeting for exon 2-5 deletion to generate genetic knockouts and Table 1 provides primer sequences for genotyping.

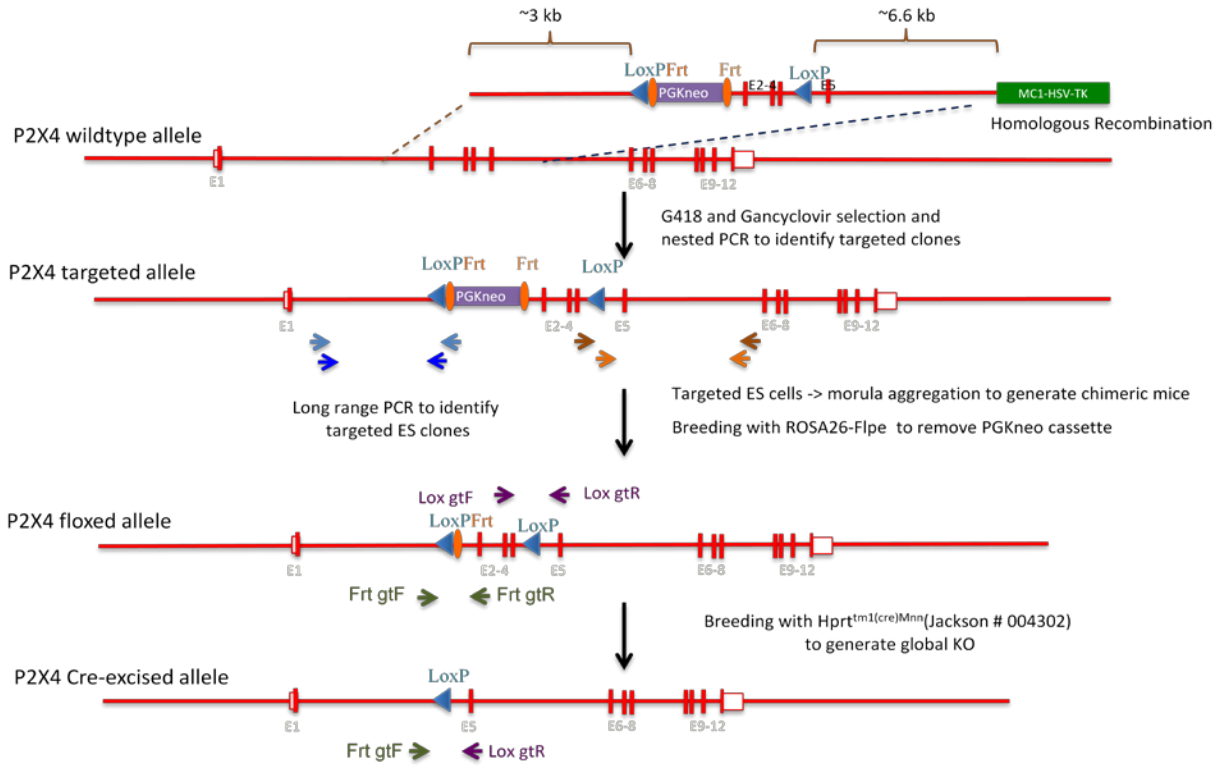

Figure 1: $P2X_4R$ Gene Structure and Targeting for knockout generation

aMHC Linker Forward	GTC GAC TGA CTA ACT AGA AGC T
P2X4 Linker Reverse	CTG AGC TGG TAT CAC ATA ATC C
$P2X4^{floxed/floxed}$ mice	
Lox gtF	TTG CGA TTC AGA CGC CAA CT
LoxgtR	TCT ATT GCA GAC ATG CTA CC
Frt gtF	TTC TGC CTT GGG TTC AAA TC
Frt gtR	AGC CCC TTA CCC AGC TAC TC
$Hprt^{tm1(cre)Mnn}$/J mice	
Transgene Forward	GCG GTC TGG CAG TAA AAA CTA TC
Transgene Reverse	GTG AAA CAG CAT TGC TGT CAC TT
Wildtype Forward	CAC AGT AGC TCT TCA GTC TGA TAA AA
Wildtype Reverse	TTT CTA TAG GAC TGA AAG ACT TGC TC

Table 1. Primer Sequences for genotyping

References

1. Sonin D, Zhou SY, Cronin C, Sonina T, Wu J, Jacobson KA, Pappano A, Liang BT. Role of p2x purinergic receptors in the rescue of ischemic heart failure. *Am. J. Physiol. Heart Circ. Physiol.* 2008;295:H1191-H1197
2. World Health Organization (Shanthi Medndis) WHFPP, and the World Stroke Organization (Bo Norrving). Global atlas on cardiovascular disease prevention and control. 201
3. CDC N. Underlying cause of death 1999-2013 on cdc wonder online database, released 2015. 2015
4. Control CfD. Cdc heart failure fact sheet.2015
5. Drury AN, Szent-Györgyi A. The physiological activity of adenine compounds with especial reference to their action upon the mammalian heart. *The Journal of physiology*. 1929;68:213-237
6. Grant AO. Cardiac ion channels. *Circulation: Arrhythmia and Electrophysiology*. 2009;2:185-194
7. Stern MD, Lakatta EG. Excitation-contraction coupling in the heart: The state of the question. *The FASEB Journal*. 1992;6:3092-3100
8. Fabiato A. Time and calcium dependence of activation and inactivation of calcium- induced release of calcium from the sarcoplasmic reticulum of a skinned canine cardiac purkinje cell. *The Journal of General Physiology*. 1985;85:247-289
9. Hodgkin AL, Huxley AF. A quantitative description of membrane current and its application to conduction and excitation in nerve. *The Journal of physiology*. 1952;117:500-544
10. Noble D. Cardiac action and pacemaker potentials based on the hodgkin-huxley equations. *Nature*. 1960;188:495-497
11. DiFrancesco D, Noble D. *A model of cardiac electrical activity incorporating ionic pumps and concentration changes*. 1985.
12. Luo CH, Rudy Y. A model of the ventricular cardiac action potential. Depolarization, repolarization, and their interaction. *Circ. Res.* 1991;68:1501-1526
13. Greenstein JL, Winslow RL. An integrative model of the cardiac ventricular myocyte incorporating local control of ca2+ release. *Biophys. J.* 2002;83:2918-2945
14. Greenstein JL, Hinch R, Winslow RL. Mechanisms of excitation-contraction coupling in an integrative model of the cardiac ventricular myocyte. *Biophys. J.* 2006;90:77-91
15. Bondarenko VE, Szigeti GP, Bett GC, Kim SJ, Rasmusson RL. Computer model of action potential of mouse ventricular myocytes. *American journal of physiology.Heart and circulatory physiology*. 2004;287:H1378-1403
16. Mullins PD, Bondarenko VE. A mathematical model of the mouse ventricular myocyte contraction. *PLoS ONE*. 2013;8:e63141
17. Sabir IN, Killeen MJ, Grace AA, Huang CLH. Ventricular arrhythmogenesis: Insights from murine models. *Prog. Biophys. Mol. Biol.* 2008;98:208-218
18. Bassani JW, Bassani RA, Bers DM. Relaxation in rabbit and rat cardiac cells: Species-dependent differences in cellular mechanisms. *The Journal of physiology*. 1994;476:279-293
19. Kaese S, Verheule S. Cardiac electrophysiology in mice: A matter of size. *Frontiers in Physiology*. 2012;3:345
20. Bers DM. Cardiac na/ca exchange function in rabbit, mouse and man: What's the difference? *J. Mol. Cell. Cardiol.*;34:369-373
21. Burnstock G. Purinergic receptors. *J. Theor. Biol.* 1976;62:491-503
22. Fredholm BB, Abbracchio MP, Burnstock G, Daly JW, Harden TK, Jacobson KA, Leff P, Williams M. Nomenclature and classification of purinoceptors. *Pharmacol. Rev.* 1994;46:143-156

23. Coddou C, Yan Z, Obsil T, Huidobro-Toro JP, Stojilkovic SS. Activation and regulation of purinergic p2x receptor channels. *Pharmacol. Rev.* 2011;63:641-683
24. Ecke D, Hanck T, Tulapurkar ME, Schafer R, Kassack M, Stricker R, Reiser G. Hetero-oligomerization of the p2y11 receptor with the p2y1 receptor controls the internalization and ligand selectivity of the p2y11 receptor. *The Biochemical journal*. 2008;409:107-116
25. Khakh BS, Burnstock G. The double life of atp. *Sci. Am.* 2009;301:84-90, 92
26. Szentmiklósi AJ. Novel trends in the treatment of cardiovascular disorders: Site- and event-selective adenosinergic drugs. *Curr. Med. Chem.* 2011;18(8):1164-1187
27. Olivier CB, Diehl P, Schnabel K, Weik P, Zhou Q, Bode C, Moser M. Third generation p2y12 antagonists inhibit platelet aggregation more effectively than clopidogrel in a myocardial infarction registry. *Thromb. Haemost.* 2014;111
28. Arulkumaran N, Unwin RJ, Tam FW. A potential therapeutic role for p2x7 receptor (p2x7r) antagonists in the treatment of inflammatory diseases. *Expert Opinion on Investigational Drugs*. 2011;20:897-915
29. Petit P, Lajoix A-D, Gross R. P2 purinergic signalling in the pancreatic β-cell: Control of insulin secretion and pharmacology. *Eur. J. Pharm. Sci.* 2009;37:67-75
30. Soares-Bezerra R, Calheiros A, da Silva Ferreira N, da Silva Frutuoso V, Alves L. Natural products as a source for new anti-inflammatory and analgesic compounds through the inhibition of purinergic p2x receptors. *Pharmaceuticals*. 2013;6:650-658
31. Kuzmin AI, Lakomkin VL, Kapelko VI, Vassort G. Interstitial atp level and degradation in control and postmyocardial infarcted rats. *American Journal of Physiology - Cell Physiology*. 1998;275:C766-C771
32. Stoner HB, Green HN. Experimental limb ischaemia in man with especial reference to the role of adenosine triphosphate. . *Clin Sci.* 1945;5:159-175
33. Stoner HB, Green HN, Threlfall CJ. Bodily reactions to trauma. A possible role of nucleotides in cardiac ischaemia. *Br. J. Exp. Pathol.* 1948;29:419-446
34. Forrester T, Williams CA. Release of adenosine triphosphate from isolated adult heart cells in response to hypoxia. *The Journal of physiology*. 1977;268:371-390
35. Hopkins SV. The action of atp in the guinea-pig heart. *Biochem. Pharmacol.* 1973;22:335-339
36. Camm AJ, Garratt CJ. Adenosine and supraventricular tachycardia. *N. Engl. J. Med.* 1991;325:1621-1629
37. Sharma AD, Klein GJ, Yee R. Intravenous adenosine triphosphate during wide qrs complex tachycardia: Safety, therapeutic efficacy, and diagnostic utility. *The American Journal of Medicine*.88:337-343
38. BjÖRnsson ÓG, Monck JR, Williamson JR. Identification of p2y purinoceptors associated with voltage-activated cation channels in cardiac ventricular myocytes of the rat. *Eur. J. Biochem.* 1989;186:395-404
39. Gergs U, Boknik P, Schmitz W, Simm A, Silber R-E, Neumann J. A positive inotropic effect of atp in the human cardiac atrium. *American Journal of Physiology - Heart and Circulatory Physiology*. 2008;294:H1716-H1723
40. Musa H, Tellez JO, Chandler NJ, Greener ID, Maczewski M, Mackiewicz U, Beresewicz A, Molenaar P, Boyett MR, Dobrzynski H. P2 purinergic receptor mrna in rat and human sinoatrial node and other heart regions. *Naunyn-Schmiedeberg's Arch. Pharmacol.* 2009;379:541-549
41. Banfi C, Ferrario S, De Vincenti O, Ceruti S, Fumagalli M, Mazzola A, D'Ambrosi N, Volonte C, Fratto P, Vitali E, Burnstock G, Beltrami E, Parolari A, Polvani G, Biglioli P, Tremoli E, Abbracchio MP. P2 receptors in human heart: Upregulation of $p2x_6$ in patients undergoing heart transplantation, interaction with tnfα and potential role in myocardial cell death. *J. Mol. Cell. Cardiol.* 2005;39:929-939

42. Danziger RS, Raffaeli S, Moreno-Sanchez R, Sakai M, Capogrossi MC, Spurgeon HA, Hansford RG, Lakatta EG. Extracellular atp has a potent effect to enhance cystolic calcium and contractility in single ventricular myocytes. *Cell Calcium*. 1988;9:193-199
43. De Young MB, Scarpa A. Atp receptor-induced ca2+ transients in cardiac myocytes: Sources of mobilized ca2+. *The American Journal of Physiology*. 1989;257:C750-758
44. Scamps F, Vassort G. Pharmacological profile of the atp-mediated increase in l-type calcium current amplitude and activation of a non-specific cationic current in rat ventricular cells. *Br. J. Pharmacol.* 1994;113:982-986
45. Christie A, Sharma VK, Sheu SS. Mechanism of extracellular atp-induced increase of cytosolic ca2+ concentration in isolated rat ventricular myocytes. *The Journal of physiology*. 1992;445:369-388
46. Zhang B-X, Desnoyer RW, Bond M. Extracellular adenosine triphosphate triggers arrhythmias and elemental redistribution in electrically stimulated rat cardiac myocytes. *Microsc. Microanal.* 2001;7:48-55
47. Shen JB, Pappano AJ, Liang BT. Extracellular atp-stimulated current in wild-type and $p2x_4$ receptor transgenic mouse ventricular myocytes: Implications for a cardiac physiologic role of $p2x_4$ receptors. *FASEB J.* 2006;20:277-284
48. Parker KE, Scarpa A. An atp-activated nonselective cation channel in guinea pig ventricular myocytes. *Am. J. Physiol.* 1995;269:H789-797
49. Mei Q, Liang BT. P2 purinergic receptor activation enhances cardiac contractility in isolated rat and mouse hearts. *Am. J. Physiol. Heart Circ. Physiol.* 2001;281:H334-341
50. Erga KS, Seubert CN, Liang H-X, Wu L, Shryock JC, Belardinelli L. Role of a2a-adenosine receptor activation for atp-mediated coronary vasodilation in guinea-pig isolated heart. *Br. J. Pharmacol.* 2000;130:1065-1075
51. Hu B, Mei QB, Yao XJ, Smith E, Barry WH, Liang BT. A novel contractile phenotype with cardiac transgenic expression of the human $p2x_4$ receptor. *FASEB J.* 2001;15:2739-2741
52. Yang A, Sonin D, Jones L, Barry WH, Liang BT. A beneficial role of cardiac $p2x_4$ receptors in heart failure: Rescue of the calsequestrin overexpression model of cardiomyopathy. *American journal of physiology.Heart and circulatory physiology*. 2004;287:H1096-1103
53. Shen JB, Cronin C, Sonin D, Joshi BV, Gongora Nieto M, Harrison D, Jacobson KA, Liang BT. P2x purinergic receptor-mediated ionic current in cardiac myocytes of calsequestrin model of cardiomyopathy: Implications for the treatment of heart failure. *American journal of physiology.Heart and circulatory physiology*. 2007;292:H1077-1084
54. Ohata Y, Ogata S, Nakanishi K, Kanazawa F, Uenoyama M, Hiroi S, Tominaga S, Kawai T. Expression of p2x4r mrna and protein in rats with hypobaric hypoxia-induced pulmonary hypertension. *Circulation Journal*. 2011;75:945-954
55. Shen JB, Shutt R, Pappano A, Liang BT. Characterization and mechanism of p2x receptor-mediated increase in cardiac myocyte contractility. *Am. J. Physiol. Heart Circ. Physiol.* 2007;293:H3056-3062
56. Yamamoto K, Sokabe T, Matsumoto T, Yoshimura K, Shibata M, Ohura N, Fukuda T, Sato T, Sekine K, Kato S, Isshiki M, Fujita T, Kobayashi M, Kawamura K, Masuda H, Kamiya A, Ando J. Impaired flow-dependent control of vascular tone and remodeling in p2x4-deficient mice. *Nat. Med.* 2006;12:133-137
57. Stokes L, Scurrah K, Ellis JA, Cromer BA, Skarratt KK, Gu BJ, Harrap SB, Wiley JS. A loss-of-function polymorphism in the human p2x4 receptor is associated with increased pulse pressure. *Hypertension*. 2011:1092-1092
58. Hammond J, Balligand JL. Nitric oxide synthase and cyclic gmp signaling in cardiac myocytes: From contractility to remodeling. *J. Mol. Cell. Cardiol.* 2012:340-340

59. Bers D. *Excitation-contraction coupling and cardiac contractile force*. Dordrecht, The Netherlands: Springer; 2008.
60. Glitsch HG. Electrophysiology of the sodium-potassium-atpase in cardiac cells. *Physiol. Rev.* 2001;81:1791-1826
61. Kimura J, Miyamae S, Noma A. Identification of sodium-calcium exchange current in single ventricular cells of guinea-pig. *The Journal of Physiology*. 1987;384:199-222
62. Hinata M, Kimura J. Forefront of na^+/ca^{2+} exchanger studies: Stoichiometry of cardiac na^+/ca^{2+} exchanger; 3:1 or 4:1? *Journal of Pharmacological Sciences*. 2004;96:15-18
63. North RA. Molecular physiology of p2x receptors. *Physiol. Rev.* 2002;82:1013-1067
64. Ralevic V, Burnstock G. Receptors for purines and pyrimidines. *Pharmacol. Rev.* 1998;50:413-492
65. Garcia-Guzman M, Soto F, Gomez-Hernandez JM, Lund PE, Stühmer W. Characterization of recombinant human $p2x_4$ receptor reveals pharmacological differences to the rat homologue. *Mol. Pharmacol.* 1997;51:109-118
66. Shen JB, Shutt R, Agosto M, Pappano A, Liang BT. Reversal of cardiac myocyte dysfunction as a unique mechanism of rescue by $p2x_4$ receptors in cardiomyopathy. *Am. J. Physiol. Heart Circ. Physiol.* 2009;296:H1089-1095
67. Ginsburg KS, Bers DM. Isoproterenol does not enhance ca-dependent na/ca exchange current in intact rabbit ventricular myocytes. *J. Mol. Cell. Cardiol.* 2005;39:972-981
68. Wang W, Gao J, Entcheva E, Cohen I, Gordon C, Mathias R. A transmural gradient in the cardiac na/k pump generates a transmural gradient in na/ca exchange. *J. Membr. Biol.* 2010;233:51-62
69. Su Z, Zou A, Nonaka A, Zubair I, Sanguinetti MC, Barry WH. Influence of prior na^+ pump activity on pump and na^+/ca^{2+} exchange currents in mouse ventricular myocytes. *Am. J. Physiol.* 1998;275:H1808-1817
70. Verdonck F, Volders PG, Vos MA, Sipido KR. Intracellular na^+ and altered na^+ transport mechanisms in cardiac hypertrophy and failure. *J. Mol. Cell. Cardiol.* 2003;35:5-25
71. Luo CH, Rudy Y. A dynamic model of the cardiac ventricular action potential. I. Simulations of ionic currents and concentration changes. *Circ. Res.* 1994;74:1071-1096
72. You Y, Pelzer DJ, Pelzer S. Modulation of l-type ca2+ current by fast and slow ca2+ buffering in guinea pig ventricular cardiomyocytes. *Biophys. J.* 1997;72:175-187
73. Iwamoto T, Kita S. Ym-244769, a novel na+/ca2+ exchange inhibitor that preferentially inhibits ncx3, efficiently protects against hypoxia/reoxygenation-induced sh-sy5y neuronal cell damage. *Mol. Pharmacol.* 2006;70:2075-2083
74. Satoh H, Ginsburg KS, Qing K, Terada H, Hayashi H, Bers DM. Kb-r7943 block of ca^{2+} influx via na^+/ca^{2+} exchange does not alter twitches or glycoside inotropy but prevents ca^{2+} overload in rat ventricular myocytes. *Circulation*. 2000;101:1441-1446
75. Swift F, Tovsrud N, Enger UH, Sjaastad I, Sejersted OM. The na+/k+-atpase alpha2-isoform regulates cardiac contractility in rat cardiomyocytes. *Cardiovasc. Res.* 2007;75:109-117
76. Lederer WJ, Niggli E, Hadley RW. Sodium-calcium exchange in excitable cells: Fuzzy space. *Science*. 1990;248:283
77. Carmeliet E. A fuzzy subsarcolemmal space for intracellular na^+ in cardiac cells? *Cardiovasc. Res.* 1992;26:433-442
78. Levi AJ, Boyett MR, Lee CO. The cellular actions of digitalis glycosides on the heart. *Prog. Biophys. Mol. Biol.* 1994;62:1-54
79. Satoh H, Mukai M, Urushida T, Katoh H, Terada H, Hayashi H. Importance of ca^{2+} influx by na^+/ca^{2+} exchange under normal and sodium-loaded conditions in mammalian ventricles. *Mol. Cell. Biochem.* 2003;242:11-17

80. Resasco DC, Gao F, Morgan F, Novak IL, Schaff JC, Slepchenko BM. Virtual cell: Computational tools for modeling in cell biology. *Wiley Interdisciplinary Reviews: Systems Biology and Medicine*. 2012;4:129-140
81. Lee EC, Yu D, Martinez de Velasco J, Tessarollo L, Swing DA, Court DL, Jenkins NA, Copeland NG. A highly efficient escherichia coli-based chromosome engineering system adapted for recombinogenic targeting and subcloning of bac DNA. *Genomics*. 2001;73:56-65
82. Vassort G. Adenosine 5′ -triphosphate: A p2-purinergic agonist in the myocardium. *Physiol. Rev.* 2001;81:767-806
83. Jameson HS, Pinol RA, Kamendi H, Mendelowitz D. Atp facilitates glutamatergic neurotransmission to cardiac vagal neurons in the nucleus ambiguus. *Brain Res.* 2008;1201:88-92
84. Gourine AV, Wood JD, Burnstock G. Purinergic signalling in autonomic control. *Trends Neurosci.* 2009;32:241-248
85. Fu L-W, Longhurst JC. A new function for atp: Activating cardiac sympathetic afferents during myocardial ischemia. *American Journal of Physiology - Heart and Circulatory Physiology*. 2010;299:H1762-H1771
86. Gurung IS, Kalin A, Grace AA, Huang CL. Activation of purinergic receptors by atp induces ventricular tachycardia by membrane depolarization and modifications of ca2+ homeostasis. *J. Mol. Cell. Cardiol.* 2009;47:622-633
87. Jarvis MF, Khakh BS. Atp-gated p2x cation-channels. *Neuropharmacology*. 2009;56:208-215
88. Erlinge D, Burnstock G. P2 receptors in cardiovascular regulation and disease. *Purinergic signalling*. 2008;4:1-20
89. Balogh J, Wihlborg AK, Isackson H, Joshi BV, Jacobson KA, Arner A, Erlinge D. Phospholipase c and camp-dependent positive inotropic effects of atp in mouse cardiomyocytes via p2y11-like receptors. *J. Mol. Cell. Cardiol.* 2005;39:223-230
90. Harzheim D, Movassagh M, Foo RS-Y, Ritter O, Tashfeen A, Conway SJ, Bootman MD, Roderick HL. Increased insp3rs in the junctional sarcoplasmic reticulum augment ca2+ transients and arrhythmias associated with cardiac hypertrophy. *Proceedings of the National Academy of Sciences*. 2009;106:11406-11411
91. Hong T-T, Smyth JW, Gao D, Chu KY, Vogan JM, Fong TS, Jensen BC, Colecraft HM, Shaw RM. Bin1 localizes the l-type calcium channel to cardiac t-tubules. *PLoS Biol*. 2010;8:e1000312
92. Kennedy C, Leff P. How should p2x purinoceptors be classified pharmacologically? *Trends Pharmacol. Sci.* 1995;16:168-174
93. Dorigo P, Gaion RM, Maragno I. Negative and positive influences exerted by purine compounds on isolated guinea-pig atria. *J. Auton. Pharmacol.* 1988;8:191-196
94. Froldi G, Varani K, Chinellato A, Ragazzi E, Caparrotta L, Borea PA. P2x-purinoceptors in the heart: Actions of atp and utp. *Life Sci.* 1997;60:1419-1430
95. Takikawa R, Kurachi Y, Mashima S, Sugimoto T. Adenosine-5'-triphosphate-induced sinus tachycardia mediated by prostaglandin synthesis via phospholipase c in the rabbit heart. *Pflugers Arch.* 1990;417:13-20
96. Schwartzman M, Pinkas R, Raz A. Evidence for different purinergic receptors for atp and adp in rabbit kidney and heart. *Eur. J. Pharmacol.* 1981;74:167-173
97. Solaro RJ. Mechanisms of the frank-starling law of the heart: The beat goes on. *Biophys. J.* 2007;93:4095-4096
98. Seddon M, Shah AM, Casadei B. *Cardiomyocytes as effectors of nitric oxide signalling*. 2007.
99. Shibata K, Shimokawa H, Yanagihara N, Otsuji Y, Tsutsui M. Nitric oxide synthases and heart failure — lessons from genetically manipulated mice. *Journal of UOEH*. 2013;35:147-158

100. Barouch LA, Harrison RW, Skaf MW, Rosas GO, Cappola TP, Kobeissi ZA, Hobai IA, Lemmon CA, Burnett AL, O'Rourke B, Rodriguez ER, Huang PL, Lima JA, Berkowitz DE, Hare JM. Nitric oxide regulates the heart by spatial confinement of nitric oxide synthase isoforms. *Nature*. 2002;416:337-339
101. Otani H. The role of nitric oxide in myocardial repair and remodeling. *Antioxidants & redox signaling*. 2009
102. McQuade LE, Ma J, Lowe G, Ghatpande A, Gelperin A, Lippard SJ. Visualization of nitric oxide production in the mouse main olfactory bulb by a cell-trappable copper(ii) fluorescent probe. *Proceedings of the National Academy of Sciences*. 2010;107:8525-8530
103. Sartoretto JL, Kalwa H, Pluth MD, Lippard SJ, Michel T. Hydrogen peroxide differentially modulates cardiac myocyte nitric oxide synthesis. *Proceedings of the National Academy of Sciences*. 2011;108:15792-15797
104. Ghosh M, van den Akker NMS, Wijnands KAP, Poeze M, Weber C, McQuade LE, Pluth MD, Lippard SJ, Post MJ, Molin DGM, van Zandvoort MAMJ. Specific visualization of nitric oxide in the vasculature with two-photon microscopy using a copper based fluorescent probe. *PLoS ONE*. 2013;8:e75331
105. Nakayama H, Bodi I, Correll RN, Chen X, Lorenz J, Houser SR, Robbins J, Schwartz A, Molkentin JD. A1g-dependent t-type ca(2+) current antagonizes cardiac hypertrophy through a nos3-dependent mechanism in mice. *The Journal of clinical investigation*. 2009;119:3787-3796
106. Podrasky E, Xu D, Liang BT. A novel phospholipase c- and camp-independent positive inotropic mechanism via a p2 purinoceptor. *Am. J. Physiol.* 1997;273:H2380-2387
107. Shen J-B, Yang R, Pappano A, Liang BT. *Cardiac p2x purinergic receptors as a new pathway for increasing na+ entry in cardiac myocytes*. 2014.
108. Ghafourifar P, Parihar MS, Nazarewicz R, Zenebe WJ, Parihar A. Detection assays for determination of mitochondrial nitric oxide synthase activity; advantages and limitations. In: Enrique C, Lester P, eds. *Methods in enzymology*. Academic Press; 2008:317-334.
109. Traynham CJ, Roof SR, Wang H, Prosak RA, Tang L, Viatchenko-Karpinski S, Ho H-T, Racoma IO, Catalano DJ, Huang X, Han Y, Kim S-U, Gyorke S, Billman GE, Villamena FA, Ziolo MT. Diesterified nitrone rescues nitroso-redox levels and increases myocyte contraction via increased sr ca^{2+} handling. *PLoS ONE*. 2012;7:e52005
110. Förstermann U, Sessa WC. *Nitric oxide synthases: Regulation and function*. 2012.
111. Sharp BR, Jones SP, Rimmer DM, Lefer DJ. *Differential response to myocardial reperfusion injury in enos-deficient mice*. 2002.
112. Janssens S, Pokreisz P, Schoonjans L, Pellens M, Vermeersch P, Tjwa M, Jans P, Scherrer-Crosbie M, Picard MH, Szelid Z, Gillijns H, Van de Werf F, Collen D, Bloch KD. Cardiomyocyte-specific overexpression of nitric oxide synthase 3 improves left ventricular performance and reduces compensatory hypertrophy after myocardial infarction. *Circ. Res.* 2004;94:1256-1262
113. Elrod JW, Greer JJM, Bryan NS, Langston W, Szot JF, Gebregzlabher H, Janssens S, Feelisch M, Lefer DJ. Cardiomyocyte-specific overexpression of no synthase-3 protects against myocardial ischemia-reperfusion injury. *Arterioscler. Thromb. Vac. Biol.* 2006;26:1517-1523
114. Kondo K, Bhushan S, King AL, Prabhu SD, Hamid T, Koenig S, Murohara T, Predmore BL, Gojon G, Wang R, Karusula N, Nicholson CK, Calvert JW, Lefer DJ. H(2)s protects against pressure overload induced heart failure via upregulation of endothelial nitric oxide synthase (enos). *Circulation*. 2013;127:1116-1127
115. Ruetten H, Dimmeler S, Gehring D, Ihling C, Zeiher AM. *Concentric left ventricular remodeling in endothelial nitric oxide synthase knockout mice by chronic pressure overload*. 2005.
116. Haldar SM, Stamler JS. S-nitrosylation: Integrator of cardiovascular performance and oxygen delivery. *The Journal of clinical investigation*. 2013;123:101-110

117. Kessler S, Clauss WG, Fronius M. Laminar shear stress modulates the activity of heterologously expressed p2x(4) receptors. *Biochim Biophys Acta.* 2011;1808(10):2488-2495
118. Prosser BL, Ward CW, Lederer WJ. X-ros signaling: Rapid mechano-chemo transduction in heart. *Science*. 2011;333:1440-1445
119. Miklavc P, Mair N, Wittekindt OH, Haller T, Dietl P, Felder E, Timmler M, Frick M. Fusion-activated ca2+ entry via vesicular p2x4 receptors promotes fusion pore opening and exocytotic content release in pneumocytes. *Proc. Natl. Acad. Sci. U. S. A.* 2011;108:14503-14508
120. Zhang YH, Youm JB, Earm YE. Stretch-activated non-selective cation channel: A causal link between mechanical stretch and atrial natriuretic peptide secretion. *Prog. Biophys. Mol. Biol.* 2008;98:1-9
121. Leychenko A. Stretch-induced hypertrophy activates nfkb-mediated vegf secretion in adult cardiomyocytes. *ONE Alerts*. 2011
122. Okada S, Yokoyama M, Toko H, Tateno K, Moriya J, Shimizu I, Nojima A, Ito T, Yoshida Y, Kobayashi Y, Katagiri H, Minamino T, Komuro I. Brain-derived neurotrophic factor protects against cardiac dysfunction after myocardial infarction via a central nervous system-mediated pathway. *Arterioscler. Thromb. Vac. Biol.* 2012
123. de Rivero Vaccari JP, Bastien D, Yurcisin G, Pineau I, Dietrich WD, De Koninck Y, Keane RW, Lacroix S. P2x4 receptors influence inflammasome activation after spinal cord injury. *The Journal of neuroscience : the official journal of the Society for Neuroscience*. 2012;32:3058-3066
124. Antman EM, DeMets D, Loscalzo J. Cyclooxygenase inhibition and cardiovascular risk. *Circulation*. 2005;112:759-770
125. Funk CD, FitzGerald GA. Cox-2 inhibitors and cardiovascular risk. *J. Cardiovasc. Pharmacol.* 2007;50:470-479
126. Tsuda M, Kuboyama K, Inoue T, Nagata K, Tozaki-Saitoh H, Inoue K. Behavioral phenotypes of mice lacking purinergic p2x(4)receptors in acute and chronic pain assays. *Molecular Pain*. 2009;5:28-28
127. Frangogiannis NG. The immune system and cardiac repair. *Pharmacol. Res.* 2008;58:88-111
128. van den Akker F, Deddens JC, Doevendans PA, Sluijter JPG. Cardiac stem cell therapy to modulate inflammation upon myocardial infarction. *Biochimica et Biophysica Acta (BBA) - General Subjects*. 2013;1830:2449-2458
129. Yang T, Shen J-B, Yang R, Redden J, Dodge-Kafka K, Grady J, Jacobson KA, Liang BT. A novel protective role of endogenous cardiac myocyte $p2x_4$ receptors in heart failure. *Circulation: Heart Failure*. 2014
130. Yamamoto K, Korenaga R, Kamiya A, Ando J. Fluid shear stress activates ca2+ influx into human endothelial cells via p2x4 purinoceptors. *Circ. Res.* 2000;87:385-391
131. Gu BJ, Baird PN, Vessey KA, Skarratt KK, Fletcher EL, Fuller SJ, Richardson AJ, Guymer RH, Wiley JS. A rare functional haplotype of the p2rx4 and p2rx7 genes leads to loss of innate phagocytosis and confers increased risk of age-related macular degeneration. *The FASEB Journal*. 2013;27:1479-1487
132. Morotti S, Edwards AG, McCulloch AD, Bers DM, Grandi E. A novel computational model of mouse myocyte electrophysiology to assess the synergy between na+ loading and camkii. *The Journal of physiology*. 2014;592:1181-1197
133. Lou Q, Janardhan A, Efimov IR. Remodeling of calcium handling in human heart failure. *Adv. Exp. Med. Biol.* 2012;740:1145-1174
134. Karantalis V, Schulman IH, Hare JM. Nitroso-redox imbalance affects cardiac structure and function. *J. Am. Coll. Cardiol.* 2013;61:933-935

135. Khan SA, Lee K, Minhas KM, Gonzalez DR, Raju SV, Tejani AD, Li D, Berkowitz DE, Hare JM. Neuronal nitric oxide synthase negatively regulates xanthine oxidoreductase inhibition of cardiac excitation-contraction coupling. *Proc. Natl. Acad. Sci. U. S. A.* 2004;101:15944-15948
136. Gonzalez DR, Treuer AV, Castellanos J, Dulce RA, Hare JM. Impaired s-nitrosylation of the ryanodine receptor caused by xanthine oxidase activity contributes to calcium leak in heart failure. *J. Biol. Chem.* 2010;285:28938-28945
137. Givertz MM, Mann DL, Lee KL, Ibarra JC, Velazquez EJ, Hernandez AF, Mascette AM, Braunwald E. Xanthine oxidase inhibition for hyperuricemic heart failure patients: Design and rationale of the exact-hf study. *Circulation: Heart Failure*. 2013;6:862-868
138. Liu Y, Huang H, Xia W, Tang Y, Li H, Huang C. Nadph oxidase inhibition ameliorates cardiac dysfunction in rabbits with heart failure. *Mol. Cell. Biochem.* 2010;343:143-153
139. Saavedra WF, Paolocci N, St. John ME, Skaf MW, Stewart GC, Xie J-S, Harrison RW, Zeichner J, Mudrick D, Marbán E, Kass DA, Hare JM. Imbalance between xanthine oxidase and nitric oxide synthase signaling pathways underlies mechanoenergetic uncoupling in the failing heart. *Circ. Res.* 2002;90:297-304
140. Moens AL, Leyton-Mange JS, Niu X, Yang R, Cingolani O, Arkenbout EK, Champion HC, Bedja D, Gabrielson K, Chen J, Xia Y, Hale AB, Channon KM, Halushka M, Barker N, Wuyts FL, Kaminski PM, Wolin MS, Kass DA, Barouch LA. Adverse ventricular remodeling and exacerbated nos uncoupling from pressure-overload in mice lacking the beta3-adrenoreceptor. *J. Mol. Cell. Cardiol.* 2009
141. Wihlborg AK, Balogh J, Wang L, Borna C, Dou Y, Joshi BV, Lazarowski E, Jacobson KA, Arner A, Erlinge D. Positive inotropic effects by uridine triphosphate (utp) and uridine diphosphate (udp) via p2y2 and p2y6 receptors on cardiomyocytes and release of utp in man during myocardial infarction. *Circ. Res.* 2006;98:970-976
142. Nishidaa M, Ogushia M, Sudaa R, Toyotakaa M, Saikia S, Kitajimaa N, Nakayaa M, Kimb KM, Idec T, Satod Y, Inouee K, Kurosea H. Heterologous down-regulation of angiotensin type 1 receptors by purinergic p2y2 receptor stimulation through s-nitrosylation of nf-kb. *Proc.Natl.Acad.Sci.U.S.A.* 2011;108:6662-6667
143. Vessey DA, Li L, Kelley M. Pannexin-i/p2x 7 purinergic receptor channels mediate the release of cardioprotectants induced by ischemic pre- and postconditioning. *Journal of cardiovascular pharmacology and therapeutics*. 2010;15:190-195
144. Cosentino S, Banfi C, Burbiel JC, Luo H, Tremoli E, Abbracchio MP. Cardiomyocyte death induced by ischemic/hypoxic stress is differentially affected by distinct purinergic p2 receptors. *J. Cell. Mol. Med.* 2012:1074-1084
145. Hattori M, Gouaux E. Molecular mechanism of atp binding and ion channel activation in p2x receptors. *Nature*. 2012;doi: 10.1038/nature11010 [Epub ahead of publication]
146. Kumar TS, Zhou SY, Joshi BV, Balasubramanian R, Yang T, Liang BT, Jacobson KA. Structure-activity relationship of (n)-methanocarba phosphonate analogues of 5'-amp as cardioprotective agents acting through a cardiac p2x receptor. *J. Med. Chem.* 2010;53:2562-2576
147. Smith NP, Crampin EJ. Development of models of active ion transport for whole-cell modelling: Cardiac sodium–potassium pump as a case study. *Prog. Biophys. Mol. Biol.* 2004;85:387-405
148. Tran K, Smith NP, Loiselle DS, Crampin EJ. A thermodynamic model of the cardiac sarcoplasmic/endoplasmic ca(2+) (serca) pump. *Biophys. J.* 2009;96:2029-2042
149. Saucerman JJ, Brunton LL, Michailova AP, McCulloch AD. Modeling β-adrenergic control of cardiac myocyte contractility in silico. *J. Biol. Chem.* 2003;278:47997-48003
150. Soltis AR, Saucerman JJ. Synergy between camkii substrates and β-adrenergic signaling in regulation of cardiac myocyte ca2+ handling. *Biophys. J.*;99:2038-2047

151. Cortassa S, Aon MA, Marbán E, Winslow RL, O'Rourke B. An integrated model of cardiac mitochondrial energy metabolism and calcium dynamics. *Biophys. J.* 2003;84:2734-2755
152. Kembro Jackelyn M, Aon Miguel A, Winslow Raimond L, O'Rourke B, Cortassa S. Integrating mitochondrial energetics, redox and ros metabolic networks: A two-compartment model. *Biophys. J.* 2013;104:332-343
153. Gauthier Laura D, Greenstein Joseph L, O'Rourke B, Winslow Raimond L. An integrated mitochondrial ros production and scavenging model: Implications for heart failure. *Biophys. J.* 2013;105:2832-2842
154. Lopez-Perez A, Sebastian R, Ferrero JM. Three-dimensional cardiac computational modelling: Methods, features and applications. *BioMedical Engineering OnLine*. 2015;14:35